

ANALYSIS OF V AMYLOSE IN CONTROLLED DRUG DELIVERY

A thesis submitted to the
UPES

For the award of
Doctor of Philosophy
in
Chemistry

BY
Rabab Fatima

December 2023

SUPERVISOR
Dr. Parteek Prasher



School of Advanced Engineering
UPES
Dehradun 248007 Uttarakhand

ANALYSIS OF V AMYLOSE IN CONTROLLED DRUG DELIVERY

A thesis submitted to the
UPES

For the award of
Doctor of Philosophy
in
Chemistry

BY
Rabab Fatima

December 2023
(SAP ID: 500087091)

SUPERVISOR
Dr. Parteek Prasher



School of Advanced Engineering
UPES
Dehradun 248007 Uttarakhand

Declaration

I declare that the thesis entitled “**Analysis of V Amylose in Controlled Drug Delivery**” has been prepared by me under the guidance of Dr. Parteek Prasher, Department of Chemistry, SOAE, UPES. No part of this thesis has formed the basis for the award of any degree or fellowship previously.



Rabab Fatima

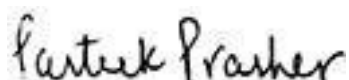
School of Advanced Engineering (SOAE), UPES

Dehradun 248007, Uttarakhand

Thesis completion certificate

This is to certify that the thesis on “**Analysis of V Amylose in controlled drug delivery**” by **Rabab Fatima** in partial completion of the requirement for the award of the degree of Doctor of Philosophy to University of Petroleum and Energy Studies (School of Advanced Engineering) is an original work carried out by her under my supervision.

It is certified that the work, in full or parts, have not been submitted to any other institute or university for the award of any other degree or diploma.



(Supervisor)

Dr. Parteek Prasher

Department of Chemistry

School of Advanced Engineering (SOAE), UPES

Dehradun 248007, Uttarakhand

Date:28.12.2023

Dedication

I want to dedicate my thesis to my deceased parents (Late) Mr. Syed Mohd. Askari and (Late) Mrs. Tahseen Fatima.

-

Abstract

Polysaccharides are characterized by the repetitive mono or disaccharide units linked through glycosidic bonds, rendering them susceptible to enzymatic activity and highly suitable as carriers for controlled release of various therapeutically significant drugs. Their exceptional physicochemical and physiological attributes such as biocompatibility, biodegradability, non-toxicity, ease of availability and limited immunogenicity, underscore their aptness for drug delivery applications. Obtained from diverse origins such as plants, animals, and microbes, these natural polysaccharides offer a wide spectrum of biomedically relevant physicochemical properties. Non-steroidal anti-inflammatory drugs (NSAIDs) are usually prescribed for chronic rheumatic and arthritic conditions and act as inhibitors of cyclooxygenase 1/2 (COX-1/2). One such NSAID, Flufenamic acid (FFA), from the member of fenamate family, also known as N-(α,α,α -trifluoro-m-tolyl) anthranilic acid, demonstrate robust non-steroidal analgesic and anti-inflammatory attributes, rendering it invaluable in treating rheumatic ailments. Reportedly, uncontrolled or burst release of FFA within the gastrointestinal tract compromises the protective mucosal barrier, resulting in ulcer development. This burst release increases the local drug concentrations beyond therapeutic thresholds while exacerbating the physiological toxicity. In contrast, controlled drug delivery systems facilitate sustained release, maintaining optimal therapeutic concentrations for targeted cells.

The gastrointestinal milieu exhibits varying pH gradients, with gastric acidity shifting towards gradual alkalinity towards the small and large intestines. This pH heterogeneity offers opportunities for colon targeted drug delivery by natural and modified polysaccharide based carrier systems. A pivotal criterion for such carriers involves their propensity to hydrate and swell, forming diffusion barrier upon contact with solid dosage forms during gastrointestinal transit. These hydrated polymer layers permit the ingress of colonic enzymes and microbes, prompting polysaccharide barrier degradation and releasing the drug at the desired site

subsequently. Polysaccharides, endowed with abundant derivatizable groups, diverse molecular weights, varied chemical compositions, and crucially, stability, safety, and biodegradability, confer distinct advantages over alternative strategies. NSAIDs, due to their propensity for burst release forming ulcers in gut mucosa. Effective implementation of controlled delivery systems with drug loaded polysaccharides attenuates ulcerogenicity index, ensuring sustained drug release for prolonged therapeutic efficacy. Unlike other polysaccharides, V-amylose from starch exhibits excellent resistance to enzymatic degradation, further substantiating its controlled release profile. Experimental in vitro release profiles of several NSAIDs with V-amylose within simulated intestinal media corroborate these findings, underscoring V-amylose's potential as a prospective drug delivery platform. Importantly, V-amylose's unique helical structure helps accommodate hydrophilic and hydrophobic drug molecules further augmenting its versatility for encapsulating diverse drug molecules. The work established the idea of using V Amylose, a form of resistant starch, as drug delivery vehicle for slow or controlled release of ulceronegic fenamates, a class of NSAIDs by successfully accommodating in the helix of V Amylose as demonstrated by CP MAS NMR, XRD and FTIR and by preparing matrix dispersion tablets. The matrix tablets achieved a controlled release profile for various members of fenamate family such as flufenamic acid, tolfenamic acid, maclofenamic acid, and mefenamic acid in GI tract owing to the cleavage of imine functionality and remarkable swelling in gastric media. The tablets demonstrated enzyme responsive release of fenamates in simulated conditions of intestines, thus preventing the burst release of fenamates after their intake. Furthermore, in order to establish controlled drug release in presence of magnetic field, magnetic nanoparticles prepared from V Amylose flufenamic acid complex serving as shell with iron oxide as core further instigated successful encapsulation and can be utilised for theranostic applications.

Keywords: Polysaccharides, Drug Delivery, V Amylose, controlled drug release, Matrix tablets, Mucoadhesive

Acknowledgement

I wish to express my profound gratitude to the Almighty God for granting me the privilege of attaining my doctoral degree from the distinguished **UPES, Dehradun**. My sincere appreciation and heartfelt thanks go to my esteemed mentor, **Dr. Parteek Prasher**, whose continuous guidance and invaluable feedback have been instrumental in all my research endeavours. He introduced me to the present research topic and have since then been a continuous source of motivation and inspiration to pursue my doctorate research.

The journey has been made meaningful through the support of the **Department of Chemistry and the Applied Science Cluster** at **UPES**. Their gracious provision of a fertile research environment underscores their unwavering commitment to fostering scholarly excellence. I am also thankful to the **Central Instrumentation facility** at UPES, and indebted to **Dr. D.K. Awasthi, Dr. Pankaj Thakur, Dr. Ranjeet Kumar Brajpuriya**, entire lab staff and faculty of the Chemistry department. Their sage guidance and steadfast encouragement have been a cornerstone of my progress, underscoring the collaborative spirit that thrives within the academic community. Also, I would like to extend my sincerest regards to my DRC members Dr. Shikha Wadhwa (Associate Professor, UPES), Dr. Shilpi Agrawal (Assistant Professor, UPES), and Dr. Abhishek Kumar Mishra (Senior Associate Professor, UPES) for their valuable feedbacks and suggestions to improve my research work.

In this journey, I am also grateful to my family, especially my daughters, Alishba and Ayeza and my husband Dr. S.M. Tauseef whose unwavering moral support has provided solace during the challenges and motivation during the triumphs. My heartfelt appreciation goes to all my friends and well-wishers whose direct or indirect assistance has been instrumental in my PhD journey.

Finally, I would like to acknowledge the contribution of UPES in providing an excellent research infrastructure and work environment that helped in bringing out the best in the present thesis work.



Rabab Fatima

SAP ID: 500087091 (Junior Research Fellow)

SOAE Applied Science Cluster

UPES Dehradun

Table of Contents

Declaration.....	i
Thesis completion certificate	ii
Dedication.....	iii
Abstract.....	iv
Acknowledgement	vii
List of Figures	xii
List of Tables.....	xiv
Abbreviations.....	xv
Chapter 1: Introduction	1
1.1. Overview and background	1
1.2. Polysaccharide based gastro intestinal targeting drug delivery systems.....	2
1.2.1 Rationale for controlled and sustained drug delivery	4
1.3. Significance of chemical modification of polysaccharides.....	5
1.4. Research motivation and objectives.....	12
Chapter 2: Literature review	16
2.1. Necessity of mucoadhesive drug delivery vehicles.....	18
2.2. Status of the cationic starch for mucosal drug delivery	20
2.3. Limitations of NSAIDs	21
2.4. V-amylose characteristics.....	27
2.5. V Amylose drug complexes	29
2.6. Amylose as enteric coated and sustained release vehicle.....	32
2.7. Amylose based solid dosage formulation for controlled drug delivery	34
2.8. Amylose based magnetically guided drug delivery systems.....	35
2.9 Methodology	37
2.9.1. FTIR spectroscopy.....	37
2.9.2 13 C NMR	38
2.9.3 XRD.....	39
2.9.4. Zetasizer.....	39
2.9.5. Dissolution apparatus	40
2.9.6. Rotating cylinder	41
2.9.7. HPLC	42
2.9.8. UV Spectroscopy	43
2.9.9. TGA analysis	44

2.9.10. SEM microscopy	44
Chapter 3: Targeted drug delivery with native V Amylose.....	46
3.1. Abstract.....	46
3.2. Pictorial presentation of the proposed work.....	46
3.3. Introduction	47
3.4. Materials and Method.....	48
3.4.1. Synthesis of V Amylose-Flufenamic acid conjugates	48
3.4.2. Calculation of the amount of Flufenamic acid included in V-amylose	48
3.4.3. Release of Flufenamic acid in simulated physiological environment	49
3.4.4. Physical investigations	49
3.5. Results and discussion.....	50
3.5.1. Yield of V-Amylose-Flufenamic acid complex and drug content in the complexes	50
3.5.2. Conjugation of Flufenamic acid to V-amylose	51
3.6. Conclusion.....	57
3.7. Summary points.....	58
Chapter 4: Controlled drug delivery with chemically modified V Amylose	59
4.1. Abstract.....	59
4.2. Introduction	59
4.3. Materials and methods	61
4.3.1. Materials	61
4.3.2. Methods	61
4.3.3. Synthesis of aminated starch	61
4.3.4. Calculation of the percentage of dialdehyde modification.....	62
4.3.5. Physical Investigations	62
4.3.6. Tablet preparation	63
4.3.7. Swelling and erosion analysis.....	63
4.3.8. Drug release study	64
4.3.9. Zeta potential assessment	64
4.3.10. Mucoadhesion investigation	64
4.3.11. Drug release kinetics.....	65
4.4. Results and discussion.....	65
4.4.1. Drug release	69
4.4.2. Kinetics of Release	74
4.4.3. Swelling and matrix erosion	87

4.4.4. Mucoadhesive profile	88
4.4.5. Zeta potential	89
4.5. Discussion	90
4.6. Conclusion.....	90
4.7. Summary Points	92
Chapter 5: Design of magnetically guided drug delivery systems for V amylose drug complexes	93
5.1 Introduction and background	93
5.2. Methodology	97
5.2.1. Materials	97
5.2.2. Preparation of V Amylose flufenamic acid (NS FFA) complexes.....	97
5.2.3. Preparation of magnetic nanoparticles coated with V Amylose flufenamic acid complex (MNPs).....	97
5.2.4. Physical Investigations	97
5.3. Results and discussion.....	98
5.4. Conclusion.....	107
Conclusion and Future Prospects.....	109
References.....	111
List of Publications	123

List of Figures

Figure 1: Mucoadhesive drug delivery (Adapted from Reference [69])	19
Figure 2: Commercialized members of 1. fenamic acid-derived NSAIDs 2. Meclofenamic acid, 3. Mefenamic acid, 4. Tolfenamic acid, 5. Flufenamic acid	26
Figure 3: Applicability of Amylose in the contemporary drug delivery paradigm.....	29
Figure 4: UV-vis absorption spectra indicating the complexation of Flufenamic acid in V-amylose	51
Figure 5: Solid-state ¹³ C CP/ MAS NMR spectra of A. V-amylose and B. V-amylose-Flufenamic acid complex.....	52
Figure 6: FTIR spectra of V Amylose-Flufenamic acid for A. In PBS, B. In simulated gastric fluid, C. In simulated small intestine fluid for 12 h, D. In simulated small intestine fluid for 24 h.....	53
Figure 7: XRD diffractogram of A. V-amylose, B. V-amylose-Flufenamic acid complex.....	54
Figure 8: Release of Flufenamic acid by V-amylose: A. Dried conjugate, B. After soaking in simulated gastric fluid for 6h, C. After soaking in simulated intestinal fluid for 12h, and D. After soaking in simulated intestinal fluid for 24h	55
Figure 9: Release of Flufenamic acid by V-amylose	55
Figure 10: Effect of pH and temperature on the release of Flufenamic acid from V-amylose	56
Figure 11: In vitro release of Flufenamic acid in the simulated small intestine fluid for 5 different ratios of Flufenamic acid and V-amylose at a. 1/5, b. 1/15, c. 1/25, d. 1/35, e. 1/50	57
Figure 12: Aminated starch fenamate matrix tablet by direct compression method.....	63
Figure 13: Synthesis of aminated starch	66
Figure 14: IR-spectra of native starch, dialdehyde starch, and aminated starch.....	66
Figure 15: XRD of native starch, dialdehyde starch, and aminated starch.....	67
Figure 16: ¹ H NMR of dialdehyde starch (DAS) in D ₂ O.....	67
Figure 17: ¹ H NMR of aminated starch in D ₂ O + DMSO	67
Figure 18: TGA of native starch, dialdehyde starch, and aminated starch	68
Figure 19: Drug release profile of fenamates in simulated intestinal media	71
Figure 20: Drug release profile of fenamates in simulated intestinal media containing pancrelipase.....	72
Figure 21: Drug release profile of fenamates in simulated gastric media	73
Figure 22: Kinetics of release of Flufenamic acid in simulated conditions of intestinal medium (A), simulated intestinal medium with pancrelipase (B) and simulated gastric medium (C).....	77
Figure 23: Kinetics of release of Tolfenamic acid in simulated conditions of intestine medium (A), simulated intestinal medium with pancrelipase (B) and simulated gastric medium (C)..	80
Figure 24: Kinetics of release of Maclofenamic acid in simulated conditions of intestine medium (A), simulated intestinal medium with pancrelipase (B) and simulated gastric medium (C).....	83
Figure 25: Kinetics of release of Mefenamic acid in simulated conditions of intestine medium (A), simulated intestinal medium with pancrelipase (B) and simulated gastric medium (C)..	86
Figure 26: Swelling and matrix erosion studies for aminated-starch-fenamate tablets.....	87
Figure 27: Behaviour of tablets in bulk of simulated intestinal media containing pancrelipase.	88

Figure 28: Assessment of the mucoadhesive strength of native starch, aminated starch and chitosan by rotating cylinder method. The values shown in the figure are an average of three experiments.	88
Figure 29: Zeta potential of: Aminated starch (in black), Native starch (in red) and Chitosan (in green) at indicated pH	89
Figure 30: FTIR of flufenamic acid	99
Figure 31: FTIR of pure V Amylose, V Amylose in KOH, complex 1/5, 1/10, 1/20 and 1/80.	100
Figure 32: XRD of pure Flufenamic acid	101
Figure 33: XRD of V Amylose (black) and complex of 1/5 ratio (red).....	101
Figure 34: (a) Chromatogram for NS in KOH,(b) Chromatogram for complex 1/5, (c) Chromatogram for complex 1/10, (d) Chromatogram for complex 1/20 and (e) Chromatogram for complex 1/80.....	102
Figure 35: FTIR spectra of Native V Amylose (NS), Native V amylose nanoparticle (NS NP) and V Amylose flufenamic acid complex (C), and magnetic nanoparticles coated with V Amylose flufenamic acid complex (CNP).....	103
Figure 36: XRD diffractogram of prepared magnetic nanoparticles coated with V Amylose flufenamic acid complex (CNP)	104
Figure 37:SEM images of (A) magnetic nanoparticles at 50,000' magnifications, (B) magnetic nanoparticles at 240,000' magnification, (C) magnetic nanoparticles coated with V Amylose-flufenamic complex at 150,000' magnification (D) magnetic nanoparticles coated with V Amylose-flufenamic acid complex at 300,000' magnification	105
Figure 38: TEM images of (A) magnetic nanoparticle with 500 nm bar, (B) magnetic nanoparticle coated with V Amylose flufenamic acid complex with 100 nm magnetic bar, (C) particle diameter of magnetic nanoparticle, and (D) particle diameter of magnetic nanoparticle coated with V Amylose flufenamic acid complex	106
Figure 39: TG analysis of (A) V Amylose flufenamic acid complex (B) magnetic nanoparticles coated with V Amylose flufenamic acid complex.....	106

List of Tables

Table 1: Tabular presentation of modified polysaccharides and their applications in drug delivery	6
Table 2: Potential advantages and novelty of proposed drug delivery system	13
Table 3: Toxicity and molecular pathways affected with NSAIDs.....	22
Table 4: Variation of the Complex yield and Drug content with V-amylose-Flufenamic acid ratio#	51
Table 5: Zeta potential of Aminated starch, native starch and chitosan with respect to pH	89

Abbreviations

Ac-Dex: Acetalated Dextran

AKT: Protein Kinase B

ASC: Apoptosis-associated speck-like protein

ATRP: Atom transfer radical polymerization

BCL: B-cell lymphoma

BSA: Bovine Serum Albumin

CDDS: Controlled Drug Delivery Systems

CF₃: Trifluoromethyl

CFTR: Cystic fibrosis transmembrane conductance regulator

COX 1: Cyclooxygenase 1

COX 2: Cyclooxygenase 2

CINODs: Cyclooxygenase inhibiting nitric oxide donating drugs

CHMAC: 3-chloro-2-hydroxypropyltrimethyl ammonium chloride

CNP: Magnetic nanoparticles coated with V Amylose flufenamic acid complex

COOH: Carboxyl Group

COXIB: Cyclooxygenase 2 inhibitor

CP/MAS: Cross Polarization/Magic Angle Spinning

CX-1: Human colorectal carcinoma cell line

DAS: Dialdehyde Starch

DCC: N, N-dicyclohexylcarbodiimide

DM: Dialysis Membrane

DMAP: 4-(N,N-dimethylamino) Pyridine

DMSO: Dimethyl Sulfoxide

DU-145: Human prostate adenocarcinoma cell line

EC: Enteric Coating

EPR: Enhanced Permeability and Retention

FFA: Flufenamic Acid

FTIR: Fourier Transform Infrared

GI: Gastrointestinal

GIT: Gastrointestinal Tract

GSH: Glutathione

Hep G2: Hepatocellular carcinoma cell line

HIV: Human Immunodeficiency Virus

IL-17 A: Interleukin-17 A

HCl: Hydrochloric Acid

HPLC: High-Performance Liquid Chromatography

Mg: Magnesium

MDF: Maximum Detachment Force

MNPs: Magnetic Nanoparticles

MRI: Magnetic Resonance Imaging

NF κ B: Nuclear factor kappa B

NMR: Nuclear Magnetic Resonance

NSAID: Non-Steroidal Anti-Inflammatory Drug

NSAIDs: Nonsteroidal Anti-Inflammatory Drugs

NS: Native Starch

NP: Nanoparticle

NS: Native V Amylose

NS NP: Native V amylose nanoparticle

OH: Hydroxyl

OPTICORE: Optimal Performance in Targeted colorectal delivery

PBS: Phosphate Buffer Solution

PMMA: Poly (methyl Methacrylate)

PVA: Polyvinyl Alcohol

Q starch: Quarternary starch

rpm: Revolutions Per Minute

SEM: Scanning Electron Microscope

siRNA: short interfering RNA

SR: Sustained Release

TDDS: Traditional Drug Delivery Systems

TGA: Thermogravimetric Analysis

TNF- α : Tumor Necrosis Factor-alpha

TRPC6: Transient receptor potential cation channel subfamily C member 6

TRAIL: Tumor necrosis factor related apoptosis inducing ligand

TWA: Total Work of Adhesion

UV: Ultraviolet

UV VIS: Ultraviolet-Visible Spectroscopy

V: Viscosity

VEGFR: Vascular endothelial growth factor receptor

XRD: X-Ray Diffraction

Chapter 1: Introduction

1.1. Overview and background

Polysaccharides are composed of repetitive mono or disaccharides units linked together by enzyme susceptible glycosidic bonds, making them ideal for controlled release drug carriers. Their exceptional physiological and physicochemical features such as biodegradability, biocompatibility and low immunogenicity, further support their suitability for drug delivery applications [1]. The natural polysaccharides are readily available from various sources such as plants, animals, and microbes, offering a wide range of physicochemical properties such as neutral or positive/negative charges, linear or branched molecular structures, and variable molecular weight [2]. Numerous polysaccharides exhibit the ability to stick to the physiological mucus layer covering the epithelial surfaces in the body enhancing the residence time of drugs in the gastrointestinal (GI) tract and leading to increased bioavailability of drugs [3]. Cationic polysaccharides such as chitosan and its derivatives possess the capability to cleave the tight junctions of epithelial cells, enhancing the permeability of hydrophilic drugs through mucus membranes [4]. By modifying the functional groups such as -OH, -NH₂, -COOH on polysaccharide structure, new polysaccharide derivatives with enhanced property for various applications can be generated. Interaction with these functional groups further allows the therapeutic drugs to incorporate into the main chain through covalent bonds or electrostatic interactions, subsequently leading to the release of the incorporated drug at the deliberated site under suitable physiological conditions [5]. Polysaccharides possessing an abundance of modifiable functional groups, a wide spectrum of molecular weights, diverse chemical compositions, and, crucially, attributes of stability, safety, low immunogenicity and biodegradability, manifest advantageous characteristics.

A diverse array of water-soluble polymers with both natural and synthetic origin, have been subject to investigation due to their inherent capacity to undergo chemical conjugation with

therapeutic drugs [6]. Examination into the pharmacokinetics of drug-conjugated polysaccharides have underscored the significance of leveraging natural and environmentally viable polymers as resilient platform for drug delivery. In combination with their synthetic water-soluble counterparts, natural polymers such as starch, pectin, dextran, chitosan, hyaluronic acid, guar gum, and cellulose, exhibit substantial promise for therapeutic cargo transport [7].

1.2. Polysaccharide based gastro intestinal targeting drug delivery systems

A range of challenges arise in the oral administration of various protein and peptide drugs due to their vulnerability to degradation by digestive enzymes within the gut region. Various approaches are employed to achieve drug targeting to the colon area, including prodrug formation, time-dependent multicoating delivery vehicles, pH-sensitive polymer coatings and biodegradable polymers [8]. A promising alternative involves the introduction of peptide and protein prodrugs into the systemic circulation primarily through colonic absorption. This approach holds particular promise for substances displaying suboptimal absorption characteristics within the upper GI tract, as the colon hosts specific digestive enzymes that are absent in the upper GI tract. Furthermore, in the context of treating localized colonic ailments such as Crohn's disease, ulcerative colitis and colon cancer, targeted prodrug delivery not only curtails the requisite dosage but also mitigates potential adverse events linked to therapeutic agents [9].

The GIT exhibits varying pH levels, with acidity prevailing in the stomach and a gradual increase as it progresses through the intestinal tract. The pH diversity along different GI tract segments has been leveraged for targeted drug delivery to the colon by coating the therapeutic molecule with pH sensitive polymers such as Eudragit [10] which remain insoluble in strong acidic environments of stomach but dissolve at a pH of 6 or higher, protecting the drug from the acidity of stomach and small intestine and ensure colonic specific drug release [11].

The colon's diverse microflora derives its energy by fermenting undigested substrates, such as di and tri saccharides and polysaccharides, left over from the small intestine [12]. In order to facilitate fermentation, the microflora makes an array of enzymes such as dextranase, nitroreductase, α -arabinosidase, β -glucuronidase, β -galactosidase, β -xylosidase, azoreductase, deaminase, amylase and urea dehydroxylase [13]. Compared to other approaches, the utilisation of microflora based degradable polymers is an attractive strategy for colon-specific drug administration because of the prevalence of these biodegradable enzymes particularly in the colon. These polymers efficiently transport the drug to the colon while shielding it from the abrasive conditions of the stomach and small intestine. The polymers eventually lose their ability to retain drug as well as its own molecular weight after degradation by microbes or enzymes in the colon. Biodegradable polymers are utilised as a linkage to create prodrugs containing the drug moiety, as a coating material to enclose the drug core, or as a medium to integrate the drug moiety into its hydrogel or matrix [14]. Various polysaccharides that undergo degradation by colonic microflora have been investigated as carriers for colon targeted drug delivery. Furthermore, utilizing naturally occurring dietary polysaccharides as drug carriers for the colon simplifies concerns related to safety, toxicity, and availability [10].

Numerous investigations have scrutinized the potential of both unmodified and derivatized variants of polysaccharides such as pectin, guar gum, dextran, and chitosan. However, relatively fewer inquiries have been undertaken with regard to chondroitin, insulin, alginates, and amylose [2]. Nevertheless, significant research remains imperative to correlate the concept of a polysaccharide-centric, colon-specific drug delivery system that is amenable to simplified formulation processes, while concurrently upholding an elevated degree of site-specificity with improved patient compliance.

1.2.1 Rationale for controlled and sustained drug delivery

In recent years, drug design has increasingly emphasized the implementation of a prodrug strategy to surmount diverse obstacles that impede efficient drug delivery. These challenges encompass issues like limited water solubility, potential tissue damage, and pharmacological complexities such as rapid absorption, elimination, or inadequate site-specificity. A prodrug refers to an inert pharmacological derivative of a drug, achieved through chemical modification, with the ability to convert into the active parent drug via enzymatic or chemical transformations during the metabolization process [15]. To target drugs to the colon effectively, it is essential to shield the drug from the harsh environments of the stomach and small intestine (SI). This protective function is achieved through conjugation with carrier moieties, leading to the formation of prodrugs. These prodrugs undergo enzymatic degradation in the colon, enabling the regeneration of the active drug form [16].

The optimal drug delivery system must possess attributes that include resistance to unintended release, inertness, biocompatibility, mechanical resilience, patient acceptability, capacity for high drug loading, and streamlined manufacturability and sterilization protocols. Traditional Drug Delivery Systems (TDDS) like tablets, capsules, and syrups demonstrate rapid systemic elimination, failing to maintain drug concentrations within the therapeutic threshold. The fast metabolism of the ingested drug after a standard single dose results in an exponential rise in drug levels followed by a sharp decline. This temporal pattern may not allow for a substantial therapeutic impact to achieve, potentially leading to inadequate therapeutic responses [7]. Controlled Drug Delivery Systems (CDDS), on the other hand, ensure sustained maintenance of drug plasma levels by precisely dispensing the appropriate drug dose within defined temporal intervals. This strategy enhances the overall effectiveness of the dosage form. Of note, by modulating the drug release kinetics, controlled delivery systems decrease the probability of exceeding safe peak concentrations, thereby mitigating potential toxicity. The steady plasma

concentration profiles engendered by these systems offer a contrast to the fluctuating levels observed in conventional delivery, contributing to more stable therapeutic responses [17]. Moreover, the tailoring of release kinetics to accommodate diverse pharmacokinetic profiles of drugs and patient populations ensure personalized and optimized therapeutic interventions. Ideally, the duration of prodrug activity should be more amenable to intentional design of rate-controlled dosage forms, rather than solely relying on the inherent kinetic properties of the prodrug. As previously mentioned, the core objectives of controlled drug delivery include safety, enhancing drug efficacy, and promoting patient adherence. These objectives can be realized by attaining finer regulation of plasma drug levels and optimizing drug dosing frequency unlike conventional dosage forms, which permit variation only in dose and dosing intervals [18].

1.3. Significance of chemical modification of polysaccharides

Chemical modification of polysaccharides offers distinctive benefit owing to their ability to encapsulate or form inclusion complexes with numerous organic and inorganic compounds, improve drug solubility and promote efficient drug delivery to various types of cells including cancer cells with minimal cytotoxicity. Chemical modifications are known to enhance the inherent properties of polysaccharides such as antioxidation, immune regulation, anti-microbial and anti tumor features [19]. The emerging applications of modified polysaccharides may revamp the realm of contemporary drug delivery, biomedicine, cell culture technology and tissue engineering. **Table1** summarizes various modified polysaccharide-based drug delivery systems and their applications. These systems offer a range of benefits, such as improved drug release, targeted delivery, and enhanced therapeutic outcomes. Notable examples include alginate-based carriers for doxorubicin and ciprofloxacin, hydrogel beads for controlled drug delivery, and nanoparticles for cancer treatment and disease management [19].

These innovative systems hold promise for more effective drug delivery and medical treatments.

Table 1: Tabular presentation of modified polysaccharides and their applications in drug delivery

Modified Polysaccharide	Active compound	Delivery system	Benefit	Reference
Dual responsive alginate	Doxorubicin	Sulphydryl dendrimer	Smart stimuli responsive controlled drug delivery system ↑ anti tumor activity in HepG2 cells 76% drug release	[20]
Carboxylated graphene oxide impregnated alginate with aminated chitosan	Ciprofloxacin	Microbeads	Enhanced drug release Targeted drug delivery ↑ swelling behaviour pH responsive delivery of antibiotics	[21]
Psyllium moringa gum alginate	Ciprofloxacin	Hydrogel beads	Anti ulcer potential ↑ anti oxidative potential Slow and sustained drug delivery	[22]
Calcium alginate based sphere-in-capsule structure	Bovine serum albumin Ranitidine hydrochloride	Microspheres	↑ Drug encapsulation 95% ranitidine hydrochloride in simulated gastric fluid 73% BSA release in simulated intestinal fluid gastro retentive drug delivery system	[23]
Alginate in polycaprolactone Chitosan	Capsaicin	Nanoparticles in nanofibers	↑ Capsaicin release from 120 h to >500 h ↓ MCF-7 cells proliferation Non toxic to human dermal	[24]

<i>Modified Polysaccharide</i>	<i>Active compound</i>	<i>Delivery system</i>	<i>Benefit</i>	<i>Reference</i>
			fibroblasts ↑ anti cancer activity	
Floatable high amylose rice starch	Glycorrhizic acid	Floatable hybrid gels	↑ water holding capacity ↑ thermal stability ↑ gastro retentive potential	[25]
Soyabean meal resistant starch	NA	Nanoscale enteric coating	Colon targeted drug delivery ↑ growth of <i>Bifidobacterium brevis</i> and <i>Lactobacillus casei</i>	[26]
Hyaluronic acid coated chitosan	Cationic anti microbial peptide	Nanoparticles	Anti tumor activity Intracellular gene delivery	[27]
Self crosslinkable chitosan and hyaluronic acid dialdehyde	siRNA	Nanoparticle	CD44 targeting siRNA drug delivery Urinary bladder cancer prevention	[28]
Alginate coated chitosan	Enoxaparin	Microbeads	↑Drug loading capacity ↑Drug delivery to colon region 60% reduction in thrombus formation in vivo ↑ Bioavailability of enoxaparin 75% permeation to intestinal epithelium	[29]
Ac-Dex	Amphotericin B	Microparticles	↑parasitic clearance using combinational therapy ↓parasitic load in vitro	[30]
Injectable Ac-Dex microconfetti	Saquinavir	Electrospun fibres	Tunable drug release profile Effective against drug resistance in HIV ↑drug encapsulation	[31]
Hydrophilic adjuvant CpG	COBRA antigen HA antigen	Microparticles	Innate immune stimulation	[32]

Modified Polysaccharide	Active compound	Delivery system	Benefit	Reference
oligonucleotides with Ac-Dex				
pH sensitive Ac-Dex	Pyraclostrobin	Microparticles	↓ acute toxicity to zebra fish ↑ fungicidal activity against <i>S.sclerotiorum</i> plant disease management	[33]
Ac-Dex with PVA coating	Tobramycin	Dry powder inhaler	↑ mucus penetration ↑ shell life ↓ risk of contamination	[34]
Mast cell activating cells encapsulated in Ac-Dex	Viral protein	Microparticles	Enhanced protection against west Nile virus ↑ Vaccine delivery Degranulation & cytokine secretion in vitro	[35]
Drug loaded silk fibroin chitosan	Dexamethasone	Hydrogel beads	Extended drug release for 16 days Encapsulation efficiency 67% Targeted drug delivery	[36]
Disulphide bridged thiolated chitosan Eudragit RS 100	Moxifloxacin	Nanoparticles	Drug loading efficiency-100.3% Encapsulation efficiency-89.67% Drug release-88.49%	[37]
Chitosan HCl/guargum loaded eletriptan pullulan hydrobromide	Potaxamers PF-127/PF-68	Nanoparticles	↑ Nose to brain drug delivery ↑ Drug release profile 84% drug release in simulated gastric media for 48 h	[38]
Poly(2-ethy-2-oxazoline) & chitosan	Ciprofloxacin	Solid lipid nanoparticles	↓ burst release ↑ drug retention ↑ mucoadhesion	[39]

<i>Modified Polysaccharide</i>	<i>Active compound</i>	<i>Delivery system</i>	<i>Benefit</i>	<i>Reference</i>
			↑ corneal retention ↓ entrapment efficiency	
Redox responsive chitosan stearic acid	Doxorubicin & curcumin	Nanoparticles	↓ premature drug leakage 98% Doxorubicin release 96% curcumin release after 136 h under GSH conditions ↑ drug retention & enhanced biodistribution with C57bL/6 mice in colon for 24 h	[40]
Gelatin chitosan	Platelet rich fibrin chitosan	Hydrogel beads	↑ anti bacterial activity ↑ cell proliferation ↑ wound healing ↑ swelling behaviour Rapid wound closure Sustained protein release from wounds	[41]
Chitosan/hyaluronan	Methotrexate, 5 amino levulinic acid	Nanogels	↓ Proinflammatory cytokines: TNF- α , IL-17 A in imiquimod-induced psoriatic mice ↑ Transdermal drug penetration & retention in vivo & in vitro ↑ Apoptosis in lipopolysaccharide-irritated HaCaT cells Effective against psoriasis	[42]
Thiolated chitosan	Paclitaxel	Nanoparticle	98.27% drug encapsulation ↑ cytotoxicity against breast carcinoma cell lines (NIH 3T3, T47D) No cytotoxicity against colon cancer cell lines (HT29, Caco2)	[43]

<i>Modified Polysaccharide</i>	<i>Active compound</i>	<i>Delivery system</i>	<i>Benefit</i>	<i>Reference</i>
Pectin with hydroxy propyl β cyclodextrin	Honokiol	Self assembled Nanoparticle	↑ Enhanced cytotoxicity in HepG2 cells ↑ Apoptosis Enhanced drug release	[44]
Pectin chitosan conjugate	Cetuximab	Nanoparticle	Effective against colorectal cancer	[45]

NA: not available

Starch is a plant carbohydrate that is produced by plants through photosynthesis [46]. Native starch provides a desirable platform for the development of advanced drug delivery systems owing to its physiological benevolence, biodegradability, susceptibility toward enzymatic degradation depending on the amylose: amylopectin ratio and remarkable swelling behaviour [47]. Furthermore, Amylose, a component of starch has recently garnered great attention due to its unique structure, physiological benevolence, biocompatibility, hydrophobic interior and hydrophilic exterior for delivering various NSAIDs and anticancer drug molecules [48], however, its full utilization as a drug carrier is yet to be realized in the contemporary era. Particularly, its application as a carrier for NSAIDs such as Ibuprofen, Indomethacin, Flufenamic acid and Nimesulide, has only been explored in preliminary investigations [49]. Moreover, the assessment of V-amylose's impact on pharmacokinetic of NSAIDs is still in its early stages, with no ongoing clinical trials in progress. Controlled drug release achieved through V-amylose delivery systems could potentially reduce the effective therapeutic dose and frequency of drug administration, but limited research exists on optimizing drug doses when using V-amylose as a carrier. Therefore, it becomes imperative to investigate and explore the versatility and physicochemical aspects of V Amylose in encapsulating fenamates, a class of NSAIDs and deliver them in a controlled and sustained manner with respect to simulated physiological conditions of stomach and intestines. Fenamates have wide implications in

management of pain, inflammation and fever associated with various rheumatic conditions and aid in management of menstrual cramps. However, the gastrointestinal toxicity generally in the form of ulcers and bleeding associated with their use limits their utility. Our aim is to deliver fenamates (Flufenamic acid, Mefenamic acid, Maclofenamic acid and Tolfenamic acid) in an effective and safer way and achieve a controlled and sustained release of drugs only in presence of a pH and colonic enzymes that specifically cleave the glycosidic linkage of amylose.

Formulating a mathematical model for drug release prediction in the field of controlled drug delivery is a meticulous but prolific task for formulation scientists. Because a solid mathematical model can predict outcomes and fewer experiments are needed to reach a conclusion. Furthermore, these approximations assist in the preparation of more effective studies to avoid wasting time or money. Many attempts have been made to date to provide a mathematical description of drug release [50]. However, these models were not appropriate for widespread usage and either did not cover the entire drug delivery region or were made for extremely rare special systems. As a result, they are unable to provide precise results, and some of them are too complicated to use in the drug release data. Legendary scientist Takeru Higuchi published his seminal work on drug distribution mathematical modelling in 1961 [51]. The accurate design of novel drug formulations and dosages was made possible by the application of established mathematical models as well as the creation of new ones. The evolution of mathematical models that concurrently integrate theories explaining drug release phenomena and the impact on pharmaceuticals during transit to the human body is currently the major concern for formulation scientists. Moreover, the task of defining models that both account for the diffusion phenomena and the cell uptake response is not straightforward. But because of its immense potential, this field of study is constantly evolving, particularly from an industrial standpoint.

Polymeric systems have been utilised in the pharmaceutical industry for many years, particularly in the provision of controlled drug release [52]. Drug polymer systems might be helpful in preventing biological deterioration of the drug before it is released. Before moving on to the use of biodegradable polymers, where swelling and erosion occur, the development of these devices began with the use of non-biodegradable polymers, which depend on the diffusion process. The following three primary processes (systems) can be used to categorize the drug release mechanism from a polymer matrix based on the physical or chemical properties of the polymer:

1. Diffusion of the drug from the non-degraded polymer (system with diffusion control).
2. Polymer swelling-induced enhanced drug diffusion (swelling-controlled mechanism).
3. Drug release as a result of erosion and polymer degradation (erosion-controlled system).

There is always diffusion at play in these three systems. Drug release in a non-biodegradable polymer matrix result from either matrix swelling (increased diffusion) or a concentration gradient caused by diffusion. In the case of biodegradable polymer matrix, diffusion may still be predominant when erosion occurs slowly, but release is typically governed by the hydrolytic breakage of polymer chains that results in matrix erosion [53]. This classification enables the development of mathematical models for various drug delivery system types in various ways. Drug release mathematical modelling sheds light on the chemical reactions and mass movement that take place in drug delivery systems as well as the impact of design variables such as drug loading and device shape on drug release mechanism [54]. As a result, a systematic technique with a minimal number of experimental trials can be used to anticipate the optimal device design for a specific drug release profile.

1.4. Research motivation and objectives

Burst release of NSAIDs in the gut causes the erosion of protective mucosal layer that result in the development of ulcers. Mainly, the burst release increases the local drug concentration at

the deliberated tissue beyond its therapeutic dose, which further enhances its physiological toxicity [21]. The controlled drug delivery systems achieve a sustained drug release, which maintains the optimal therapeutic dose to the morbid cells. A prolonged release profile achieved by these systems ensure the drug release over an extended time, which produces a long-term therapeutic effect, while lowering the effective concentration required in order to achieve the relieving effect.

V Amylose serves as potential drug delivery system for mitigating the side effects of contemporary NSAIDs and for improving the drug pharmacokinetics in order to achieve an optimal therapeutic effect. The controlled release profile minimizes the therapeutic dose of the cargo drug, which further improves its therapeutic effect [55]. We plan to study V-Amylose as a drug delivery vehicle for the intestine targeted delivery of fenamates, where a better drug absorption occurs, while bypassing the acidic pH of stomach microenvironment. Fenamates, owing to their burst release mark the onset of ulcerogenicity in the gut mucosa. The application of a favorable controlled delivery system mitigates the ulcerogenicity index, and achieve a sustained release of the drug for a prolonged relieving effect. Unlike other polysaccharides, V-Amylose display stability towards enzymatic degradation, which supports its controlled release profile. The *in vitro* release profile of Flufenamic acid by V-amylose in the simulated intestine media evidenced these observations as a novel drug delivery system. Importantly, the ability to carry both hydrophobic and hydrophilic drugs further support delivery applications of a variety of pharmaceuticals by V-amylose. The novelty and advantageous features of the proposed drug delivery system have been summarized in **Table2**.

Table 2: Potential advantages and novelty of proposed drug delivery system

Properties	Advantages
Naturally occurring	V amylose is naturally synthesized in plants and hence easily available and economically

	convenient as compared to the synthetic polymers used to deliver NSAIDs and other drugs to GI system [56]. This also promotes non toxicity and non-immunogenicity to targeted cells and neighbouring cells
Slow degradation	Owing to unique helical structure, V Amylose resist degradation and hydrolysis in presence of gastric enzymes such as amylase as compared to other counterparts which precipitates easily. This feature renders V Amylose distinct as it promotes sustained and controlled delivery of a variety of therapeutics to colon for enhanced effect with reduced biodegradability and reduced occurrence of burst effect and ulcerogenicity in intestines [57].
Mucoadhesive	The ease of chemical modification to the backbone of V Amylose rendering it cationic, makes it an ideal mucoadhesive candidate for adhering to the negatively charged mucus layer owing to the presence of primary and secondary amino groups [58]. The mucoadhesion promotes enhanced residence time of drugs to intestines and ensures controlled delivery of an active pharmaceutical agent to bloodstream.

Hence, the objectives of the present thesis are as follows:

1. To study the potential of V Amylose as a drug carrier under simulated physiological conditions
2. To investigate the release profile of V amylose from solid dosage formulation based on high amylose starch for fenamic acid NSAIDs

3. To design magnetically guided drug delivery system with V Amylose fenamic acid complex

Chapter 2: Literature review

In the domain of advanced drug delivery systems, the utilization of modified polysaccharides has yielded intricate formulations with reinforced therapeutic efficacy. The integration of dual-responsive alginate with sulfhydryl dendrimer resulted in a sophisticated smart stimuli-responsive controlled drug delivery system for doxorubicin, leading to a notable augmentation in anti-tumor activity as observed in HepG2 cells, coupled with a substantial 76% drug release [20]. Carboxylated graphene oxide impregnated in alginate, in conjunction with aminated chitosan, produced microbeads characterized by increased drug release, targeted drug delivery, and an enhanced swelling behavior, particularly advantageous for pH-responsive antibiotic delivery [21]. Hydrogel beads fashioned from Psyllium moringa gum alginate demonstrate commendable anti-ulcer potential, anti-oxidative prowess, and a proclivity for slow and sustained drug delivery [22]. In parallel, calcium alginate-based microspheres, incorporating bovine serum albumin and ranitidine hydrochloride, manifest an elevated drug encapsulation rate, with 95% ranitidine release in simulated gastric fluid and 73% bovine serum albumin (BSA) release in simulated intestinal fluid, underscoring their utility as a gastro-retentive drug delivery system [23]. These innovative formulations, spanning various nano and micro-scale carriers, exhibit promising attributes such as targeted drug delivery, prolonged drug release kinetics, and enhanced therapeutic efficacy portrayed their potential across diverse biomedical applications.

The pharmaceutical industry has a long history of using starch and its derivatives for drug delivery and tablet formulations. The physiological benevolence, biodegradability, vulnerability to enzymatic breakdown based on the amylose: amylopectin ratio, biocompatibility and extraordinary swelling behaviour make it a desirable candidate for the development of advanced drug-delivery systems [47]. Furthermore, Amylose has recently garnered great attention due to its tightly packed helical structure, biocompatibility,

hydrophobic interior and hydrophilic exterior for delivering various NSAIDs and anti cancer drug molecules [48]. The multiple advantages of combinational chemotherapy using amylose such as tumor shrinkage, less toxicity, increased response rate and targeted treatment has been extensively studied using anticancer drugs. The synergistic action of Curcumin and Doxorubicin inclusion complexes inside the hydrophobic cavity of Amylose demonstrated enhanced therapeutic effect, trivial enzymatic degradation, and minimal drug resistance [59]. Amylose when modified with synthetic polymer such as PMMA via ATRP technique induced switchable hydrophilicity and enhanced drug complexing ability [60]. Furthermore polysaccharide-capped metal nanoparticles with special reference to Amylose have been reported by Prasher et al [61] for delivery of antibiotics and anticancer drugs which possess poor availability and degrade easily due to cellular microbial efflux. Acetylation adds ester groups to starch, making it more functional, less toxic, and more stable and produce low, medium, and high degree of substitution starch relevant to controlled drug delivery systems [62]. Several studies have reported the acetylation of starch and amylose to be more beneficial than other chemical modification techniques as it improves starch retrogradability and water solubility. Najafi et al [63] synthesized *in vitro* acetylated corn starch by varying the degree of substitution to deliver the antibiotic, Ciprofloxacin for treating respiratory, urinary, corneal and gonococcal infections and demonstrated enhanced drug entrapment efficiency from 67.7 to 89.1 percent thus preventing the premature drug release with reduced toxicity. Acetylation and oxidation processes are known to impart stability to high amylose starch and ascorbyl palmitate complexes in aqueous solutions which have immense application in oral formulations and targeted delivery [64]. Moreover, where ethylation reported hydroxyl group substitution with carboxymethyl, hydroxypropyl or hydroxyethyl group, carboxyl methylated starches are extensively used as disintegrants in drug delivery due to their increased sensitivity to pH.

Chemically modified starch has also been investigated to modulate molecular pathway in cells depending on the type and degree of modification, as well as the cell or tissue type involved. These pathways are involved in various cellular processes and have been linked to several diseases, including metabolic disorders, inflammation, and cancer. Dialdehyde starch (DAS) and its derivatives have been known for inherent anti-viral, anti-inflammatory and anti-neoplastic properties. The drug dialdehyde starch nanoparticle in conjunction with 5-Fluorouracil reported significant inhibition of MCF-7 cell proliferation and reduced tumor weight *in vivo* [65]. The complex arrested various phases of cell cycle and induced necrosis in cultured cells owing to the presence of two aldehyde groups that conjugated with the imine groups in 5-Fluorouracil making it a versatile and non toxic carrier for anti cancer therapy.

2.1. Necessity of mucoadhesive drug delivery vehicles

Mucus acts as a physiological barrier against foreign agents to the underlying organs and tissues. Essentially, the permeability of the mucus mesh is controlled by interaction filtering and size filtering mechanisms, and its varied spacing spans from 20 to 1800 nm across various organs [66]. Smaller particles can pass through the mesh while the larger molecules are retained by the size filtering effect. Positively charged molecules stick to the negatively charged mucus layer, whereas similarly charged molecules neither stick to nor penetrate the mucus layer; this is why the interaction filtering mechanisms enable neutral molecules get through. The mucus layer which is generally negatively charged due to COOH and SO₄²⁻ functional groups on mucin, govern the mucoadhesive/muco-penetration capacity of logically constructed drug delivery systems [67]. The fact that drug distribution across the alveolar mucosa resists mucociliary clearance further posits challenge to drug pharmacokinetics necessitating the maintenance of an optimum therapeutic dosage. Also, in order to retain the best possible therapeutic impact, these elements require higher dosage frequencies, which may make patient compliance more difficult. The primary function of cationic polysaccharides such as chitosan

is to increase the bioadherence of the parent polymer to the physiological mucus barrier by either quaternizing NH_2 groups or chemically modifying OH groups to NH_2 and NH functionalities (**Fig 1**). Through their ability to stick to the mucus mesh and interact with its components mostly through hydrogen bonding and electrostatic forces, the cationic polysaccharides primarily aid in mucoadhesive drug delivery to the morbid cells beneath the mucus layer [68].

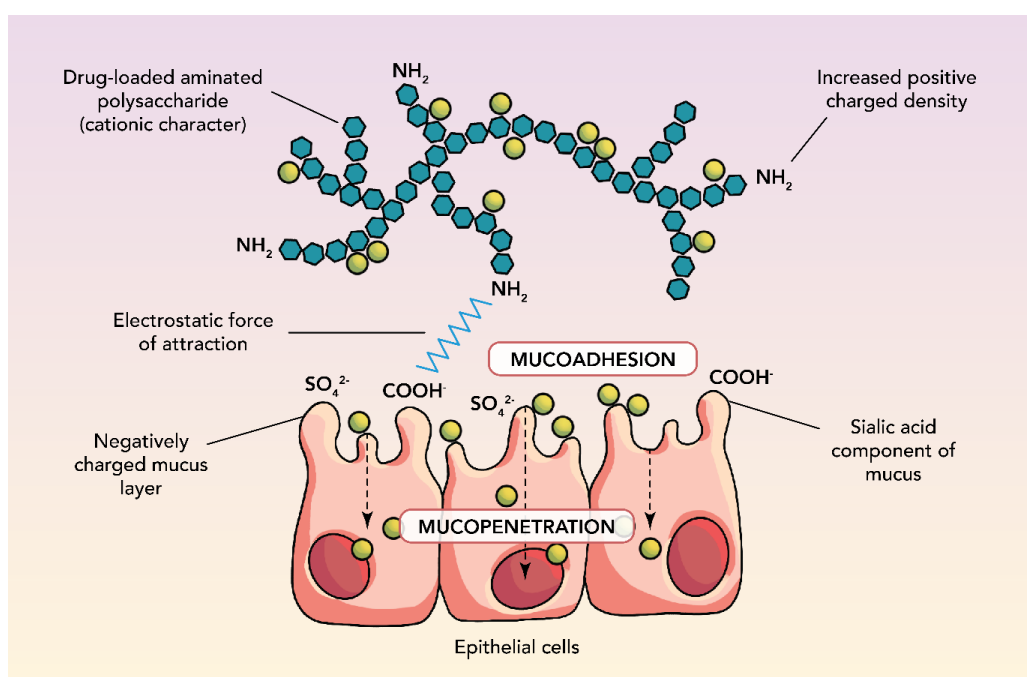


Figure 1: Mucoadhesive drug delivery (Adapted from Reference [69])

The delivery of therapeutics to mucosal tissue such as sublingual, buccal, nasal, vaginal, ocular and rectal mainly result in bypassing the first pass metabolism for successfully delivering the drugs. To enhance mucoadhesion to cellular membranes of such sites and to extend the residence time of most drugs, the local cationic charge on the surface of starches can be altered. There have been very few studies that have used diaminated or cationic starch to achieve a sustained drug release effect. In this regard Nouri et al [70] developed a cationic polysaccharide-based drug delivery system in which primary and secondary amines were introduced into the backbone of starch, resulting in an increased solubility and

mucoadhesiveness. Moreover, Jelkmann et al [71] demonstrated an improved mucoadhesion delivery system using starch as an alternative to chitosan, where amino groups when added to starch resulted in enhanced intestinal residence time than native starch or chitosan. The incorporation of amine linkages onto polysaccharides imparts versatility, significantly expanding their applicability in pharmaceutical domains while their modification facilitated drug delivery systems to meet specific therapeutic requirements, including tumor-targeted or stimuli-responsive drug release. Naturally occurring polysaccharides possessing amine linkages, such as hyaluronic acid or chitosan, demonstrated outstanding biocompatibility and biodegradability for diverse biomedical applications [72].

2.2. Status of the cationic starch for mucosal drug delivery

Comparing chemically modified starch to chitosan, the addition of NH_2 and NH groups at its OH group demonstrated significant diamination and enhanced hydrophilicity and mucoadhesion. 4-toluenesulfonyl chloride and triethylamine for 12 hours at 5°C generated diaminated starch. When starch's OH groups are chemically modified to create diaminated starch, which has both NH_2 and NH groups, the observed retention time on mucosa was ten times longer than it was with chitosan and had better water solubility and mucoadhesion at physiological pH [70]. Compared to chitosan, which protonates only at the NH_2 group at the same pH, the diaminated starch's mucoadhesive potential was further mitigated by the protonation of both the NH_2 and NH groups at an acidic pH. On the other hand, diaminated starch is protonated at the NH_2 group at neutral pH, which enabled pH-responsiveness of the cationic starch's surface charge, resulting in a noticeable mucoadhesive pH-responsive smart drug delivery system. Unlike chitosan, which only showed solubility at acidic pH, the diaminated starch demonstrated solubility over acidic, neutral, and basic pH. Due to the protonation of the NH_2 and NH groups, the diaminated starch showed a characteristic swelling behaviour and water permeability at acidic pH 1.2, resulting in a 53-fold increase in the initial

weight. A 30-fold increase in weight was seen at pH 3, and an 18-fold increase was seen at pH 5. A slight swelling of diaminated starch occurred as the pH got closer to the neutral values of 6.8 and 7.4 suggesting that the diaminated starch degraded gradually and retained water. Additionally, the total work of adhesion (TWA) and maximum detachment force (MDF) exhibited higher tensile strength and elasticity, further validating its use as a mucoadhesive material. Comparing the monoaminated counterpart with NH_2 to chitosan, it showed better mucoadhesion and water solubility, similar to diaminated starch [71].

Small interfering RNA (siRNA) is a key tool in therapies as it uses the natural RNA interference (RNAi) pathway to specifically target and silence genes that cause disease. RNAi has significant implications for precision medicine, targeted validation in drug discovery, and gene function investigations. The development of a reliable and effective siRNA delivery method is still a hurdle and, in this context, cationic starch (Q-starch) was developed by quaternizing potato starch with CHMAC to entrap negatively charged siRNA [73]. This demonstrated that siRNA effectively bind to amine groups on Q-starch by self-assembly, regardless of the pH of the surrounding environment. Upon complexing with a siRNA-based carrier, a particular size and charge are crucial for the intended gene or drug to be transfected successfully. Here, a modest diameter (~30 nm) and a positive surface charge were observed, protecting the siRNA against enzymatic attack. Additionally, the siRNA/Q starch complex showed efficient P-glycoprotein (P-gp) gene silencing in ovarian cancer cell line manifesting low cytotoxicity.

2.3. Limitations of NSAIDs

NSAIDs serve as extensively prescribed therapeutic agents for the chronic management of rheumatic and arthritic conditions. These compounds act as inhibitors of cyclooxygenase 1/2 (COX1/2) and include salicylates, oxicams, sulfonanilides, acid derivatives and selective COX-2 inhibitors (Coxibs) [74]. It is imperative to realize that the utilization of NSAIDs is associated with potential upper gastrointestinal (GI) complications, ranging from mild

dyspepsia to more severe outcomes such as hemorrhage, ulceration, and even perforation of the gastric or intestinal walls along with perturbed physiological molecular pathways (**Table 3**). Fenamates are a subgroup of NSAIDs, derived from a fenamic acid core structure and share intrinsic pharmacological traits as organic acids, predominantly characterized by a pKa value typically falling within the pH range of 3 to 5 and include Mefenamic acid, Tolfenamic acid, Flufenamic acid and Maclofenamic acid. Generally, fenamates include an acidic functional group, notably carboxylic acid or enol and is attached to an aromatic, planar moiety covalently linked to a lipophilic segment through a polar moiety, playing a crucial role in mediating their cyclooxygenase inhibitory activity [75]. Fenamates exhibit robust analgesic, antipyretic and anti-inflammatory properties, making them valuable in treating rheumatic disorders [76]. At physiological pH levels, fenamates are >99% ionised and are primarily removed in the urine through hydroxylation and glutamate conjugation within 3- 4 hours. To enhance the systemic bioavailability of fenamates, it is often desirable to escalate the dosage and dosing frequency potentiating the incidence of gastrointestinal ulcers and bleeding. To mitigate these complications, fenamates are frequently administered in the form of enteric coatings or as solid dosage formulations. This strategy facilitates the achievement of therapeutic objectives with a single dose, ensuring controlled and sustained release of the therapeutic compound, while circumventing the need for multiple administrations.

Table 3: Toxicity and molecular pathways affected with NSAIDs.

NSAID	Brand name	FDA approval status	Cell line/ animal used	Adverse effect/Toxicity	Biomarker affected	Reference
Mefenamic acid	Ponstel	approved	HepG ₂	Oxidative stress	↑SOD, ↑H ₂ O ₂ , ↑PC, ↑AOPP	[77]

NSAID	Brand name	FDA approval status	Cell line/ animal used	Adverse effect/Toxicity	Biomarker affected	Reference
Indomethacin	Tivorbex	approved	Rats	Hemorrhagic lesion on small intestine	↑COX 2, ↓PGE2	[78]
Mefanamic acid	Ponstel	approved	Hep G ₂	Oxidative stress	↑SQSTM1, ↑Nrf2, ↓Keap1	[79]
Celecoxib, Ibuprofen, Diclofenac, Flufenamic acid, Maclofenamic acid, Mefanamic acid	Celebrex, Advil, Arlef, Meclomen, Ponstel	approved	Immortalized mouse bone marrow-derived macrophages (iBMDMs)	Inhibition of Cl ⁻ channels in macrophages	↓NLRP3 inflammasome, ↓VRAC, ↓IL-1β, ↓TRPM2, ↓ASC protein, ↑Caspase 1	[80]
Mefanamic Acid, Maclofenamic acid, Niflumic acid, and Flufenamic acid	Ponstel, Meclomen, Donalgin, Arlef	approved	cultured embryonic rat hippocampal neurons	Neuroprotective efficacy against glutamate induced excitotoxicity	↓ROS, ↓NO accumulation, ↓mitochondrial cytochrome c, ↑BCL XI, Minimum cell death	[81]
Indomethacin	Tivorbex	approved	RGM1 cells	Enhance surviving degradation by ubiquitin	↓survivin, ↑TNF α	[82]

NSAID	Brand name	FDA approval status	Cell line/ animal used	Adverse effect/Toxicity	Biomarker affected	Reference
				proteasome machinery in gastric epithelial cell injury	↑ cell injury and apoptosis	
Aspirin alongwith TRAIL	Bayer	approved	Human prostate adenocarcinoma LNCaP and DU-145 cell lines, human colorectal carcinoma CX-1 cell line, and normal prostate YPEN cell line w	Activation of effector caspases related to mitochondrial apoptosis	↓ AKT NF kB, ↓ IKK B, ↑ caspase 3,6,7 ↓ BCL 2	[83]
Aspirin	Bayer	approved	human gastric epithelial cell line (AGS)	Cytochrome c release and activation of caspases 9.	↑ caspase 8,9, ↑ Bax, Bid, SMAC, ↑ cytochrome c	[84]
Celecoxib alongwith dimethyl celexib	Celebrex	approved	LN229, U251, T98G, U87 (glioblastoma), HCT116,		↓ survivin, induce apoptosis, ↑ caspases	[85]

NSAID	Brand name	FDA approval status	Cell line/ animal used	Adverse effect/Toxicity	Biomarker affected	Reference
			DLD1 (colorectal carcinoma), Raji (Burkitt's Lymphoma), T47D, MCF7 (breast carcinoma), Mia Pa Ca 2, BxPc 3 (Pancreatic carcinoma), A549 (lung carcinoma),			
Tolfenamic acid	Clotam	approved	Hep G2, HeLa cells, PC	Inhibition of VEGFR-2 tyrosine kinase in solid tumors, high docking score (ΔG) in VEGFR-2.	\uparrow caspase 4, caspase 8, \downarrow VEGFR 2, \downarrow cell cycle progression via inhibition at G2/M phase	[86]

A class of non-steroidal anti-inflammatory drugs known as fenamates includes commercially available members such as Tolfenamic acid, Flufenamic acid, Mefenamic acid, and Maclofenamic acid, all produced from fenamic acid (**Fig 2**) [87]. Flufenamic acid (FFA), (also known as 2-[3-(trifluoromethyl)anilino]benzoic acid), is an aromatic amino acid comprising anthranilic acid

with an *N*-(trifluoromethyl)phenyl substituent exhibiting IC₅₀ values of 3 μM and 9.3 μM for human COX-1 and COX-2, respectively [88]. Its anti-inflammatory and analgesic properties were acknowledged in the 1960s however, enhanced gastrointestinal side effects such as ulceration and bleeding associated with its chronic pathological use restricts its usage in humans [89]. In human polymorphonuclear leukocytes, flufenamic acid demonstrated inhibition of calcium influx induced by fMLP (formyl-methionyl-leucyl-phenylalanine), with IC₅₀ values of 29 μM and 14 μM [90]. Furthermore, flufenamic acid inhibited the activity of cystic fibrosis transmembrane conductance regulator (CFTR) and activated large-conductance calcium-activated potassium channel and transient receptor potential canonical 6 (TRPC6). This compound also effectively hindered TNF-α-induced elevation in COX-2 levels and NF-κB activation in HT-29 colon cancer cells in a concentration-dependent way [91].

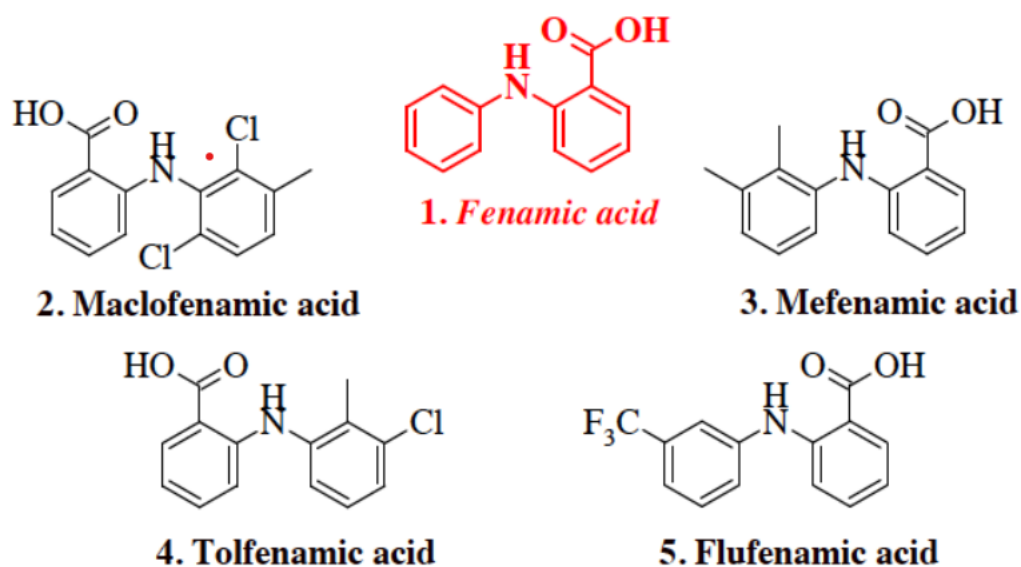


Figure 2: Commercialized members of 1. fenamic acid-derived NSAIDs 2. Meclofenamic acid, 3. Mefenamic acid, 4. Tolfenamic acid, 5. Flufenamic acid

The enzyme cyclooxygenase exists in two isoforms, COX-1 and COX-2, each fulfilling its discrete role. COX-1 is generally constitutively expressed and assumes a pivotal function in safeguarding the gastric mucosa through the synthesis of prostaglandins. In addition to being involved in the synthesis of prostaglandins, COX-1 is essential for physiological platelet

activation, GI tract mucosal protection, and renal function maintenance. On the other hand, the inflammatory response triggers the production of COX-2, inhibiting smooth cell growth, platelet suppression, and vasodilation.

The primary cause of NSAID-induced ulcer is the suppression of COX-1, which perturbs the regular defence mechanism of gastric mucosa [92]. Gastrointestinal complications attributed to NSAID use stem primarily from three distinct mechanisms: the inhibition of COX-1 enzyme and gastroprotective prostaglandins, alterations in membrane permeability, and the generation of supplementary proinflammatory mediators. To ameliorate the gastrointestinal disturbances associated with the inhibition of COX-1, COX-2 selective NSAIDs were developed manifesting adverse cardiovascular events [93]. The prevailing trend in NSAID development primarily focuses on enhancing therapeutic efficacy and mitigating upper GI side effects by modifying dosage forms to optimize drug delivery. These formulations are engineered to improve patient compliance through prolonged therapeutic effect and reduce adverse effect by lowering peak plasma concentrations. Polysaccharides exhibit a notable potential as a prospective advanced drug delivery system, attributed to their biodegradability, biocompatibility, and controlled/sustained release kinetics which further endorse the pharmacokinetics and maintains an optimal drug concentration across the physiological mucus barrier.

2.4. V-amylose characteristics

V-amylose demonstrates a unique structural composition, consisting of a hydrophobic helical core and a hydrophilic exterior, making it an attractive option for the targeted delivery of various pharmaceutical molecules [94]. Specifically, in oral drug delivery, encapsulating the drug within the V-amylose helix enhanced its resistance to acidic hydrolysis, leading to controlled release in the colon through enzymatic stimulation improving the tolerability of drug molecules that may have toxic effects during burst release. The drug molecules and amylose

combine to form inclusion complexes in which the former caused the latter to undergo a conformational change resulting in a compact helical shape with a hydrophobic interior and a hydrophilic outside. A single chain helix of amylose is stabilised by van der Waals interactions and intramolecular hydrogen bonding between the helical turns, whereas the bonds between the amylose and drug are stabilised by intramolecular forces. The hydrophilic exterior of helical amylose is formed by glycosyl OH groups, while the hydrophobic cavity of the polymer is made up of 1,4-glycosidic linkages and methylene groups broadening its ability to wrap different therapeutic molecules. The small intestine's α -amylase further acts as a catalyst for the breakdown of drug amylose conjugate and release the encapsulated drug subsequently. The rate at which amylose hydrolyzes determines the drug release and can be controlled or sustained over an extended period. But unlike amylopectin, which has additional 1,6-glycosidic linkages with highly branched structure and a greater surface area for the activity of enzymes, helical amylose has a limited rate of enzymatic hydrolysis in the small intestine due to its linear 1,4-glycosidic linkages. The amylose-to-amylopectin ratios of starch vary depending on the biological sources from which it is derived. Its processing simplicity and efficacy as an oral drug delivery vehicle are constrained by low shear stress resistance, poor aqueous/organic solubility, and poor gastrointestinal digestion. Amylose-to-amylopectin ratio is the primary factor that is changed when starch composition is modified by genetic engineering. Acetylation reduced the ability of starch to be digested by enzymes and to dissolve in water but at low pHs, carboxymethylation rendered starch acid-insoluble and aggregative. The overall effects included sustained the drug release in the upper intestine (**Fig 3**). The drug release from carboxymethylated starch that is acid-insoluble can be further decreased by aminating it to give it the ionic character needed to create hydrogels. Ionic starch indeed manifested insoluble, controlled-release complexes with drugs, non-starch polyelectrolytes, and oppositely charged starches [95].

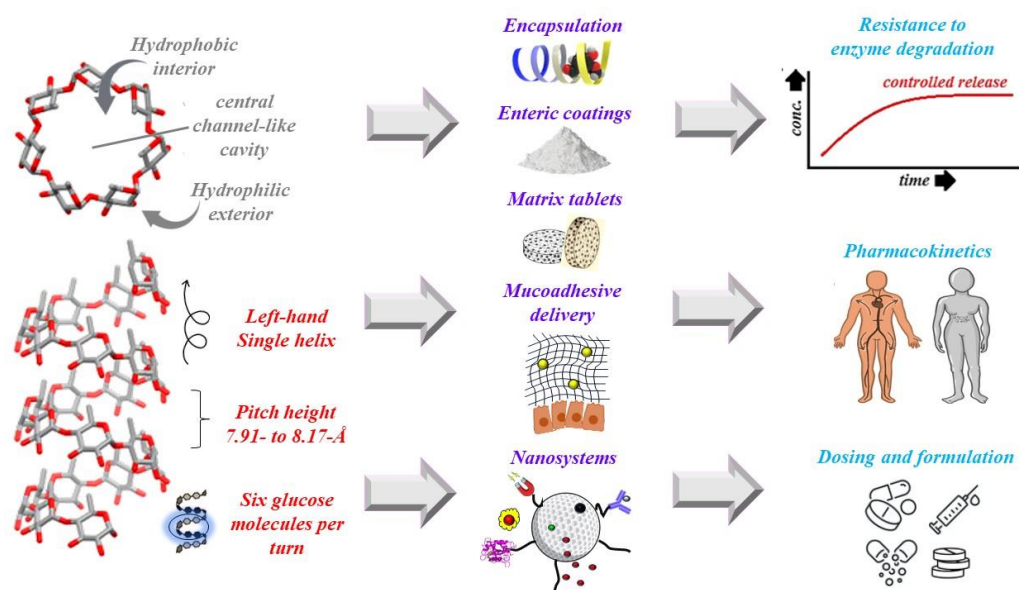


Figure 3: Applicability of Amylose in the contemporary drug delivery paradigm.

2.5. V Amylose drug complexes

V-amylose's enzymatic hydrolysis resulted in a delayed release, which is achieved by complexing it with Ibuprofen to reduce the drug's gastrointestinal side effects. When compared to the simulated gastric medium (pH 1.2) and the simulated small intestinal medium (pH 7.2), the Ibuprofen V-amylose inclusion complexes showed remarkable stability which eventually explained the gradual drug releases in the test media [96]. Further reducing the drug's effective therapeutic dosage, potential toxicity was provided by the V-amylose-ibuprofen complex. The system demonstrated only 5.5% release of the drug present in the complexes in simulated gastric medium, according to the in vitro assay used to evaluate the drug release behaviour of the inclusion complex, indicating it remarkable stability. In a manner similar to the small intestine model, these complexes demonstrated a sustained and complete release of the drug cargo in order to attain the best possible therapeutic response. Moreover, the medium's amylase content caused the complex to biodegrade, which in turn caused Ibuprofen to release gradually over the course of 8-12 hours [97]. Mainly, the ibuprofen molecules were encapsulated in the 5.4 Å diameter and 8 Å pitch height of internal hydrophobic cavity of V amylose to create

flexible helices and persistent inclusion complexes preventing the premature drug leakage from the hydrophobic cavity.

Indomethacin's release profile was ameliorated at pH 12, where the solubility reached its peak, escalating the drug's hydrolysis and resulting in the loss of 5-methoxy-2-methylindole-3-acetic acid and p-chloro benzoic acid moieties, which degraded the molecule. An innovative drug delivery system that relies on enzymes was developed when indomethacin and amylose were chemically conjugated using ester linkage, *N, N*-dicyclohexylcarbodiimide (DCC) coupling agent, and 4-(*N,N*-dimethylamino) pyridine (DMAP) catalyst [98]. Better water absorption efficiency in the conjugates with less indomethacin concentration triggered the activity and diffusion of hydrolyzing enzymes to the swollen conjugates. This characteristic promoted the amylose-indomethacin conjugates' biodegradation, resulting in a prolonged release of the conjugated drug molecules in the intestines' simulated media. At the same time, the conjugation showed a negligible drug release in the gastric fluid. Less than 2% of the drug was released by the conjugates in simulated gastric fluid after 90 minutes at 37°C. In contrast, the drug was gradually released during the 180-minute incubation period in the simulated intestinal media. Principally, when incubated in the colonic fermenter, it produced a 65% release in 36 hours, indicating a prolonged and sustained release for intestinal targeting. Indomethacin and V-amylose formed trivial complex as the drug molecules physically trap in the matrix of amylose instead of the helical hydrophobic cavity. The absence of indomethacin within the helix of V-amylose however limited the effectiveness of the drug's targeted release in the intestine and promoted early release in the stomach's acidic pH.

By physically fitting inside the helical cavity, bulkier nutraceuticals like "genistein" reported the formation of inclusion complexes with V-amylose. The complex aggregated as a result of hydrophobic interactions between V-amylose and genistein in the stomach's acidic environment and released less than 15% of the drug suggesting a discernible stability in these circumstances.

The regulated release of genistein molecules at the intended site in the digestive system in the presence of hydrolyzing gut enzymes was validated by the stability in acidic pH, which prevented the molecules from releasing prematurely in the gastric area. It's interesting to note that these compounds showed exceptional stability at 30°C and 50°C across a pH range of 4 to 8 [99]. The releasing behaviour was further enhanced by the additional pH rise, primarily as a result of their partial breakdown in alkaline environments. The partial charge that V-amylose and genistein acquire on their surfaces decreased the interactions between them and enhanced their interactions with the surrounding water molecules accelerating free genistein in the solution

An acceptable substitute for the controlled administration of Quercetin is V-amylose. The B aromatic ring in the quercetin molecule changes conformation to a more ordered state when it was encapsulated in V-amylose through hydrophobic and hydrogen-bonding with V-amylose via carbonyl (C=O) and OH groups. In simulated stomach settings, the V-amylose–quercetin complex showed a significant retention of the latter; however, in simulated small intestine conditions, the release rate gradually increased in the presence of pancreatin, reaching a maximum at 97% after 8 hours [100]. The V-amylose inclusion complexes with "nimesulide" and "praziquantel" is an excellent rationale for accomplishing site-specific drug release. The drug molecules that were encapsulated were released in an enzyme-sensitive manner as a result of the system's pH-dependent behaviour in absorbing nearby water molecules. At acidic pH levels, the protonation of polar head groups decreased electrostatic repulsion, which in turn decreased the absorption of water molecules [101]. On the other hand, at higher pH levels, the hydrophobic drug molecules that are present on the surface of these complexes were formed into crystalline structures by the ionisation of the polar head groups. These complexes' increased electrostatic repulsions, encourage the absorption of nearby water molecules and promoted delayed drug release [102]. Mainly, the V-amylose drug complexes conferred a

modest release profile in phosphate buffer (6.9) and acidic pH (1.2), however the drug release rate improved when pancreatin enzyme was specifically included.

2.6. Amylose as enteric coated and sustained release vehicle

The use of sustained release (SR) vehicles and enteric coatings (EC) in NSAIDs dosage improve their physiological tolerance by facilitating a controlled drug release rather than burst release preventing toxicity to gastric mucosa that may occur due to a rapid increase in drug concentration. The osmotically triggered slow-release version of indomethacin, which is no longer marketed, has been linked to distal side effects such as perforating colonic and ileal ulcers when used with sustained-release NSAIDs [103].

Under optimal conditions, the gelation of V-amylose yield films that exhibited remarkable resistance against pancreatic α -amylase, but gradually deteriorated when colonic microflora amylases were present. Enteric coatings made of amylose quickly swelled in gastrointestinal simulators, creating porosity and allowing drug molecules to be released from their capsules. By adding insoluble polymers like ethylcellulose to the amylose film, V-amylose's swelling characteristics were improved, which in turn improved its drug release profile [104]. The anti-inflammatory mesalazine or 5-aminosalicylic acid showed remarkable resistance to the simulated gastric and small intestinal conditions when V-amylose-ethylcellulose was coated in a 1:4 ratio preventing any drug release for 24 hours. It has been found that ethylcellulose inhibited V-amylose swelling, which ultimately delayed the drug release from the coating. However, after being added to the fermenter, the V-amylose-ethylcellulose coated 5-aminosalicylic acid released more quickly between two and five hours, and displayed eight hours for the complete release of mesalazine [105].

After two hours at 37°C, mathematical modelling of the release kinetics of antibacterial and antineoplastic limonene molecules from the V-amylose revealed exceptional resilience towards acidic environment. In six hours, the system demonstrated a controlled, delayed drug release,

increasing gradually from 34% to 79% in small intestine-simulated medium. When compared to the "Peppas model," the release pattern of limonene from V-amylose showed the highest determination coefficient, whereas the fuzzy logical intelligent modelling showed a coefficient of determination larger than 0.99. With a greater success rate than traditional experimental methods, the mathematical simulations effectively stimulated the adoption of strategies for modelling the controlled release trend of encapsulated limonene molecule and comparable nutraceuticals from V-amylose [106].

The delivery of NSAIDs to the intestines using resistant starch further exhibited considerable potential by limiting early release in the acidic environment of the upper gastrointestinal system to achieve a localised effect. Through the action of pancreatic amylase, resistant starch is only minimally broken down in the small intestine. Consequently, resistant starch containing a high percentage of amylose surpasses the small intestine's enzymatic hydrolysis and enable gut-microbiota based colon-targeted drug release [107]. The trigger mechanisms for the delayed drug release are conspicuous to the contemporary innovations such as phloral coating technology and include the microbiota trigger based on the resistant starch V-amylose and the pH trigger based on Eudragit S, which dissolves in intestinal fluid. Thus, this coating technology offered a fail-safe method for cargo drugs to be released colonically. It's noteworthy that the integrity of the coating in the upper GI tract and Eudragit S remain unaffected with resistant-starch coating [108]. Likewise, the unique OPTICORE technology presented the accelerated release as the duocoat present in the inner layers when combined with the Phloral triggered mechanism in the outer layer, quickly released drug particularly due to isolation layer separating the inner layer and the core. In essence, when the pH of the luminal fluid deviates from neutral, the presence of a Phloral outer coating facilitated enhanced drug release. Consequently, OPTICORE technology enabled specific drug delivery to the colon region for patients suffering from ulcerative colitis [109].

2.7. Amylose based solid dosage formulation for controlled drug delivery

Matrix tablets play a pivotal role in the realm of drug delivery by modulating controlled and sustained release of pharmaceuticals. These tablets are meticulously designed with the drug uniformly dispersed within a matrix or polymer, a strategic arrangement that exercises dominion over the release kinetics of the drug across an extended temporal span [110]. The significance of matrix tablets is underscored by a constellation of cardinal attributes. First and foremost, matrix tablets exhibit the phenomenon of controlled release, resulting in the preservation of therapeutic drug concentration within the body over an extended duration which is particularly advantageous for drugs harboring a slender therapeutic window or those necessitating consistent dosing regimens. Further the ability of matrix tablets to reduce dosing frequency, augment patient compliance and convenience, particularly for drugs requiring frequent administration schedules [111].

In a matrix system, the active and inactive components are combined and uniformly distributed throughout the dosage form. By controlling the release of the drug dosage from solid forms, matrix tablets mitigate the undulations and the potential undesirable side effects. For drugs characterized by short half-lives, matrix tablets based on amylose bestow a sustained release profile within the body, thus potentiating their therapeutic efficacy. Substantively, matrix tablets also curtail the fluctuations between drug peaks and troughs in plasma concentration, an aspect that holds promising clinical outcomes. By judiciously selecting polymers and formulations, amylose matrix tablets afford the luxury of tailoring drug release profiles to harmonize the idiosyncratic pharmacokinetic requisites of diverse therapeutic agents.

In the development of solid dosage formulations and enteric coated pills, high amylose maize starch has been used as a disintegrant, binder, and filler in matrix tablet preparation. Native starch can be chemically modified at primary and secondary OH groups are present for tailorable physicochemical properties. The complexation of diclofenac with high amylose

starch that has been combined with cross-linked polymers demonstrated additional control over the delivery vehicle's characteristics, resulting in a more regulated release profile and better therapeutic outcome. When a drug is added to high-amylose starch (70% amylose), the system's strength, crystallinity, and thermal stability are ameliorated. The amylose diclofenac complex, with enhanced physicochemical features, serve as an important controlled delivery method for distribution to the colon, specifically improving the degradation profile of drug conjugated with amylose. Diclofenac sodium was released under regulated conditions using tableted microparticles made of pectin blend and high-amylose starch polymers and significantly demonstrated prolonged and sustained gastrointestinal-targeted release via Fickian diffusion in vitro (95 percent release in 30 minutes) [112].

2.8. Amylose based magnetically guided drug delivery systems

Magnetic nanoparticles (MNPs) have emerged as versatile entities with multifaceted roles in advancing both targeted drug delivery and theranostics, combining therapeutic and diagnostic functionalities within a unified platform [113]. In the domain of targeted drug delivery, magnetic nanoparticles function as carriers for therapeutic agents, for transporting drugs, peptides, nucleic acids, and other cargoes to specific anatomical sites. Among several MNPs, iron oxide is the most preferred owing to its superparamagnetic nature at room temperature. But due to its hydrophobic nature, it tends to agglomerate and form large clusters with reduced colloidal stability [114]. Another hitch is the oxidation of the MNPs due to their large surface to volume ratio, necessitating the coating of the iron oxide core with functional shell containing long chain molecules enhancing colloidal stability and minimize residual magnetization [115]. Owing to their low toxicity, ease of surface modification, biocompatibility and magnetic attribute, MNPs are considered as next-generation drug/gene carriers with immense utility in diagnostics, theranostic and clinical science. Their modifiable surface properties supplement functionalization with targeting ligands, enabling precise recognition and binding to particular

cells or tissues. Following targeting, the nanoparticles can be effortlessly maneuvered and concentrated at the intended location through external magnetic field augmenting adequate drug accumulation while mitigating systemic exposure. This targeted strategy elevated the therapeutic efficacy of drugs and diminished off-target effects, ultimately enhancing patient outcomes.

In the realm of drug delivery systems, V-amylose has exhibited promising potential; however, its comprehensive utilization as a drug carrier remains unrealized in the current era. Notably, its application as a carrier for ulcerogenic flufenamic acid, Ibuprofen, Indomethacin, and Nimesulide, has only undergone preliminary investigation. Furthermore, the evaluation of V-amylose's impact on the pharmacokinetics of NSAIDs is still in its nascent stages, with limited ongoing clinical trials.

Controlled drug release facilitated by V-amylose delivery systems holds the promise of potentially reducing the effective therapeutic dose and the frequency of drug administration. This could significantly enhance patient compliance and mitigate the adverse effects associated with NSAID use, particularly the development of gastrointestinal ulcers. Despite these initial strides, a conclusive determination of V-amylose's efficacy and safety in the context of NSAID delivery awaits further research and rigorous clinical validation. A comprehensive understanding of the long-term effects and potential side effects through extensive clinical trials will be pivotal in establishing V-amylose as a reliable and effective drug delivery system. The integration of cutting-edge technologies and innovative approaches in pharmaceutical research will likely contribute to unlocking the full potential of V-amylose, paving the way for its successful integration into contemporary therapeutic strategies for NSAID delivery.

2.9 Methodology

2.9.1. FTIR spectroscopy

FTIR spectroscopy relies on the interaction of infrared radiation with the vibrational modes of molecular bonds in a sample. When infrared light passes through or interacts with a sample, specific wavelengths are absorbed, leading to characteristic peaks in the resulting spectrum. Molecules exhibit vibrational modes corresponding to stretching and bending of bonds. These vibrational transitions absorb infrared radiation at specific frequencies. In the FTIR instrument, a broadband infrared light source emits radiation. This radiation passes through or interacts with the sample, and certain wavelengths are absorbed by the sample based on its molecular composition. The transmitted or reflected light interferes with a reference beam, creating an interferogram. The interferogram is a plot of the intensity of the infrared light as a function of time. The interferogram is Fourier-transformed to generate the FTIR spectrum, which represents the intensity of absorbed infrared radiation as a function of wavenumber. Peaks in the spectrum correspond to specific vibrational frequencies, providing a "chemical fingerprint" that can be used to identify functional groups and molecular structures. Sample preparation involves mixing finely ground sample with a transparent and inert matrix material (e.g., potassium bromide) to form a pellet (~10mm) and subjected to hydraulic pellet forming machine to obtain a uniform, translucent compact pellet for final analysis. The prepared pellet was carefully handled to avoid contamination that could affect the spectrum.

Place the pellet in the sample compartment of the FTIR instrument (SP 300 PYE UNI CAM Infrared Spectrophotometer) and ensure proper alignment with the infrared beam for the sample to be analyzed in transmission mode (light passes through the sample). Pellet preparation is a crucial step in FTIR analysis, influencing the quality and reliability of the obtained spectra. Proper mixing, pressing, and handling are essential for achieving reproducible results, and attention to detail during pellet preparation contribute to the success

of FTIR experiments on solid samples. FTIR spectra of V-amylose-flufenamic acid complexes were recorded in the range 4000-450 cm^{-1} .

2.9.2 ^{13}C NMR

Nuclear Magnetic Resonance (NMR) spectroscopy was performed using Varian Infinity Plus 500 MHz spectrometer operating at 75 MHz for ^{13}C nucleus, with spinning rate of 8KHz at magic angle 54.7° . The cross polarization contact time for recording spectra of complexes was 1 ms, spectral width was 40 KHz, while the acquisition time was 12 s. In ^{13}C NMR spectroscopy, the magnetic nuclei of carbon-13 isotopes are observed. Carbon 13 nuclei possess a nuclear spin, which is a quantum mechanical property associated with their magnetic moment. This magnetic moment interacts with an external magnetic field. When placed in a strong external magnetic field, the carbon-13 nuclei align either parallel or antiparallel to the field. This results in two possible energy levels, each with a distinct magnetic moment. A radiofrequency pulse perpendicular to the external magnetic field is applied. This pulse causes a transition between the two energy levels, flipping the nuclear spins. The frequency of the RF pulse required to induce this transition corresponds to the resonance frequency of the carbon-13 nuclei and is influenced by the local chemical environment of each carbon atom. After the RF pulse is turned off, the nuclear spins return to their original alignment, releasing energy in the form of an NMR signal. The emitted NMR signals are detected, and the data are processed to generate the spectrum that provides information about the chemical environment and the number of carbon atoms in distinct environments in the molecule. The chemical shift in ^{13}C NMR represents the difference in resonance frequency due to the electronic environment around a carbon nucleus. It is measured in parts per million (ppm) and is referenced to a standard compound, usually D_2O and DMSO. ^{13}C NMR is valuable for determining the carbon framework of organic molecules. It can be used for quantitative analysis of the carbon composition in a sample. ^{13}C NMR instruments are similar to those used for ^1H NMR, but

they operate at lower frequencies due to the lower gyromagnetic ratio of carbon-13. ¹³C NMR spectroscopy aid in structural elucidation and analysis in various fields including chemistry, biochemistry, and materials science.

2.9.3 XRD

X-ray Diffraction (XRD) is a technique used to study the crystal structure of materials by analyzing the diffraction pattern produced when X-rays interact with a crystal lattice and was carried out using Philips PW 3020 powder diffractometer having graphite crystal monochromator. The generator worked at 40 kV, and 40 mA. The scanning of test samples was done over 5-30° (2θ) in steps of 0.02° (2θ) per second.

The working principle involves the diffraction of X-rays by crystal planes, resulting in constructive interference that produces diffraction patterns. The fundamental principle behind XRD is Bragg's Law, which relates the angles of incidence and the interplanar spacing of crystal lattice planes and is represented by the following equation:

$$n\lambda=2d\sin(\theta)$$

where: n is the order of the diffraction peak, λ is the wavelength of the X-rays, d is the interplanar spacing of the crystal lattice, and θ is the angle of incidence. When monochromatic X-rays interact with a crystal lattice, they are scattered by the crystal planes. The scattered waves interfere constructively at specific angles, producing diffraction peaks A detector records the intensity of diffracted X-rays at different angles. The resulting diffraction pattern in the form of a diffractogram providing information about the crystal structure, including lattice spacing and orientation and atomic arrangements.

2.9.4. Zetasizer

Zetasizer Nano ZS90 was used to calculate the particle size and zeta potential. The Zetasizer is a device commonly used for measuring particle size and zeta potential in colloidal and nanomaterial dispersions. It employs dynamic light scattering (DLS) and electrophoretic light

scattering (ELS) techniques to analyze particles in a liquid medium. A laser beam is directed through a sample containing dispersed particles. The particles in the sample scatter light, causing fluctuations in intensity over time. Particles in a fluid undergo Brownian motion due to thermal energy. The motion results in changes in the scattered light intensity, and these fluctuations are monitored by the Zetasizer. The Zetasizer analyzes the correlation function of the scattered light intensity fluctuations over time. This information is used to calculate the diffusion coefficient of the particles. The Zetasizer employs ELS to measure the zeta potential of particles. An electric field is applied to the sample, causing charged particles to move. As the charged particles move in response to the electric field, they experience a Doppler shift in the frequency of scattered light. This shift is proportional to the velocity of the particles. The Zetasizer combines DLS and ELS techniques to measure particle size and zeta potential in colloidal systems. By analyzing the dynamic behavior of scattered light and the electrophoretic mobility of particles, the zetasizer provides valuable information about the properties of nanoparticles and colloids in a liquid medium.

2.9.5. Dissolution apparatus

A dissolution apparatus is a pharmaceutical instrument used to study the rate at which a solid dosage form (e.g., tablets, capsules) dissolves under standardized conditions. This information is crucial for assessing the drug's bioavailability and its potential therapeutic efficacy. There are different types of dissolution apparatus, commonly categorized as per the United States Pharmacopeia (USP) into apparatus types I to IV. Below is a general overview of the working principle of a typical dissolution apparatus, such as Apparatus II (Paddle apparatus) or Apparatus I (Basket apparatus). We have employed basket apparatus for our study.

A dissolution test typically starts with the preparation of a dissolution medium that simulates the physiological conditions in which the drug will be administered. This medium may be an aqueous solution with specific pH conditions, reflecting the pH of the gastrointestinal tract.

The dissolution apparatus consists of a vessel containing the dissolution medium and a temperature control system to maintain the medium at a specified temperature, often 37°C. The synthesized compound was directly placed in the basket, which is then immersed in the dissolution medium. The test begins by introducing the dosage form into the dissolution medium. At predetermined time intervals, samples are withdrawn from the dissolution medium. The concentration of the drug in each sample was analyzed using an appropriate analytical method, such as UV-visible spectroscopy. The dissolution rate is calculated based on the measured drug concentration over time. The results were presented as a dissolution profile, indicating the percentage of drug dissolved versus time. The dissolution medium is designed to maintain "sink conditions," meaning that the concentration of the drug in the medium remains much lower than its solubility. Different apparatus types may be chosen based on the characteristics of the dosage form and the intended use of the drug. Dissolution testing is an essential component of quality control for pharmaceutical products, ensuring consistency in drug release and bioavailability. The dissolution apparatus serves as a critical tool in pharmaceutical development, quality control, and research, providing insights into the performance of dosage forms in simulated physiological conditions.

2.9.6. Rotating cylinder

It is a commonly used technique for studying the mucoadhesive properties of pharmaceutical formulations, especially those designed for mucosal drug delivery. The Rotating Cylinder method is employed to assess the strength and duration of adhesion between a mucoadhesive material and a biological substrate. The instrument typically consists of a rotating cylinder, which simulates the movement within the human body, and a platform to hold the mucosal substrate.

The rotating cylinder method in present work was employed to compare the mucoadhesive qualities of the native and aminated starch tablets with chitosan. A freshly cut pig intestinal

mucosa (4 x 5 cm) was adhered to a stainless-steel cylinder (apparatus 6 rotating cylinder, 2 inches) using cyanoacrylate glue. The mucosa was then covered in test tablets containing chitosan, aminated starch tablets, and native starch. After that, the cylinder was put into a dissolving equipment, which revolved at 50 rpm and held 900 mL of 0.1 M phosphate buffer pH 6.8 at 37 ± 0.2 °C, in accordance with the European Pharmacopoeia. The rotation of the cylinder simulates the shearing forces experienced in the dynamic environment of the mucosal surface. Over the course of five days, the detachment times were recorded. The Rotating Cylinder Method is widely used to assess the mucoadhesive properties of oral, nasal, ocular, and vaginal dosage forms. It helps in the development and optimization of mucoadhesive drug delivery systems, where prolonged contact with mucosal surfaces is desired for enhanced drug absorption. The method is valuable in evaluating the influence of formulation components on mucoadhesive performance. It is a valuable tool for researchers in the field of pharmaceutical sciences, aiding in the characterization and development of mucoadhesive formulations for targeted drug delivery to mucosal surfaces.

2.9.7. HPLC

HPLC was performed on Prominence-I LC-2030C from Shimadzu using C18 column (Sunfire, 4.6 x 250 mm) for chromatographic separation. Liquid mobile phase and stationary phase are used in HPLC. The stationary phase is a packed column, while the mobile phase is a solvent or combination of solvents that circulates through the apparatus. Within the HPLC system, a tiny volume of the sample is introduced. Compounds that need to be separated may be mixed together in the sample. A column filled with a stationary phase holds the sample. In order to maximise the surface area for interactions with the sample components, the column is usually packed with tiny particles. Differential interactions between the components of the sample and the stationary phase are what cause separation to occur. A plot of the detector response (signal intensity) against time is called a chromatogram, was produced by processing the data that the

detector produces. Distinct components within the sample were indicated as peaks on the chromatogram.

2.9.8. UV Spectroscopy

UV-Visible spectroscopy was performed using Shimadzu 1800. It is a widely used analytical technique that involves the absorption of ultraviolet and visible light by molecules, leading to electronic transitions. This technique was employed for qualitative and quantitative analysis of complexes, providing information about the electronic structure and concentration of analytes. UV-Visible spectroscopy involves the interaction of molecules with ultraviolet (UV) and visible light. The energy of this electromagnetic radiation matches the energy required for electronic transitions in molecules. When a molecule absorbs UV or visible light, electrons are promoted from lower energy (ground) states to higher energy (excited) states. The energy difference corresponds to the energy of the absorbed light. The absorption of light is recorded as an absorption spectrum, which is a plot of absorbance (or transmittance) versus wavelength. Peaks in the spectrum correspond to specific electronic transitions. The technique follows Beer-Lambert Law which defines the relationship between the concentration of a solute in a solution and the absorbance of light is described by the Beer-Lambert Law and is represented by the following equation: $A = \epsilon \cdot c \cdot l$ where: A is the absorbance, ϵ is the molar absorptivity (extinction coefficient), c is the concentration of the solute, l is the path length of the sample. The Beer-Lambert Law is fundamental for quantitative analysis using UV-Visible spectroscopy. The choice of solvent can influence the absorption spectrum. Polar solvents may shift absorption bands compared to nonpolar solvents due to solute-solvent interactions. UV-Visible spectroscopy was performed using a UV-1800 spectrophotometer, which consists of a light source, monochromator, sample holder, and detector, operating on a 240V. The monochromator selects a specific wavelength of light, and the detector measures the intensity of light before and after it passes through the sample. UV-Visible spectroscopy is widely used for quantitative

analysis of compounds and concentration in solution and is also employed for quality control in various pharmaceuticals, food, and beverages industries.

2.9.9. TGA analysis

The TGA, or Thermogravimetric Analysis was carried out using NEXTA STA 200 model from HITACHI to study the weight changes of a sample as a function of temperature (or time) in a controlled atmosphere. The principle behind TGA is based on the measurement of the weight of a sample as it undergoes physical or chemical changes. 5 milligrams of the sample was weighed and placed in a crucible on a sensitive balance inside the thermal analyser. The crucible with the sample was subjected to a controlled temperature program under the atmosphere of nitrogen. The temperature can be increased linearly or held constant. As the sample is heated, it may undergo physical or chemical changes which are reflected by a change in the weight of the sample and the data is recorded over time and analyzed to determine the nature and extent of the weight loss occurring in the sample.

2.9.10. SEM microscopy

SEM images were obtained by using Carl Zeiss EVO 50 VP scanning electron microscope operating at an accelerating voltage of 10 kV, and 30 Pa. The dried sample was loaded on stub SCM and gold coated under spatter coater to obtain the micrographs. It is a powerful imaging technique that uses a focused beam of electrons to create detailed three-dimensional images of the surface of a sample. It uses an electron gun to generate a beam of electrons that is then focused into a fine point with the help of electromagnetic lenses. The sample was placed in a vacuum chamber to prevent scattering of the electron beam by air molecules. The vacuum also facilitates the movement of electrons without interference. The signals collected by the detectors are used to generate images of the sample surface. By scanning the electron beam across the sample at different angles, SEM provide a series of images that can be used to reconstruct a three-dimensional representation of the sample's surface. SEM is used to study

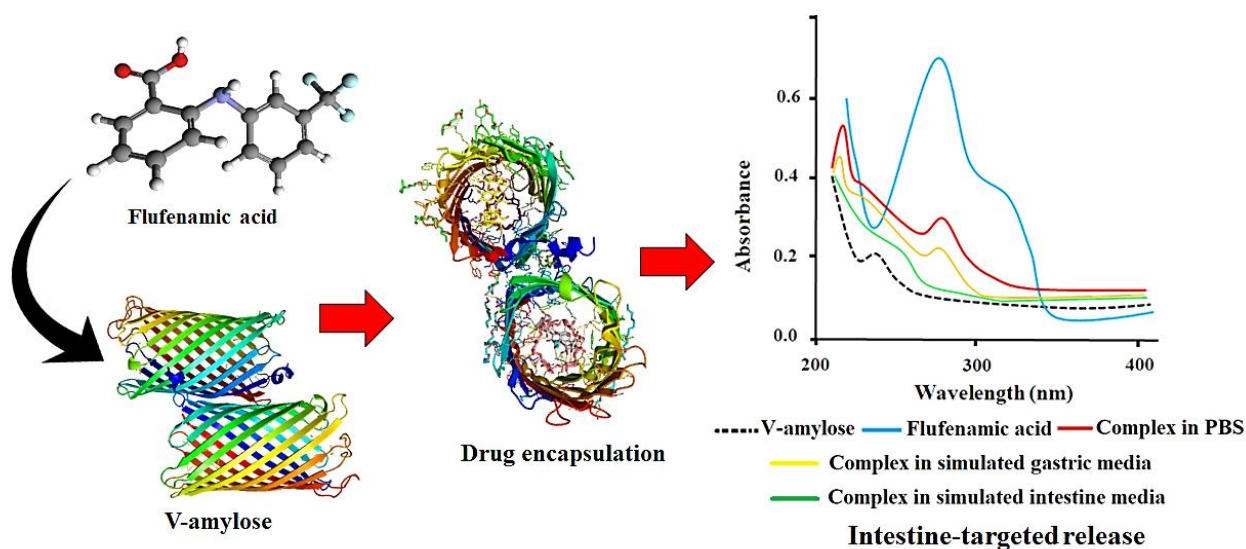
the morphology and topography of materials at a high resolution. It is particularly valuable for imaging surfaces at a nanoscale level and is an essential tool in materials science, biology, geology, and other disciplines.

Chapter 3: Targeted drug delivery with native V Amylose

3.1. Abstract

Encapsulation of Flufenamic acid by V-amylose offers its targeted delivery to the intestine. The V-amylose-Flufenamic acid complex presents a considerable stability over a range of pH, and at elevated temperatures. Solid-state ^{13}C CP/ MAS NMR, FTIR and XRD analysis indicated the entrapment of cargo drug molecules inside the helical structure of V-amylose. SEM investigations suggested that the conjugates display a marked stability in simulated gastric environment (pH 1.2), while the degradation of V-amylose in simulated intestine media (pH 7.2) containing hydrolyzing enzyme led to a rapid release of cargo drug molecules. UV-visible analysis for the appraisal of the drug release property of V-amylose indicated intestine-targeted release of Flufenamic acid. The V-amylose-Flufenamic acid complex displayed a sustained release of the cargo drug molecule for 12h at different drug/amylose ratios.

3.2. Pictorial presentation of the proposed work



3.3. Introduction

The helical structure of V-amylose, its resistance towards enzymatic degradation, and ability to encapsulate the drug molecules in helical cavity makes it a superior drug delivery vehicle compared to the other polysaccharides [48]. Mainly, the glycosidic bonds and glycosyl hydroxyl groups constitute the hydrophobic cavity and the hydrophilic periphery respectively, of the helical V-amylose [46]. The helical cavity of V-amylose having a pitch height of 7.91-8.17 Å provides a privilege drug delivery system for carrying a variety of molecules [101]. The tight packing of the helical structure of V-amylose possesses considerable resistance towards degradation by amylases, which supports its application as a controlled-release drug delivery vehicle for a targeted release of the cargo therapeutics [116]. These characteristics play an important role in minimizing the limitations posed by the gastrointestinal delivery of drugs. As such, the targeted sustained release by V-amylose provided a robust candidature for the safer delivery of NSAIDs that reportedly corrode the gastric mucosa following their burst release in the gut [117]. Reportedly, the inclusion complexes of Ibuprofen with V-amylose significantly lowered the effective therapeutic dose of the drug, in addition to achieving a sustained release in the simulated intestine media, which manifested minimal side effects [96]. The encapsulation of poorly soluble Indomethacin within the hydrophobic cavity of V-amylose prevented its early release in acidic gastric media, while promoting a sustained release in the intestine owing to slow degradation by α -amylase [118]. In the present communication, we report the intestine targeted delivery of Flufenamic acid by V-amylose. The drug molecules encapsulate in the helical cavity of V-amylose while achieving intestine targeted release of the cargo drug. The drug-amylose complex displayed a marked stability in the simulated gastric media with pH 1.2, which prevented the early release in gastric setting. These investigations suggested V-amylose as a candidate delivery system for the sustained release of gut corroding NSAIDs.

3.4. Materials and Method

Flufenamic acid (analytical standard), and Potato Amylose, α -Amylase from porcine pancreas (>1000 units/ mg protein), and Pancreatin were procured from Sigma-Aldrich Chemical Company. Analytical grade chemicals and solvents were used for performing synthesis and experimentation.

3.4.1. Synthesis of V Amylose-Flufenamic acid conjugates

The conjugates were prepared by the dissolution of 1g of amylose to 250 ml of KOH solution (0.1 mol/L) at 80 °C, with constant stirring until the solution turns into a homogenous paste. The paste was further cooled to 35 °C followed by the addition of Flufenamic acid in different amounts. The pH of the solution was maintained at 4.7 by the addition of H₃PO₄ (0.1 mol/L) with gentle stirring, which led to the appearance of precipitates. The precipitates were isolated by centrifugation of the solution (10000 g, 15 min, 10 °C), and purified with 30% (v/v) ethanolic solution. Freeze-drying of purified precipitates followed by milling through 100-mesh sieve led to the procurement of V-amylose-Flufenamic acid complexes [119]. Percentage yield of the complexes was calculated with the help of **Equation 2.1** [96].

$$\% \text{ Yield} = \frac{\text{Mass of complex}}{\text{Mass of Amylose} + \text{Mass of Flufenamic acid}} \times 100 \quad \dots \quad \text{Eq 2.1}$$

3.4.2. Calculation of the amount of Flufenamic acid included in V-amylose

The quantification of included drug was done by incubation with Pancreatin solution, for which a 0.180 g pancreatin was dissolved in 20 mL of 20mM solution of PBS (containing 0.04 % brine) buffer at pH 6.9. The centrifugation of this solution (500 g/ 15 min.) followed by filtration provided supernatant, which was used for performing the experiments. A predetermined amount of complexes (20 mg) was incubated with the above pancreatin solution at 37 °C for 24h, which led to the digestion of complexes thereby releasing Flufenamic acid in the parent solution. The free drug was extracted from solution with ethanol and the amount

extracted was calculated by UV-vis spectrophotometry [99]. The percentage of included flufenamic acid was calculated with the help of Equation 2.2

$$\% \text{ Complexed drug} = \frac{\text{Quantified mass of drug in pancreatin solution}}{\text{Theoretical mass of drug in the complexes}} \times 100 \quad \text{Eq. 2.2}$$

3.4.3. Release of Flufenamic acid in simulated physiological environment

Predetermined amount of V-amylose-Flufenamic acid complex was incubated with 1.5 ml of simulated gastric fluid (0.1 M HCl, pH 1.2) for 5 h at 35 °C with constant stirring. The samples were then diluted with 165 mL PBS buffer (pH 6.9) followed by centrifugation (5000 g, 10 min).

The simulated intestine medium was prepared by using PBS buffer (pH 7.2) containing 30 units/ mL of α -amylase enzyme. To 20 mL of this medium, 165g of sample complex was incubated at 37 °C with constant stirring. The amount of drug release in the presence of simulated media was quantified with UV-vis spectrophotometry by using Equation 2.2.

3.4.4. Physical investigations

XRD diffractograms were obtained by using Philips PW 3020 powder diffractometer having graphite crystal monochromator. The generator was worked at 40 kV, and 40 mA. The scanning of test samples was done over 5-30° (2θ) in steps of 0.02° (2θ) per second.

Solid state ¹³C CP/MAS NMR was performed by using Varian Infinity Plus 500 MHz spectrometer operating at 75 MHz for ¹³C nucleus, with spinning rate of 8KHz at magic angle 54.7°. The cross polarization contact time for recording spectra of complexes was 1 ms, spectral width was 40 KHz, while the acquisition time was 12 s.

FTIR spectra of V-amylose-flufenamic acid complexes were recorded in the range 4000-450 cm⁻¹, by using SP 300 PYE UNI CAM Infrared Spectrophotometer.

SEM images were obtained by using Carl Zeiss EVO 50 VP scanning electron microscope operating at an accelerating voltage of 10 kV, and 30 Pa. The dried sample was loaded on stub SCM and gold coated under spatter coater to obtain the micrographs.

Extreme caution was exercised while preparing samples for analyzing FTIR, CP MAS NMR, XRD, UV VIS, and SEM so as to ensure the following errors do not affect the quality of sample prepared and final measurement:

- i) Static error which includes reading, characteristic and environmental error.
- ii) Instrument loading error
- iii) Systemic or random errors

All the instruments were handled with precision and care following the standard operating procedure.

3.5. Results and discussion

3.5.1. Yield of V-Amylose-Flufenamic acid complex and drug content in the complexes

The percentage yield of the complex and its drug content was calculated by using the equations 1, and 2. As depicted in **Table 4**, the increment in V-amylose-Flufenamic acid ratios in the order 5:1-25:1 caused an increase in the percentage yield of the complex and the drug content. However, further increase in the ratio by 35:1 to 50:1 caused a decline in these parameters. The maximum percentage yield of the complex and highest percentage of encapsulated drug were observed as 55.8 ± 0.2 and 21.2 ± 0.1 respectively, at 25:1 (w/w) ratio of V-amylose: Flufenamic acid. These observations suggested a moderate loading capacity of V-amylose for Flufenamic acid.

Table 4: Variation of the Complex yield and Drug content with V-amylose-Flufenamic acid ratio[#]

V-amylose: Flufenamic acid (w/w)	% content of Flufenamic acid in the complex	% yield of complex
5:1	18.3±0.4	50.5±0.3
15:1	19.7±0.2	54.2±0.5
25:1	21.2±0.1	55.8±0.2
35:1	17.9±0.2	40.5±0.3
50:1	13.3±0.4	32.5±0.3

[#]Data shown in mean ± standard deviation

%w/w: weight of solute in a given weight of solution

3.5.2. Conjugation of Flufenamic acid to V-amylose

Fig 4 indicates the absorption spectra of V-amylose, Flufenamic acid and their conjugation in the presence of PBS buffer. The complex remained intact in the presence of simulated gastric media with acidic pH without showing any visible signs of degradation. However, in the simulated intestinal media containing amylase and slightly basic pH, the absorption spectra undergo a marked change, thereby indicating the onset of degradation process.

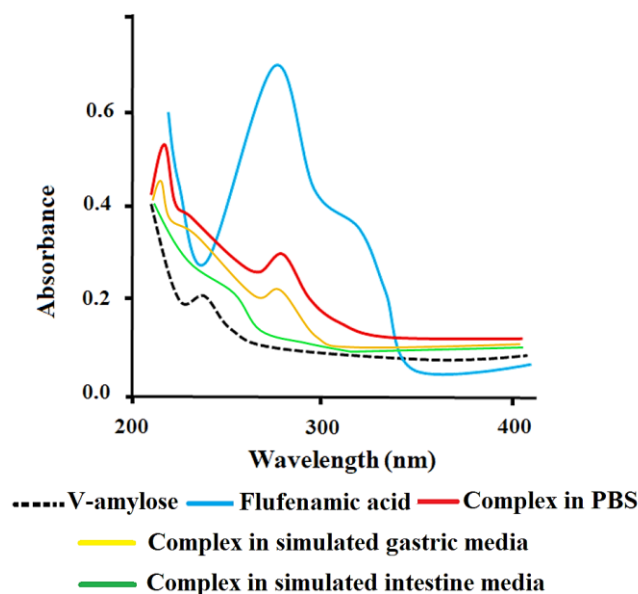


Figure 4: UV-vis absorption spectra indicating the complexation of Flufenamic acid in V-amylose

Solid-state ¹³C CP/MAS NMR spectra of V-amylose and its complex with Flufenamic acid is given in Fig 5. Doublet at 102.0 and 104.5 ppm corresponds to the C-1 of hexapyranose of V-

amylose, while the broad peak at 81.5 ppm belongs to the C-4. The overlapping peaks at 73.0 ppm appear for C-2, C-3, and C-5; whereas the peak at 61.9 ppm designates C-6 of the $-\text{CH}_2\text{OH}$ group. For the V-amylose-Flufenamic acid complex, the singlet at 73.0 ppm confirms the inclusion of drug molecule in the helical conformation of amylose [120].

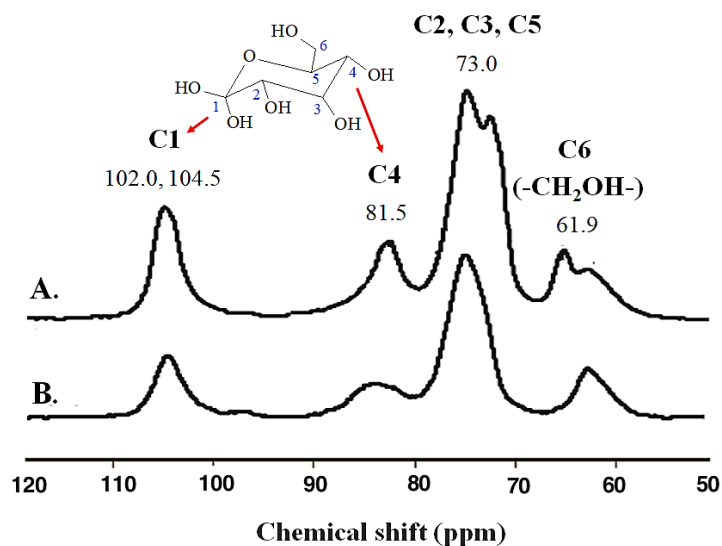


Figure 5: Solid-state ^{13}C CP/MAS NMR spectra of A. V-amylose and B. V-amylose-Flufenamic acid complex

FTIR spectra of V-amylose-Flufenamic acid complex in the simulated physiological medium is represented in **Fig 6**. The FTIR spectra for the V-amylose-Flufenamic acid conjugates in simulated gastric fluid demonstrated only a trivial degradation as indicated by the peak at 1096 cm^{-1} , which broadens in simulated gastric medium while retaining its original intensity. This indicates that the structures of V-amylose-Flufenamic acid conjugates do not undergo degradation in acidic pH. However, in the simulated small intestine fluid, the peak at 1096 cm^{-1} disappeared thereby indicating the hydrolysis of the glycosidic bonds ($-\text{C}-\text{O}-\text{C}-$) in V-amylose backbone by the intestinal α -amylase[121][48].

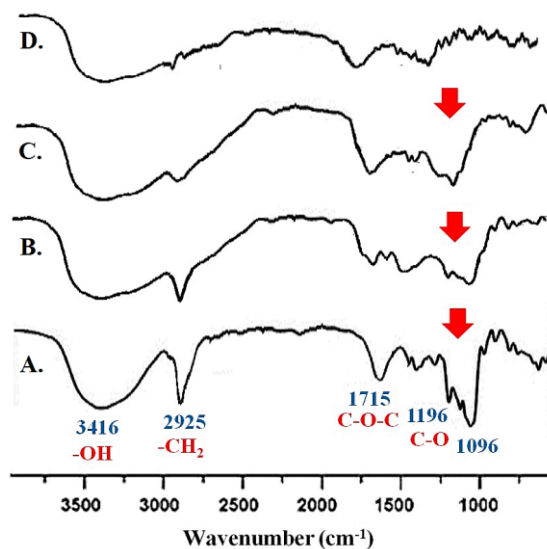


Figure 6: FTIR spectra of V Amylose-Flufenamic acid for A. In PBS, B. In simulated gastric fluid, C. In simulated small intestine fluid for 12 h, D. In simulated small intestine fluid for 24 h.

Fig 7. indicates the XRD diffractograms of Flufenamic acid, V-amylose (a) and their complexes. On the complexation of V-amylose with Flufenamic acid, the characteristic bands of the drug become feeble. However, the peak intensity around 13° and 20° increased on increasing the drug-amylose ratio by 1/50 (b), 1/25 (c), and 1/5 (d); that indicated the V-shaped inclusion complexes of amylose with Flufenamic acid [122].

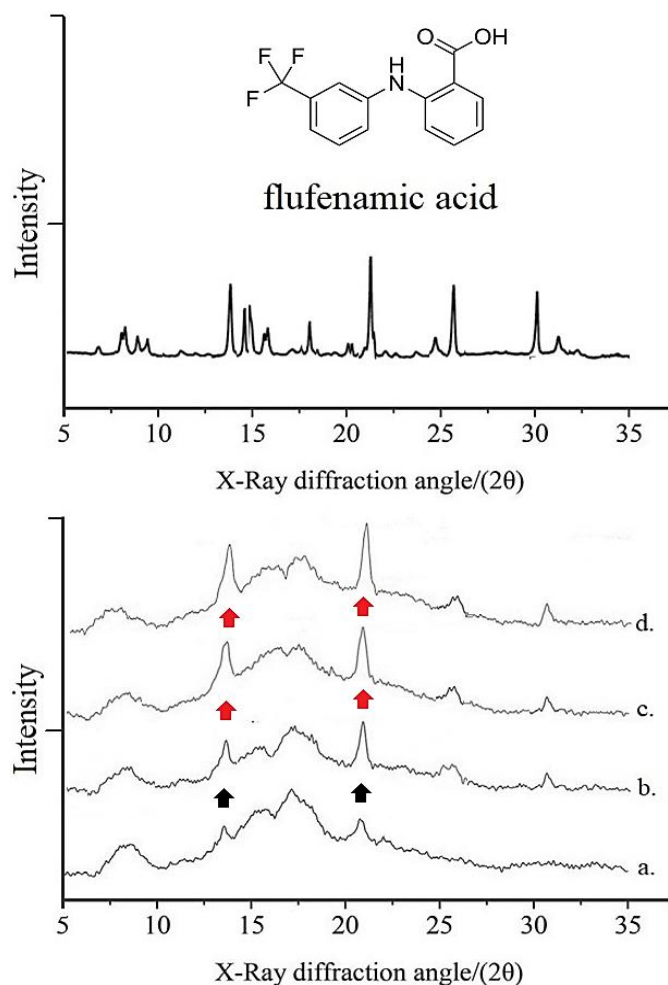


Figure 7: XRD diffractogram of A. V-amylose, B. V-amylose-Flufenamic acid complex

SEM images of V-amylose-Flufenamic acid conjugates in **Fig 8** indicated the retention of the original structure of the dried conjugate after soaking in simulated gastric media for 4h, hence indicating stability of the V-amylose-Flufenamic acid conjugate in the acidic pH of gastric environment where negligible degradation takes place. However, the treatment with simulated intestinal fluid led to the degradation and erosion of the V-amylose-Flufenamic acid conjugate. The degradation occurred due to the enzymatic action of amylase on the glycosidic bonds of V-amylose. The controlled intestinal release of the Flufenamic acid utilizes this property of V-amylose that ameliorates the impending side effects of the drug.

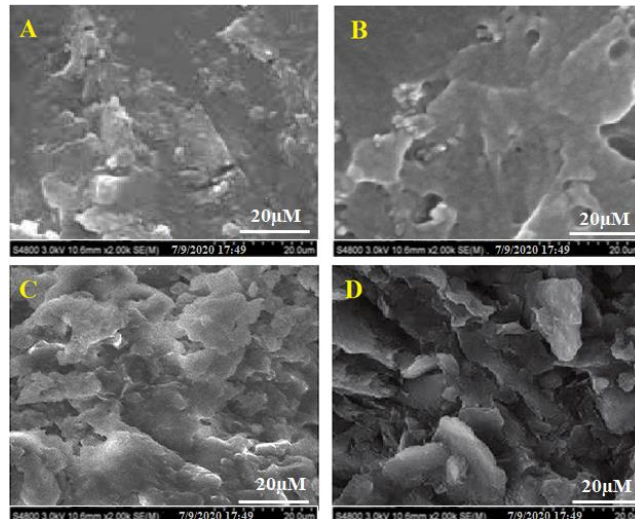


Figure 8: Release of Flufenamic acid by V-amylose: A. Dried conjugate, B. After soaking in simulated gastric fluid for 6h, C. After soaking in simulated intestinal fluid for 12h, and D. After soaking in simulated intestinal fluid for 24h

Fig 9 represents the release profile of Flufenamic acid from V-amylose, as compared to starch. V-amylose undergoes a rapid drug release as compared to starch in pancreatin containing simulated intestine medium, mainly due to the hydrolysis of its glycosidic bonds in this environment. However, V-amylose in simulated gastric medium with acidic pH displayed remarkable resistance towards hydrolysis compared to starch as indicated by the drug release characteristics. This prevents the early release of cargo drug molecules from V-amylose in gastric environment.

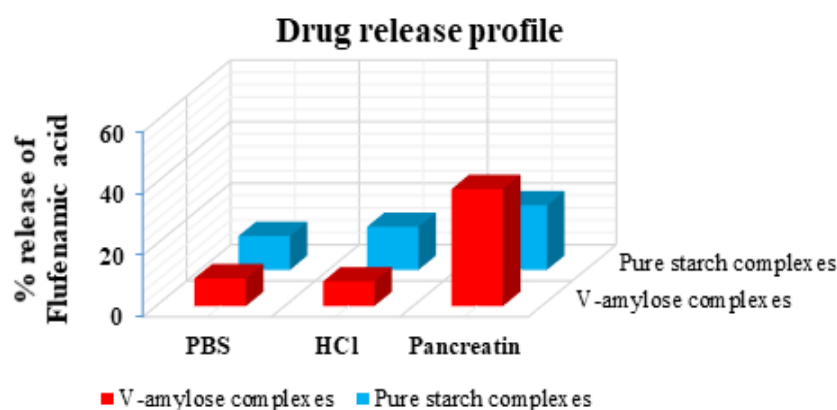


Figure 9: Release of Flufenamic acid by V-amylose

Fig 10 highlights the effect of physicochemical parameters typical to gastric environment, on the drug release profile of V-amylose. The maintenance of gastric stability of an ideal drug

delivery system necessitates the protecting of cargo molecules from the acidic pH and high temperature in the stomach and food matrix. Highest amount of the cargo drug released at pH 8, due to the dissolution of V-amylose-Flufenamic acid complex mainly due to the appearance of partial charge on V-amylose and Flufenamic acid that increases their hydrostatic interactions with surrounding water molecules. This event escalates the amount of Flufenamic acid in the parent solution. Similarly, the release of cargo drug from V-amylose increases with temperature. However, lower amount of drug release occurs at pH 4-5. Nevertheless, under a range of pH and from 30-60 °C, <12% of drug release occurred that indicated the considerable physicochemical stability of the V-amylose-Flufenamic acid conjugates.

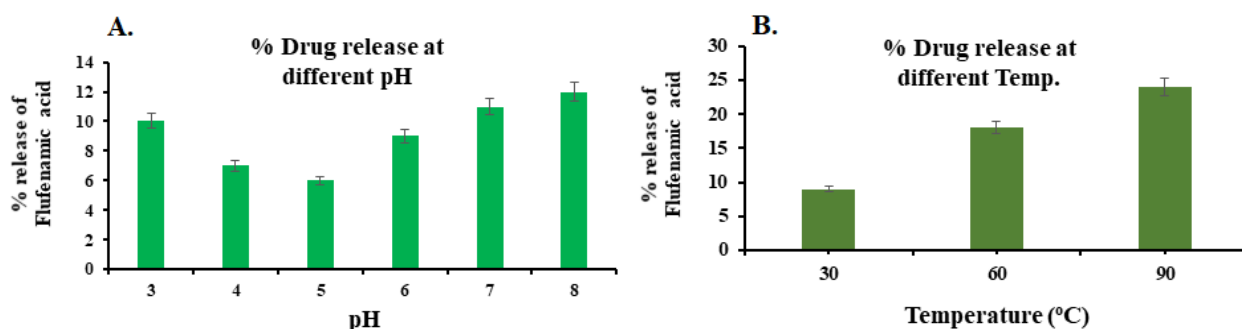


Figure 10: Effect of pH and temperature on the release of Flufenamic acid from V-amylose

The cumulative release profile of V-amylose-Flufenamic acid complexes in **Fig 11** indicated a sustained release of the cargo drug in 12 h in the simulated small intestine medium at different drug-amylose ratio. The cumulative release of the drug by the complexes strongly depended on the Flufenamic acid-V-amylose ratio and the amount of amylose present in the simulated small intestine medium.

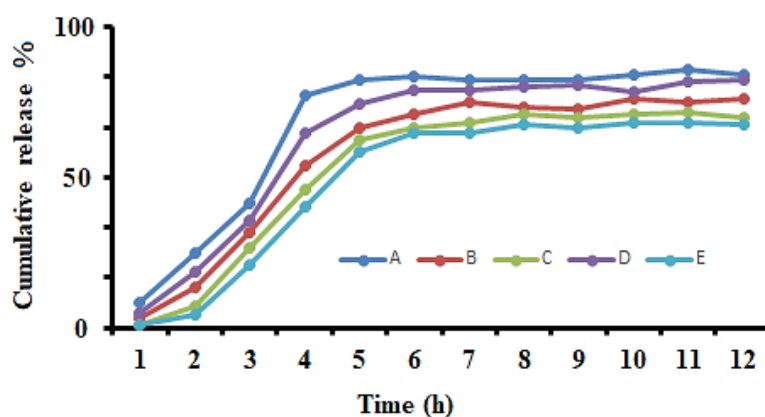


Figure 11: In vitro release of Flufenamic acid in the simulated small intestine fluid for 5 different ratios of Flufenamic acid and V-amylose at a. 1/5, b. 1/15, c. 1/25, d. 1/35, e. 1/50

3.6. Conclusion

Inclusion complexes of V-amylose with Flufenamic acid presents an anticipated profile for the targeted release of cargo drug to the intestine. The physical investigations by XRD, FTIR, and ^{13}C CP/MAS NMR confirmed the encapsulation of drug in V-amylose helix. Drug release profile of the complex in simulated gastric/ small intestine medium indicated a sustained release owing to the digestion of carrier system in the presence of amylase enzyme. The complex presents a considerable stability over a range of pH, and at elevated temperature, that further supports its potential intestine drug delivery applications. The inclusion complexes of V-amylose with Flufenamic acid prove highly advantageous in mitigating the gastrointestinal side effects of the drug by preventing its burst release in the gut. Further studies will be performed for testing the pharmacokinetics, and toxicity profiling of drug loaded V-amylose in the intestine.

3.7. Summary points

- V-amylose promotes targeted delivery of flufenamic acid
- The V-amylose-flufenamic acid complex is stable in acidic pH of simulated gastric setting
- The V-amylose-flufenamic acid complex achieves controlled drug release in the simulated intestine media
- V-amylose-flufenamic acid complex shows considerable stability at elevated temperatures for food matrix applications in nutraceutical delivery system
- Intestine delivery by V-amylose support its potential applications as enteric coatings

Chapter 4: Controlled drug delivery with chemically modified V Amylose

4.1. Abstract

Aim: To develop controlled release tablets based on aminated starch. **Materials and methods:** Aminated starch was characterized with Fourier transform Infrared (FTIR) spectroscopy, and X-ray diffraction (XRD) studies, which also indicated the preferential oxidation of crystalline region. Thermogravimetric analysis (TGA) further confirmed these observations. The drug release profile was studied in simulated gastric media, and simulated intestinal media with and without pancrelipase enzyme and the data was fitted to various mathematical models to evaluate the release kinetics. Rotating cylinder method was used to study mucoadhesive potential of tablets. **Results and discussion:** The tablets achieved an initial fast release of fenamates, which slows down after 12 hours. Drug release was not completed in the simulated intestinal media (both with and without pancrelipase) which may be due to the stability of imine bond in aminated starch at weakly acidic pH. Drug release was completed in simulated acidic media even though initial release kinetics resembled that of the simulated intestinal media due to the hydrolysis of imine functionality at strongly acidic pH. The protonation of primary amine groups leading to considerable swelling prevents premature release of drug from tablets in both simulated gastric and intestinal media. **Conclusion:** Aminated starch containing primary amine group and an imine functionality may serve as an ideal intestine-targeted drug delivery system due to stability at weakly acidic pH, controlled drug release profile, and a remarkable mucoadhesive potential.

4.2. Introduction

Since their inception, non-steroidal anti-inflammatory drugs (NSAIDs) represent the frontline treatment regime for the management of chronic inflammation and related exigencies. Despite

their benefits, the non-selective inhibition of cyclooxygenases (COX-1 and COX-2) by a majority of NSAIDs results in serious health complications, including gastrointestinal (GI) ulcers [123]. Mechanistically, the inhibition of constitutive cyclooxygenase (COX-1) in the GI tract by NSAIDs causes a significant reduction in the secretion of prostaglandins, apparently lowering their cytoprotective affinity thereby increasing the incidence of mucosal injury [124]. These challenges have been countered with the development of COXIBs and CINODs, however the former exert adverse cardiovascular events, whereas the latter pose a poor patient compliance [125]. The delivery of NSAIDs with controlled release systems has been identified as a potential strategy to improve the patient compliance by lowering the dosing frequency of NSAIDs that possibly mitigates the GI side effects arising from the overuse of the latter [126]. Native starch provides a desirable platform for the development of advanced drug delivery systems owing to its physiological benevolence, biodegradability, susceptibility towards enzymatic degradation depending on the amylose: amylopectin ratio, and remarkable swelling behaviour. Furthermore, the native starch has been utilized as binder, filler, and as disintegrant in the production of solid dosage formulations and as enteric coated tablets. The presence of primary and secondary -OH groups on native starch serve as the site for its chemical modification to tailor the physicochemical properties [127].

Aminated starch possesses cationic properties comparable to chitosan that can be utilized for the development of mucoadhesive and colon targeted delivery of pharmaceuticals. Chitosan has been utilized for colon-targeted drug delivery due to its swelling at intestinal pH and dissolution at acidic stomach pH. However, the aminated starch presents a remarkable swelling behaviour and water penetration tendency at pH 1.2 mainly due to the protonation of amine groups [70]. This supports its stability at acidic pH, which the colon-targeted delivery systems must bypass. Furthermore, the amination of high amylose starch is highly desirable for GI targeted release owing to a slow degradation of amylose content by α -amylases released in the

GI tract by pancreas. In this short communication, we aim to present the aminated starch-supported GI specific delivery of fenamates, a class of NSAIDs.

4.3. Materials and methods

4.3.1. Materials

High amylose starch and Pancrelipase were obtained from Sigma Aldrich, Flufenamic acid, Mefenamic acid, Tolfenamic acid, and Maclofenamic acid were obtained from TCI Chemicals (India) Pvt. Ltd.

4.3.2. Methods

4.3.3. Synthesis of aminated starch

2g of high amylose corn starch was dissolved in 30 ml deionized water to obtain a suspension. 5 ml of KIO_3 (0.7M) was added to this suspension followed by heating to 35 °C and stirring at 550 rpm on a magnetic stirrer for 120 minutes. Further, 30 ml acetone was added to the above mixture to obtain white precipitates of dialdehyde starch. These precipitates were separated by filtration followed by several washings with deionized water to remove excess unreacted KIO_3 . The qualitative analysis of dialdehyde starch was confirmed with Schiff's reagent that gave magenta colour on reaction with dialdehyde starch. The washed precipitates of dialdehyde starch were then dried in vacuum oven at 35 °C for 24 h and finally submitted for characterization by XRD and FTIR spectroscopy. Dialdehyde starch was then treated with 0.05 ml of ethylenediamine and agitated in an agate mortar at room temperature for 2 minutes without a solvent. The mechanochemical reaction resulted in the formation of imine functionality between ethylenediamine and dialdehyde starch in the form of a white solid, which was labelled as aminated starch. This white solid after multiple washings with deionized water was dried in a vacuum oven at 24 °C for 24 h and stored for further use [128].

4.3.4. Calculation of the percentage of dialdehyde modification

The percentage of aldehyde content on starch was calculated by rapid quantitative alkali consumption method. 0.2 g of dried dialdehyde starch was added to a 250 ml conical flask containing 25 ml of the standard NaOH solution (0.2 M). The conical flask was heated over a water bath maintained at 80°C for 5 minutes, followed by rapid cooling under running tap water. 25 ml of a standard solution of H₂SO₄ (0.2 M) was then added to the conical along with 100 ml of water and a few drops of phenolphthalein indicator. The solution in the conical flask was then titrated with 0.2 M NaOH solution to calculate the percentage of dialdehyde content by using Equation 3.1 [129].

$$DAS (\%) = \frac{C_1V_1 - 2C_2V_2}{W/161} 100 \quad \dots \text{Eq 3.1}$$

Where % DAS is the percentage of dialdehyde, C₁ and C₂ are concentration of H₂SO₄ and NaOH respectively, W is the dry weight of oxidized starch, and 161 is the average molecular weight of the repeat unit in dialdehyde starch.

4.3.5. Physical Investigations

The XRD diffractograms were recorded with Philips PW 3020 powder diffractometer fitted with a graphite crystal monochromator. The generator was run at 40 kV and 40 mA and the samples were scanned over 10-40° (2θ) in the steps of 0.02° (2θ) per second. The FTIR spectra was recorded in the range 500-4500 cm⁻¹ with SP 300 PYE UNI CAM Infrared Spectrophotometer. Thermal analyzer (Perkin Elmer TGA 4000) was used to obtain TGA curves.

Extreme caution was exercised while preparing samples for analyzing FTIR, XRD, UV VIS, HPLC, and TGA so as to ensure the following errors do not affect the quality of sample prepared and final measurement:

- i) Static error which includes reading, characteristic and environmental error.
- ii) Instrument loading error

- iii) Systemic or random errors

All the instruments were handled with precision and care following the standard operating procedure.

4.3.6. Tablet preparation

The tablets were prepared by direct compression method. The ingredients of the tablet were passed through a 0.150 mm sieve to achieve a uniform particle size distribution before mixing. Predetermined weight of the drug and aminated starch were then mixed for 10 minutes in a cubic mixer followed by the addition of magnesium stearate as binder and Aerosil® 200 as a coating agent. The contents were then blended for another 5 minutes. The tablets were compressed with the help of single-punch tablet machine with 7-mm round flat punch set. The weight of the tablets was kept constant as 1000 mg and their thickness were adjusted to ~2.5 mm (**Fig 12**). The tablets were then stored away from light in an airtight container for further studies [130].



Figure 12: Aminated starch fenamate matrix tablet by direct compression method.

4.3.7. Swelling and erosion analysis

The tablets were weighed and fixed on glass slides followed their immersion in Petri dish containing simulated intestinal media (pH 7.2) at a constant temperature of 37 °C. The tablets were removed after fixed time intervals, excess media was wiped with filter papers, and the swollen tablets were weighed to check the swelling index (SI). These tablets were then kept at 60 °C for 24h to remove the excess water and their dry weight was then checked until a constant value is attained to calculate matrix erosion (ME) [131].

$$SI (\%) = \frac{100 (W_t - W_o)}{W_o} \quad \dots \text{Eq 3.2}$$

$$ME (\%) = \frac{100 (W_o - W_d)}{W_o} \quad \dots \text{Eq 3.3}$$

Where, W_t is the weight of swollen tablet at a given time interval; W_o is the initial weight of the tablet; and W_d is the weight of tablet after drying.

4.3.8. Drug release study

The tablets were added to simulated intestinal fluid (20 mL) containing pancrelipase at 28 °C kept in glass vials with constant stirring at 150 rpm. The media was withdrawn periodically at different time intervals and replaced with fresh medium. The amount of drug released in the simulated intestinal media was assessed with the help of HPLC by a pre-validated protocol.

4.3.9. Zeta potential assessment

Zeta potential measurements were employed to evaluate the impact of various diamine substructures on the surface electric charges of starch when subjected to acidic conditions. The zeta potential of diamine-modified starch was assessed in comparison to that of chitosan and unmodified starch. This assessment was conducted at a concentration of 1 mg/mL in a 0.1 mM citric acid-sodium phosphate dibasic buffer with pH values ranging from 3 to 7, all maintained at room temperature. The zeta potential measurements were carried out using a Zetasizer Nano ZSP instrument from Malvern Instruments.

4.3.10. Mucoadhesion investigation

The mucoadhesive properties of the tablets were studied by rotating cylinder method. Porcine intestinal mucosa was freshly obtained from a local slaughterhouse and fixed on a stainless-steel cylinder. The Tablets were fixed on the mucosa with the help of cyanoacrylate glue, followed by the placing of cylinder in dissolution apparatus containing 0.1 M phosphate buffer maintained at 37°C and pH 6.8. The cylinder was then rotated at 35 rpm and the detachment time of tablets was recorded over 24 hours [132].

4.3.11. Drug release kinetics

The drug release kinetics were assessed with Higuchi, Hixson-Crowell, and Korsmeyer-peppas mathematical equations [131] [110] as given below:

Higuchi Equation

$$Q = K_H \cdot t^{1/2} \quad \dots\text{Eq 3.4}$$

Where 'Q' is the cumulative amount of drug released in time 't' and K_H is Higuchi constant.

Hixson-Crowell Equation

$$Q_0^{1/3} - Q^{1/3} = K_{HC} \cdot t \quad \dots\text{Eq 3.5}$$

Where Q_0 is the initial amount of drug, Q is the amount of drug remaining after time t, and k_{HC} is the rate constant.

Korsmeyer-peppas equation

$$Mt/M = K_m \cdot t^n \quad \dots\text{Eq 3.6}$$

Where Mt/M is the fraction of drug released in time t, K_m is the kinetic constant, and n is the diffusion or release exponent.

4.4. Results and discussion

Aminated starch was prepared by **Fig 13** and its formation was confirmed with IR-spectra. The native starch was first oxidized to dialdehyde starch, which was qualitatively confirmed with Schiff's reagent. The appearance of a prominent peak at 1710 cm^{-1} in the IR spectra further confirms the presence of an aldehyde group. The percentage of aldehyde content was calculated rapid quantitative alkali consumption method and it was found to be 69%. Mechanochemical reaction of dialdehyde starch with ethylene diamine results in the formation of aminated starch, which gives negative test with Schiff's reagent thereby confirming the consumption of dialdehyde groups. The peak at 1630 cm^{-1} and a broad peak 3195 cm^{-1} in the IR spectra confirms the presence of imine linkage and primary amine functionality respectively (**Fig 14**).

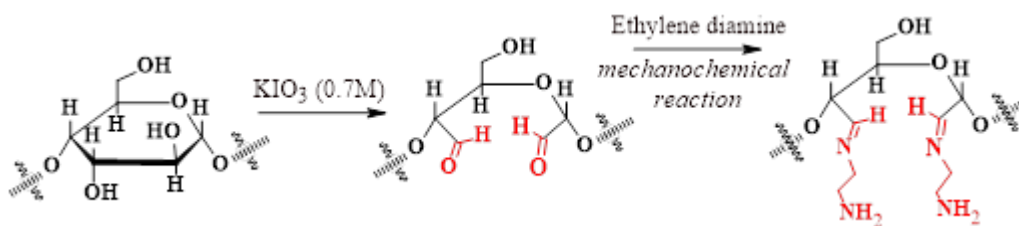


Figure 13: Synthesis of aminated starch

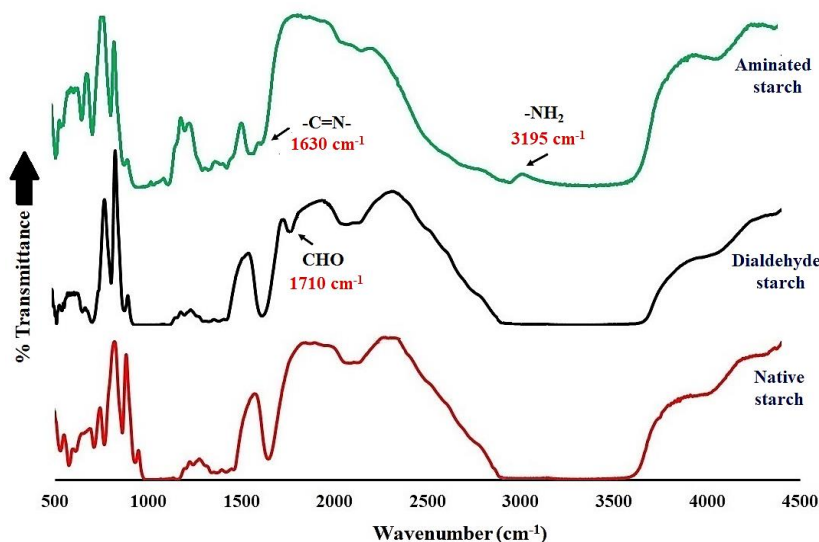


Figure 14: IR-spectra of native starch, dialdehyde starch, and aminated starch

The chemical modification of native starch results in a significant loss of crystallinity as suggested in the XRD spectra (**Fig 15**) where the intensity of peaks corresponding to the amylose and amylopectin in the native starch at $2\theta = 15^\circ$, 23.5° , and a doublet between $2\theta = 16^\circ - 18^\circ$ saw a significant decrease. The XRD pattern of the amorphous region in the starch is still retained. This may be an indication of a preferential oxidation of the amylose content and double helices of amylopectin in native starch that resulted in a loss of crystal structure thereby causing a loss of peak intensity in the crystalline region of native starch. Although amorphous regions are more prone to oxidation, the retention of amorphous region on XRD might be due to a low oxidation rate (69%) in the presence of KIO_3 [133].

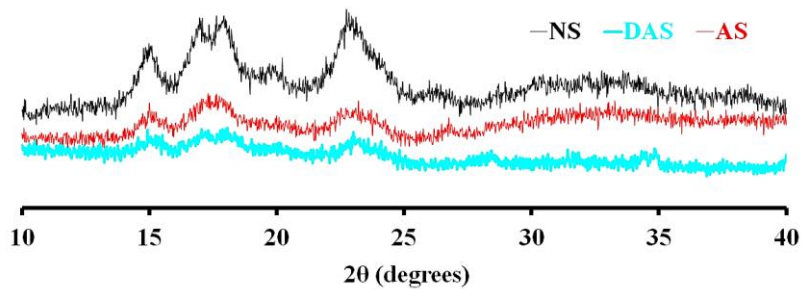


Figure 15: XRD of native starch, dialdehyde starch, and aminated starch

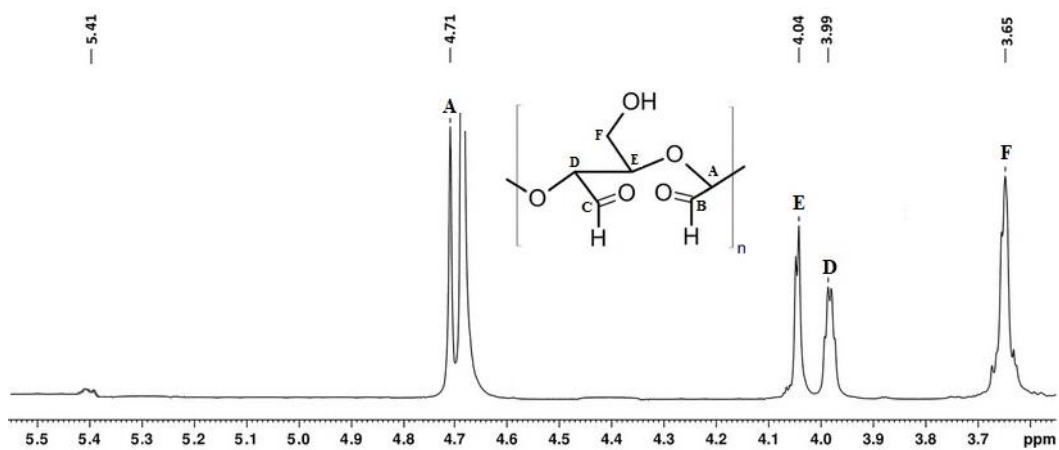


Figure 16: ^1H NMR of dialdehyde starch (DAS) in D_2O

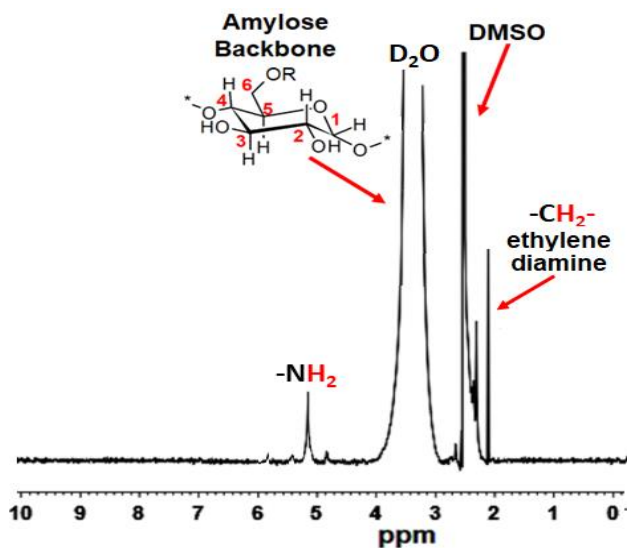


Figure 17: ^1H NMR of aminated starch in $\text{D}_2\text{O} + \text{DMSO}$

¹H NMR of DAS indicates peaks corresponding to all the CH protons on the intact monomer of starch except CH protons corresponding to C_c and C_b which are normally observed at 5.41. For the reported DAS, these protons are only observed as minor peaks, and not as sharp signals as for the other CH protons. This may be due to 69% conversion of NS to DAS. The peaks corresponding to CHO protons were very feeble. Thus, Schiff's reagent was used to further confirm the synthesis of DAS (**Fig 16**). ¹H NMR of AS was recorded with a mixture of D₂O and DMSO. The spectra show the peaks corresponding to CH₂ protons and NH₂ protons whereas most of the protons corresponding to the native starch backbone were merged into the solvent signals (**Fig 17**).

Thermogravimetric analysis (TGA) of native starch, dialdehyde starch, and aminated starch further indicates the loss of crystallinity or preferential oxidation of amylose content (**Fig 18**). The native starch shows a fast rate of decomposition which begins at 300 °C, with only 10% of the remaining material at 500 °C and complete decomposition is reached at 650 °C. The sharp decomposition near 300 °C is an indicative of high percentage of crystalline amylose in the native starch. In comparison, the decomposition of dialdehyde and aminated starches starts before 300°C, and follows a slower rate, with 25% of the material remaining at 500 °C. In addition, the decomposition is not completed till 700 °C with 15% and 10% of the material corresponding to dialdehyde starch and aminated starch respectively remaining.

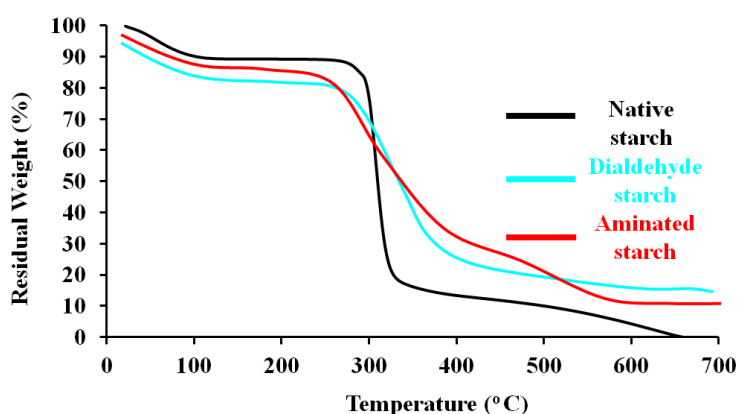


Figure 18: TGA of native starch, dialdehyde starch, and aminated starch

4.4.1. Drug release

The drug release profile was studied for aminated starch-fenamate formulations for flufenamic acid, maclofenamic acid, tolfenamic acid, and mefenamic acid. The release media was chosen as simulated intestinal media (**Fig 19**), simulated intestinal media with pancrelipase enzyme (**Fig 20**), and simulated gastric media (**Fig 21**). A controlled release profile was observed for the drugs from tablets in the simulated intestinal media where the drug release was sustained after an initial fast release and the plateau was reached at 10 hrs. Mainly, 60% of the drug was released into the simulated intestinal media at 10 hrs, which reached up to a maximum of 80% till 24 hrs, meaning that the drug release was not completed even at 24 hrs. This observation may be arising due to an initial release of free drug molecules, whereas the stability of imine linker of aminated starch prevented the premature drug release into the simulated intestinal media [49]. However, a different trend was observed for the simulated intestinal media containing pancrelipase enzyme. In this case, the drug release was quite rapid initially and continued till 14 hrs where an average of 75% drug was released in most cases. Plateau is not reached in this case, however the further release of the drug is decelerated as for the next 12 hours, an average of 15% of the drug was released in all the cases. Overall, a total of 90% drug release was completed in the simulated intestinal media containing pancrelipase. The release profile can be justified due to the presence of the enzyme which facilitates the degradation of glycosidic bonds in aminated starch thereby accelerating drug release. However, the stability of imine linker still maintains the controlled release profile of aminated starch. Alternatively, a completely different trend was observed for simulated gastric media where the drug release was 60% till 12 hrs and it completed to 100% at the end of 24 hrs. The drug release profile in simulated gastric media followed an almost similar trend during the first 10-12 hrs as that of the simulated intestinal media with and without pancrelipase. This observation might be arising due to a significant swelling behaviour of aminated starch-fenamate tablets due to protonation of amine groups at acidic pH which prevent the premature drug release in the dissolution media

[134]. However, the drug release accelerated further and reached completion due to the susceptibility of imine linkage of aminated starch towards acidic pH, which results in the completion of drug release in the simulated gastric media [135]. Nevertheless, in all the cases, the drug release was not rapid throughout, and it mainly slowed down after 12 hrs. This observation may be ascribed to the excellent swelling behaviour of aminated starch and increase in the amorphous nature during chemical modification, however further studies are needed to validate this hypothesis.

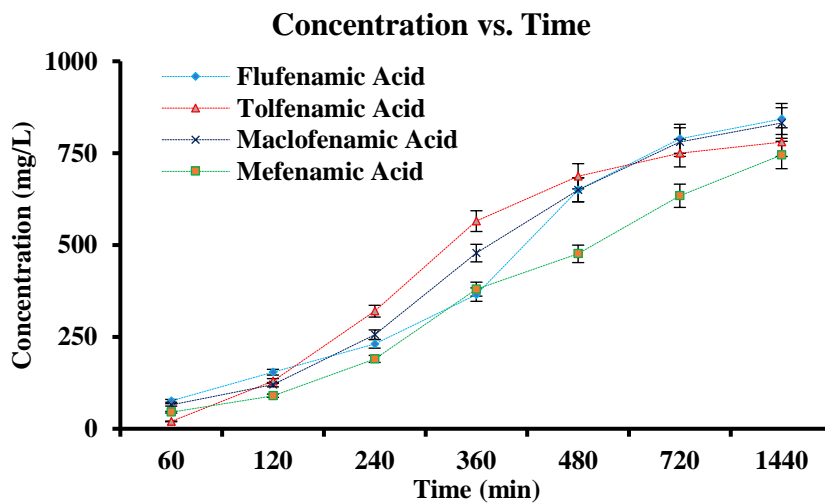
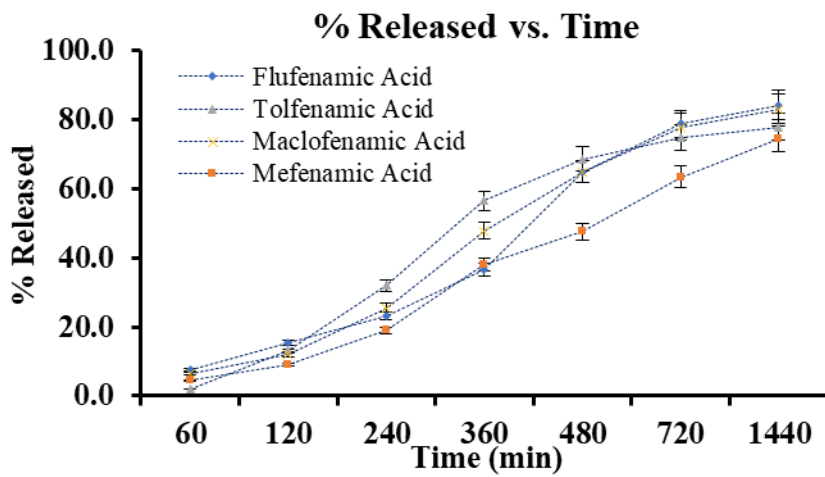
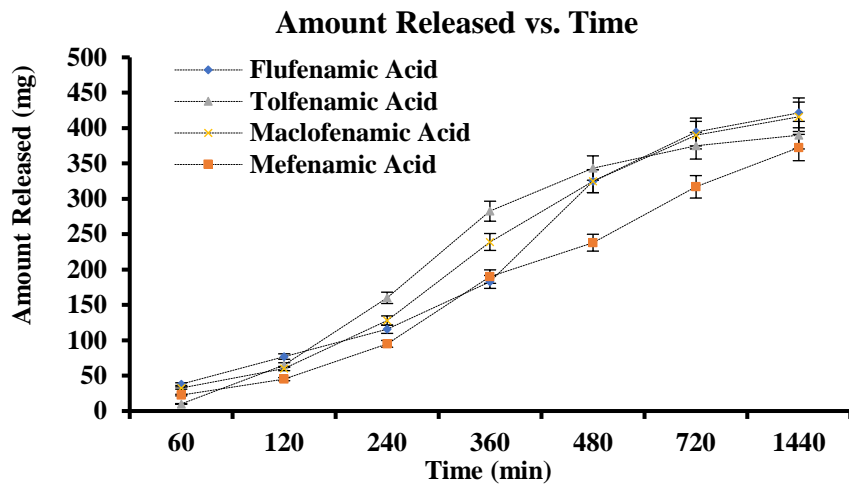


Figure 19: Drug release profile of fenamates in simulated intestinal media

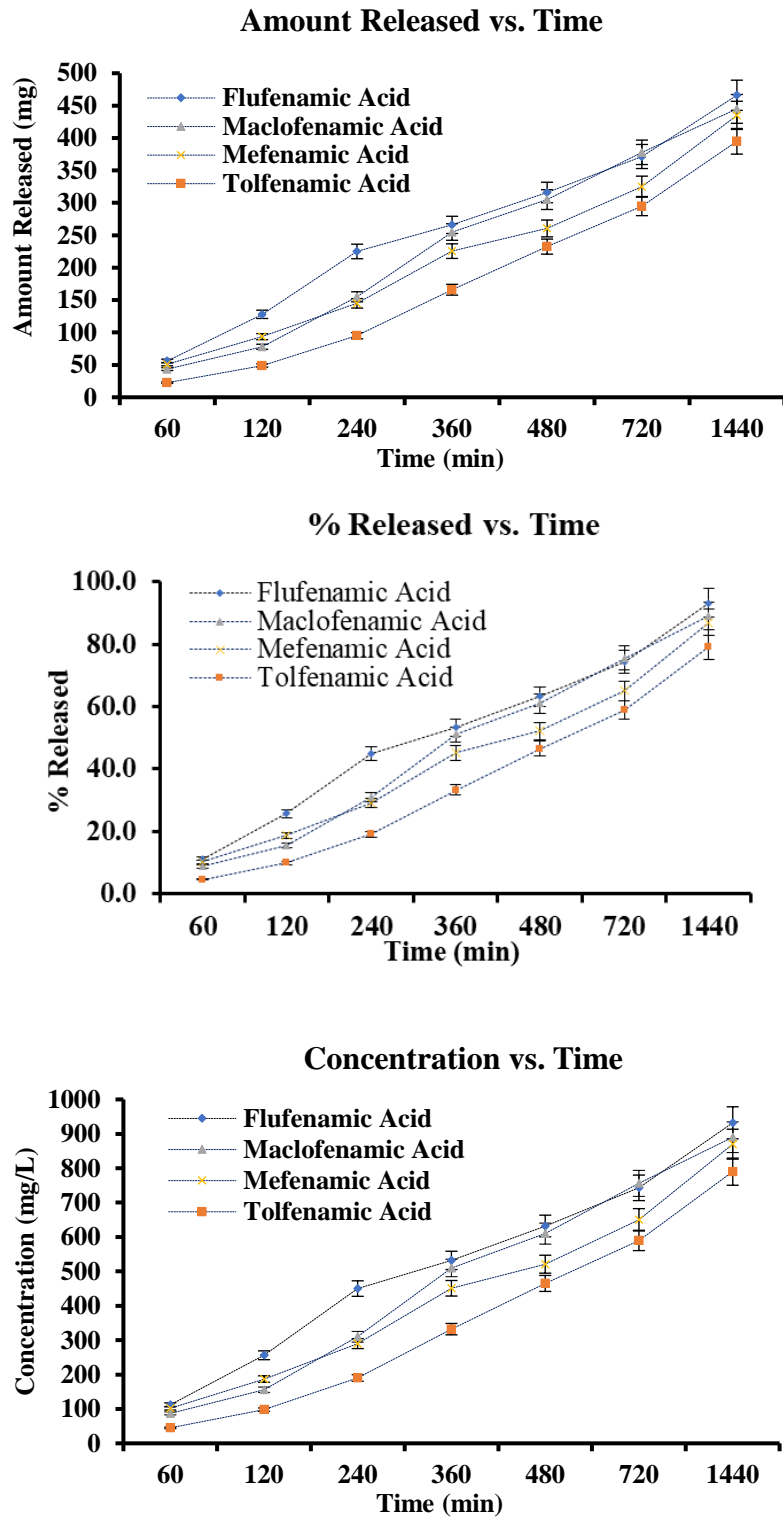


Figure 20: Drug release profile of fenamates in simulated intestinal media containing pancrelipase

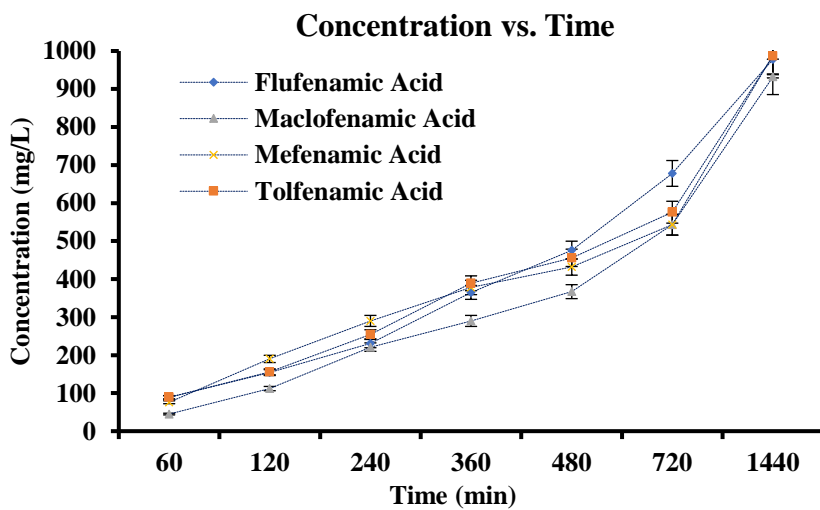
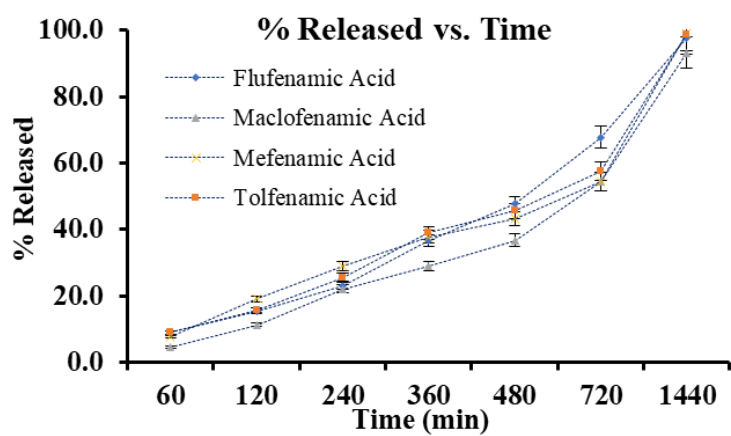
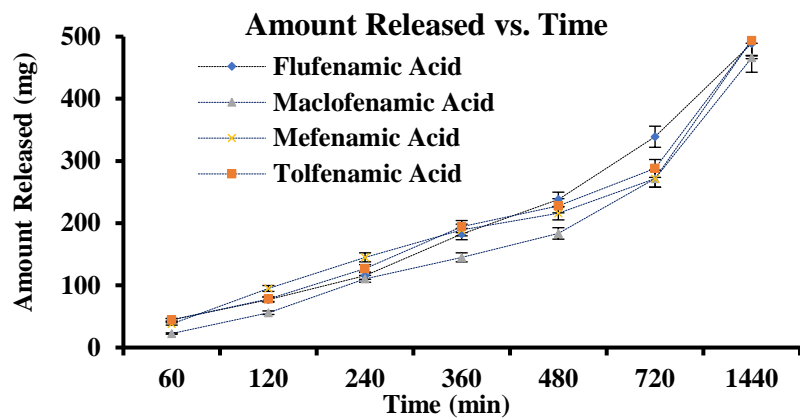
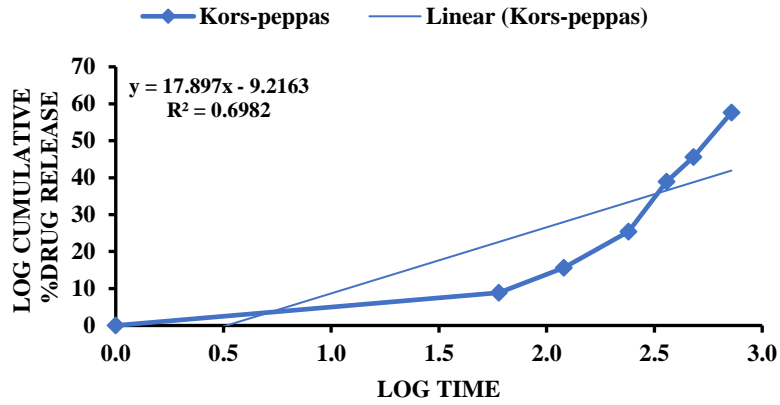


Figure 21: Drug release profile of fenamates in simulated gastric media

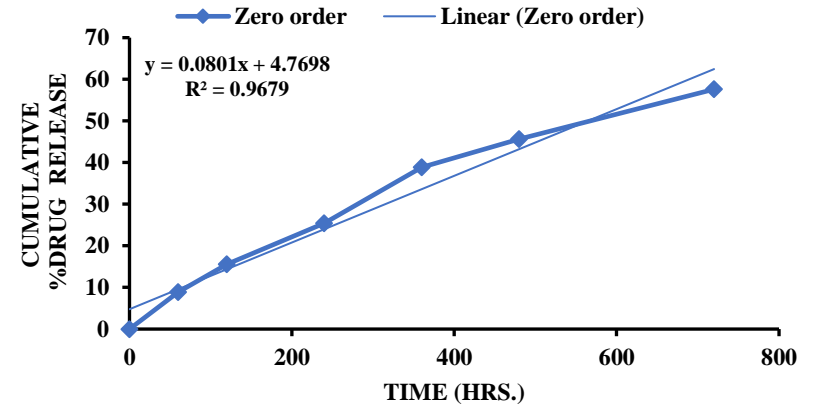
4.4.2. Kinetics of Release

The behaviour of release of all the four drugs used in the present study was assessed and the release data obtained in vitro was fitted to various kinetic models for calculating the drug release kinetic constants and correlation coefficients (R^2) of each drug in all the simulated conditions applied in the experiment. Data from in vitro drug release studies were plotted as log cumulative percentage drug release vs log time in order to analyse the release kinetics. Zero order kinetics provided best correlation coefficients thereby indicating the mechanism of drug release to be independent of its initial concentration. Furthermore, while fitting data to Korsmeyer-peppas model, a non-Fickian kinetics for drug release was observed. It is because on contacting the dissolution media (simulated intestinal media containing pancrelipase), the aminated starch-fenamate tablets undergo rapid swelling and erosion of the tablet matrix over time causing a release of the drug molecules. However, the transferring of dissolution media after fixed time intervals provides time for regeneration of the gel layer present on the surface of tablets (due to rapid swelling), thereby controlling the release rate of the drug. Furthermore, degradation of glycosidic bonds in the parent polymer molecules (aminated starch) by pancrelipase in the dissolution media facilitates drug release (**Fig 22-25**). Overall, both diffusion from the aminated starch matrix, and erosion/ degradation of glycosidic bonds of aminated starch by pancrelipase are the contributing factors for drug release in the Korsmeyer-peppas model.

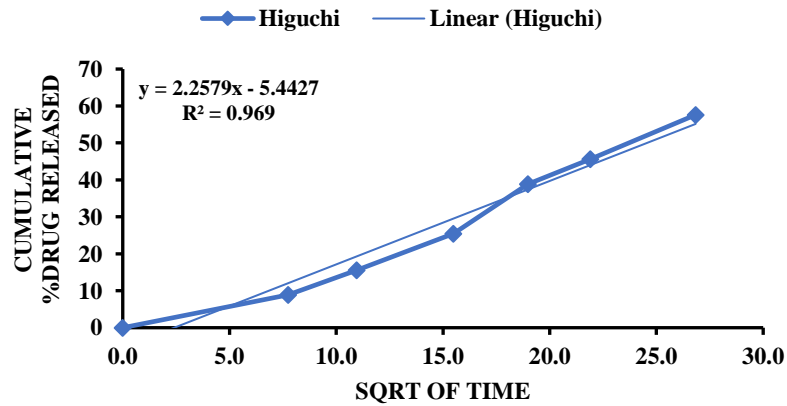
KORS-PEPPAS



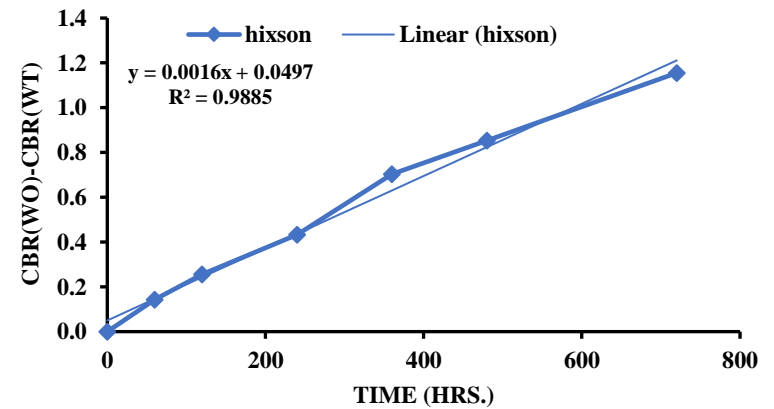
ZERO ORDER



HIGUCHI

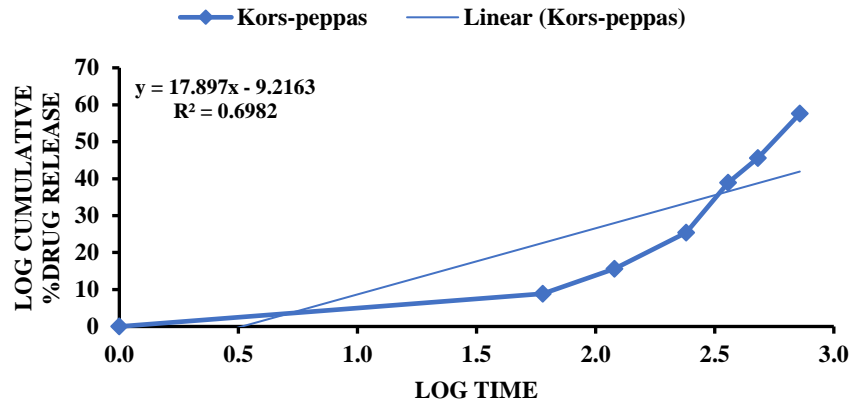


HIXSON

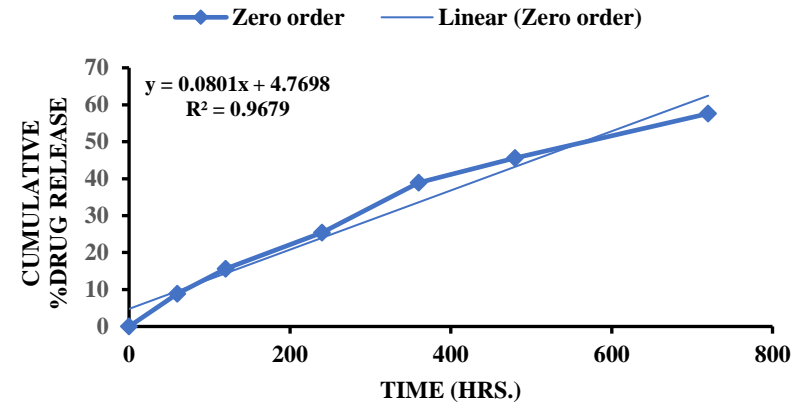


(A) Flufenamic acid in simulated intestinal medium

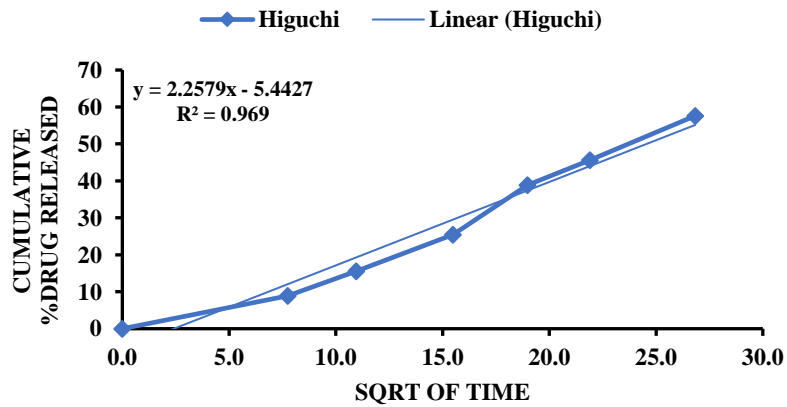
KORS-PEPPAS



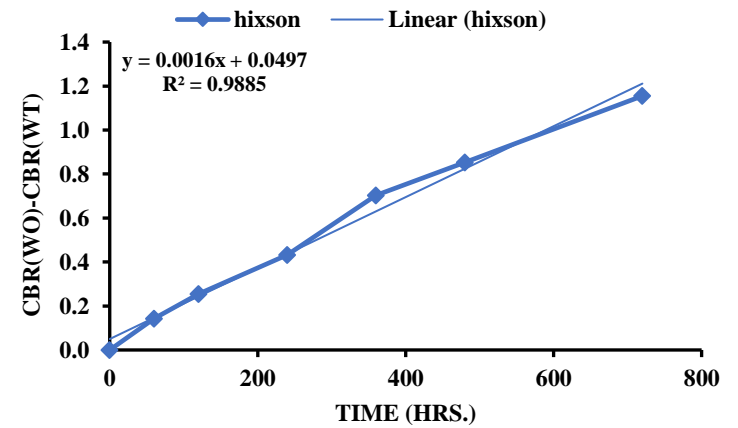
ZERO ORDER



HIGUCHI

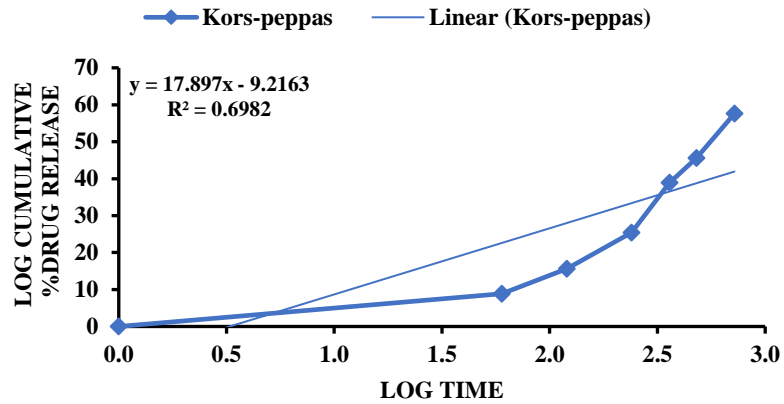


HIXSON

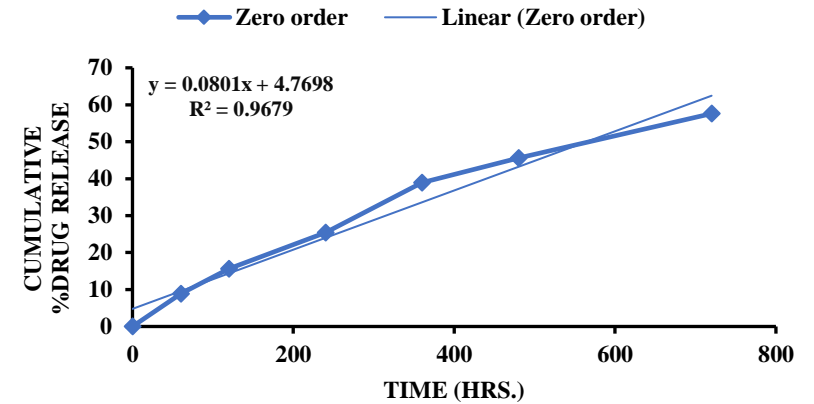


(B) Flufenamic in simulated intestinal medium with pancrelipase

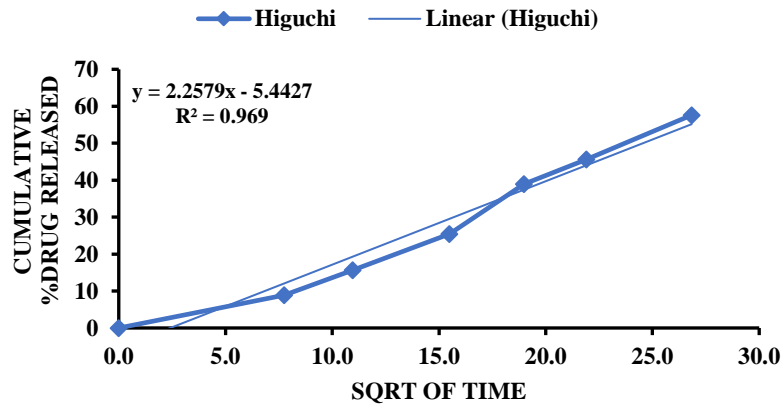
KORS-PEPPAS



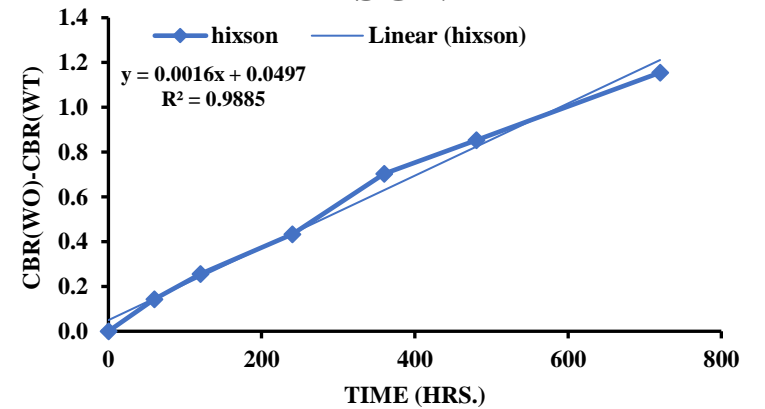
ZERO ORDER



HIGUCHI



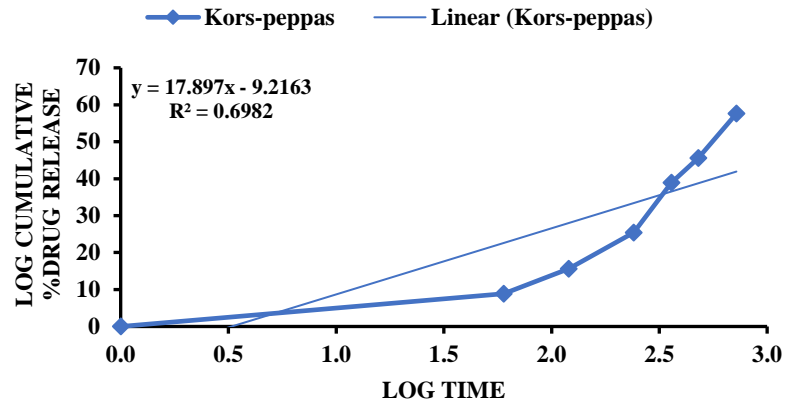
HIXSON



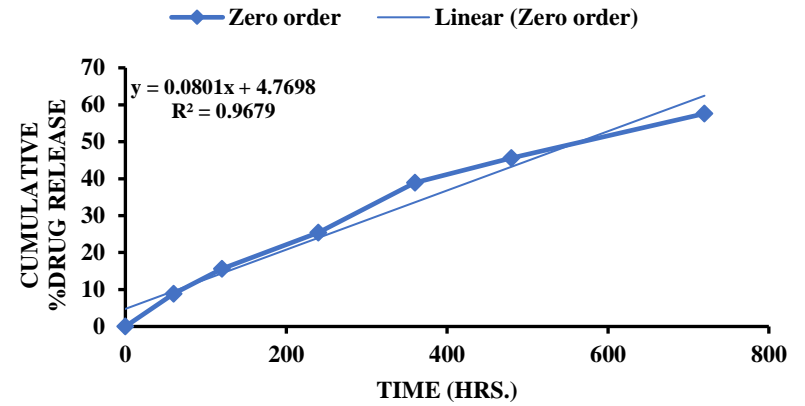
(C) Flufenamic acid in simulated gastric medium

Figure 22: Kinetics of release of Flufenamic acid in simulated conditions of intestinal medium (A), simulated intestinal medium with pancrelipase (B) and simulated gastric medium (C)

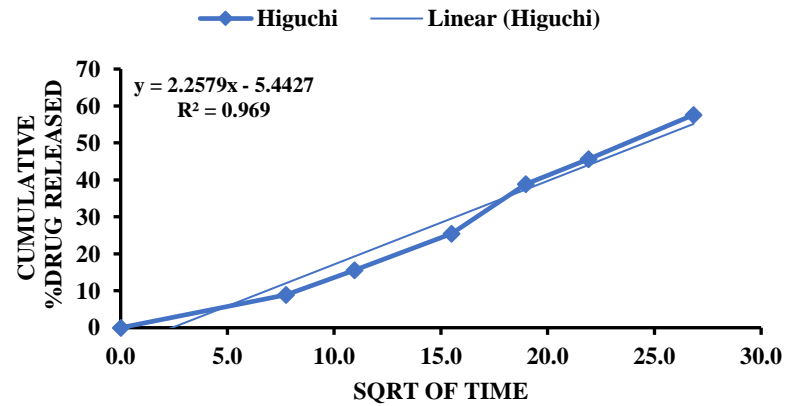
KORS-PEPPAS



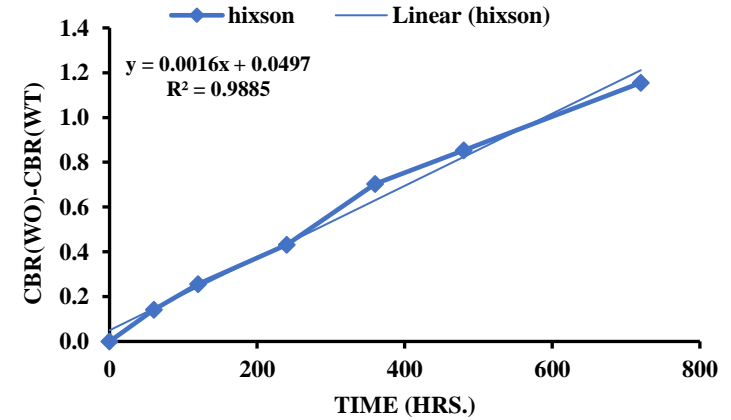
ZERO ORDER



HIGUCHI

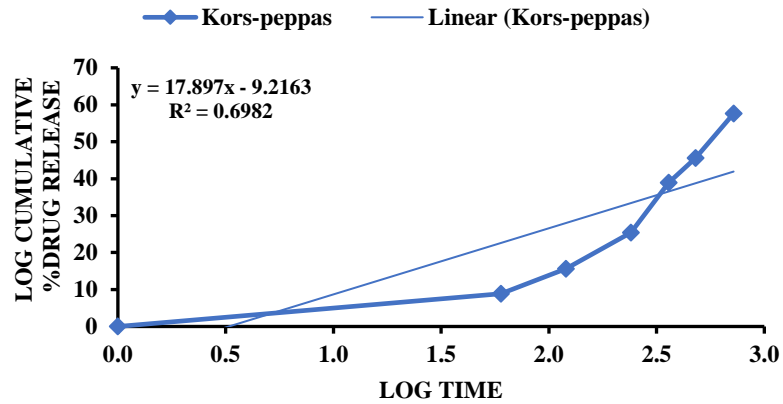


HIXSON

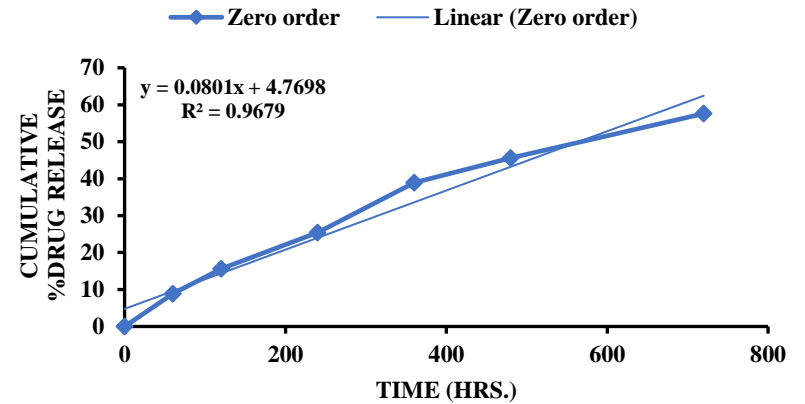


(A) Tolfenamic acid in simulated intestinal medium

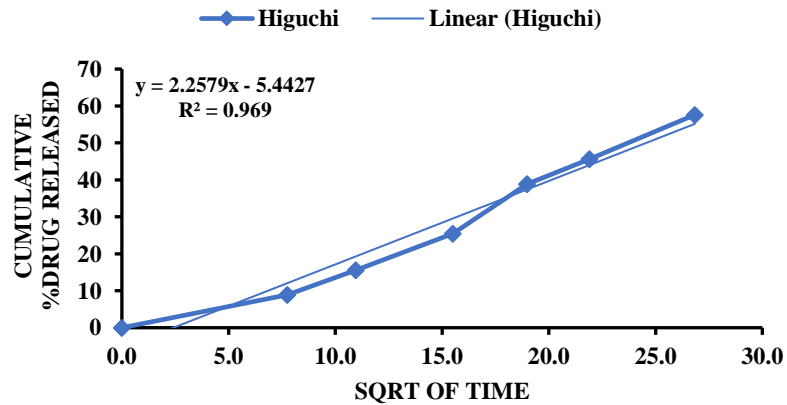
KORS-PEPPAS



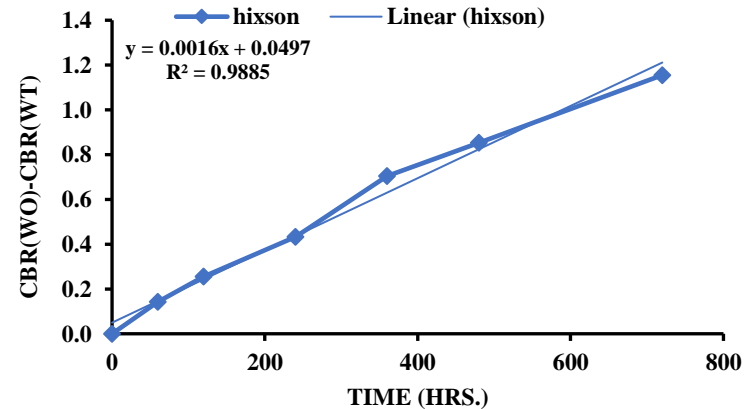
ZERO ORDER



HIGUCHI

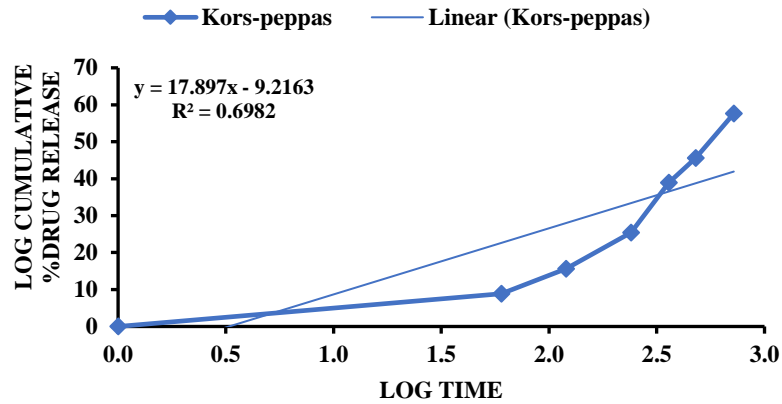


HIXSON

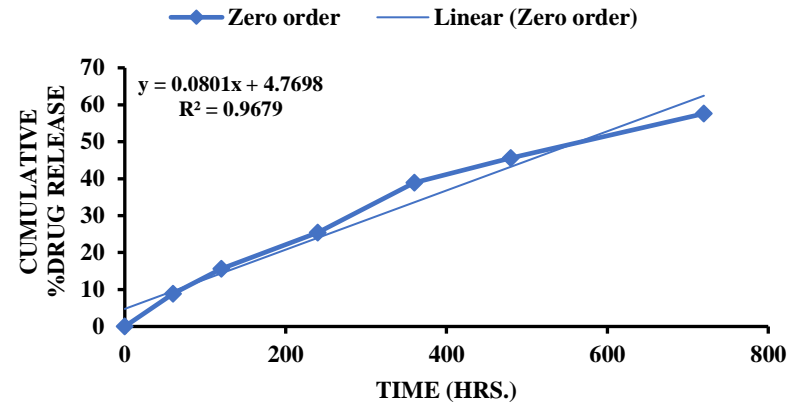


(B) Tolfenamic acid in simulated intestinal medium with pancrelipase

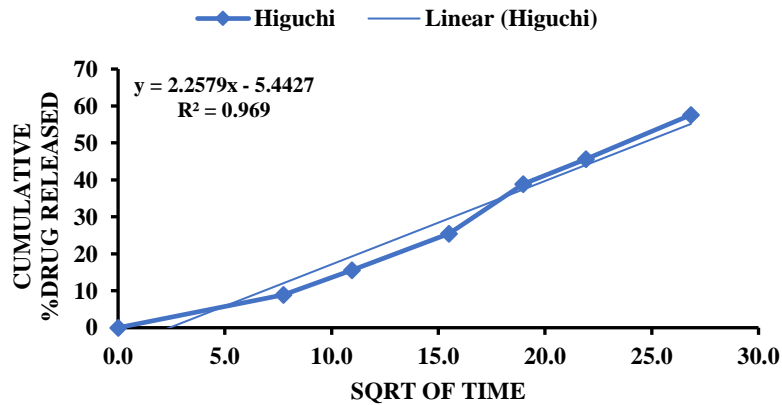
KORS-PEPPAS



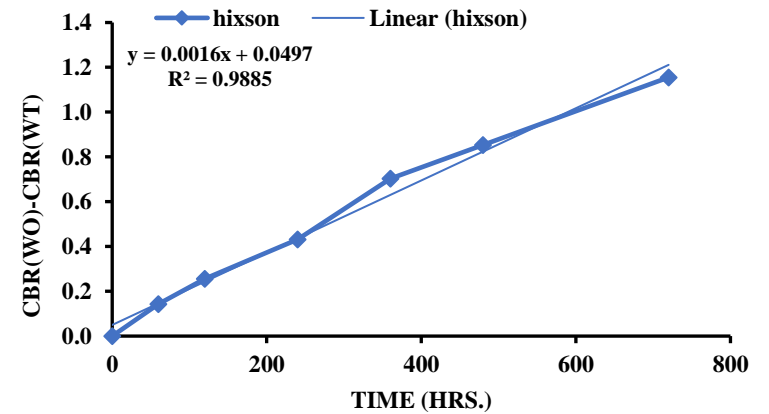
ZERO ORDER



HIGUCHI



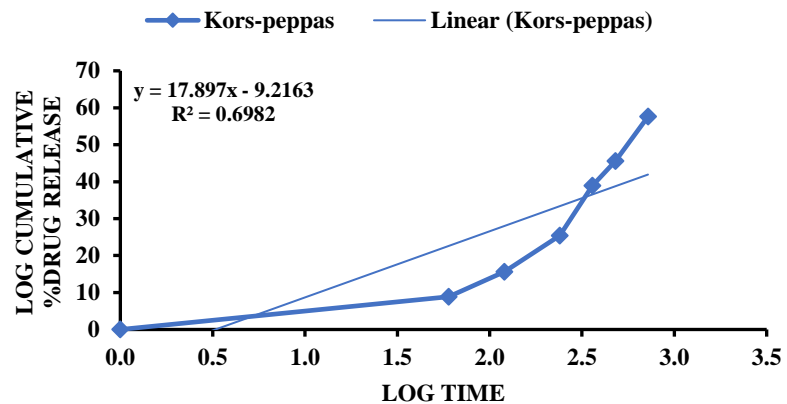
HIXSON



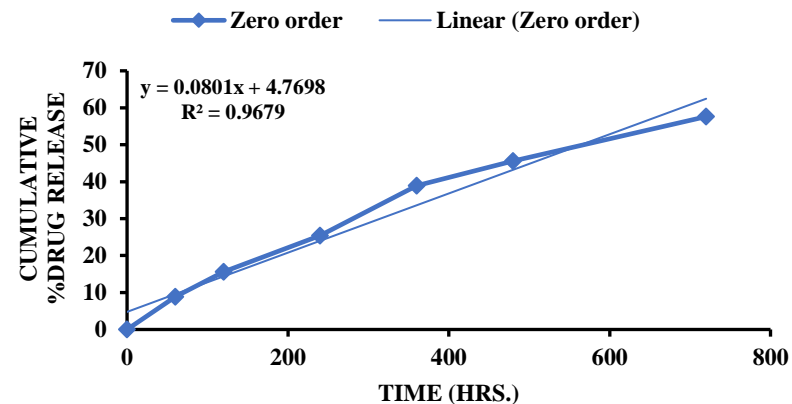
(C) Tolfenamic acid in simulated gastric medium

Figure 23: Kinetics of release of Tolfenamic acid in simulated conditions of intestine medium (A), simulated intestinal medium with pancrelipase (B) and simulated gastric medium (C).

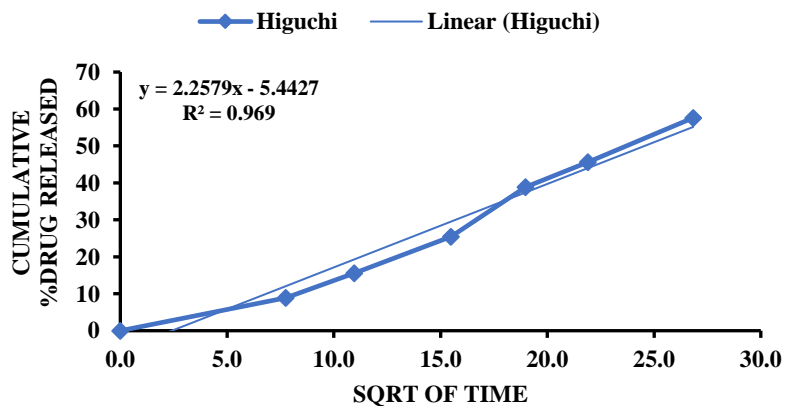
KORS-PEPPAS



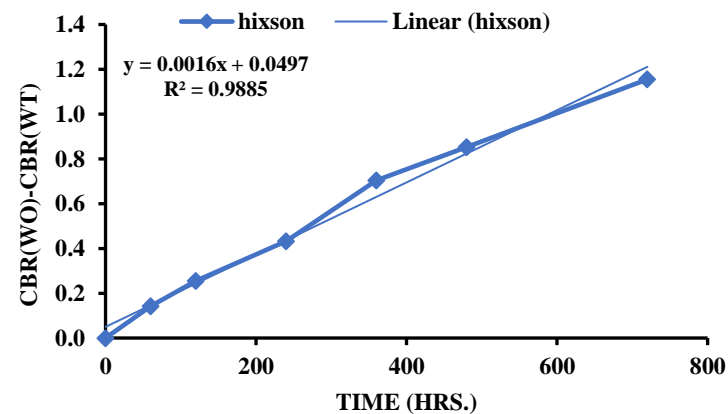
ZERO ORDER



HIGUCHI

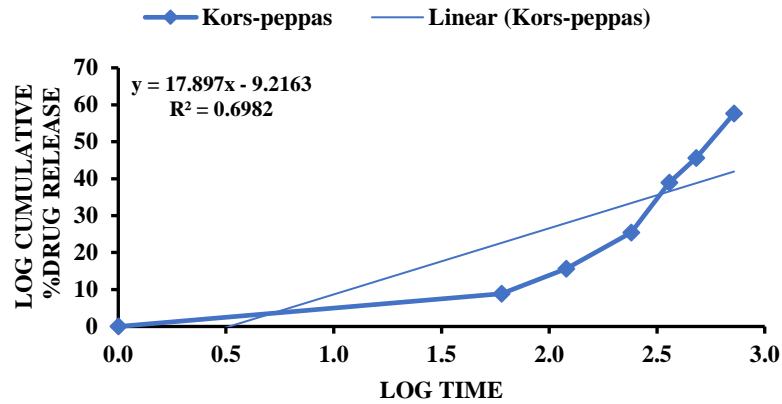


HIXSON

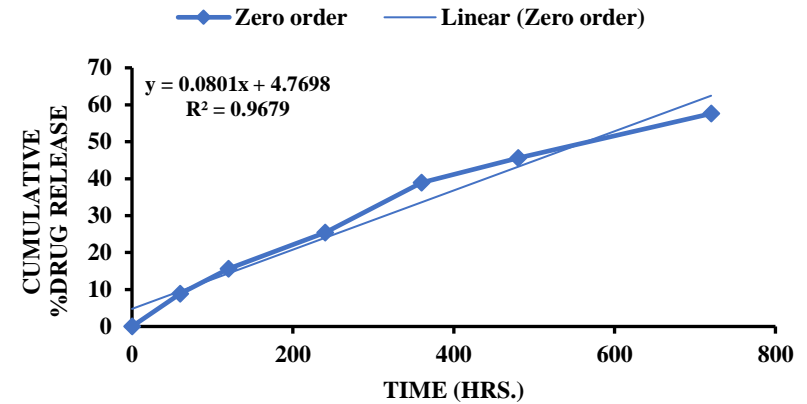


(A) Maclofenamic acid in simulated intestinal medium

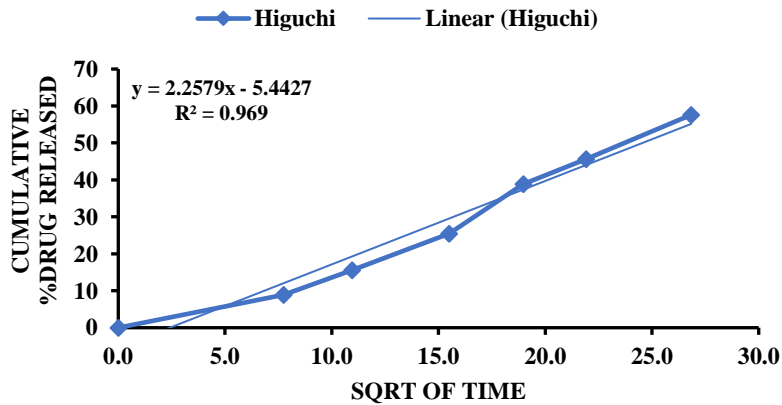
KORS-PEPPAS



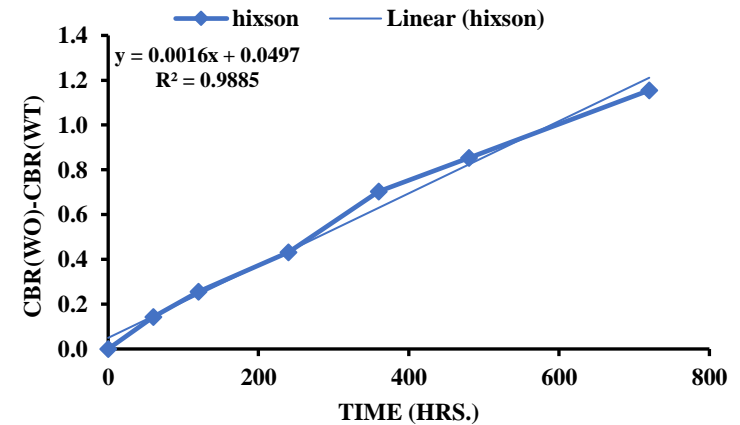
ZERO ORDER



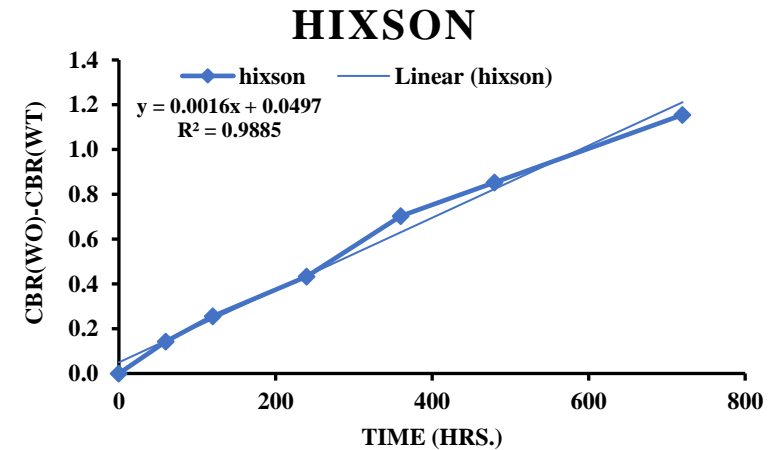
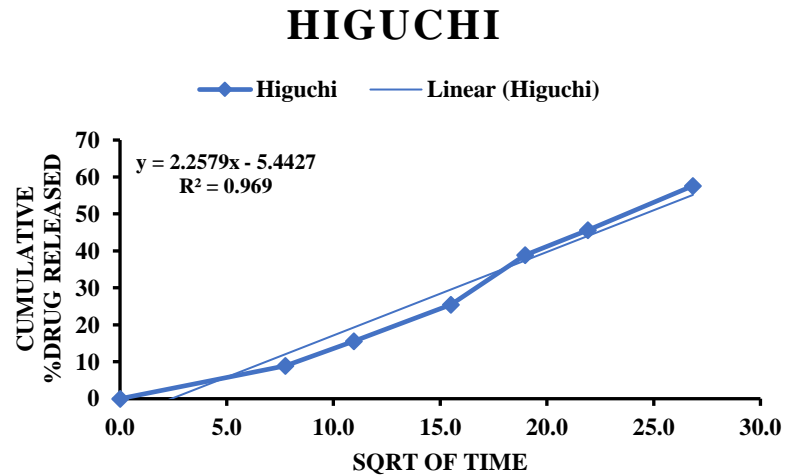
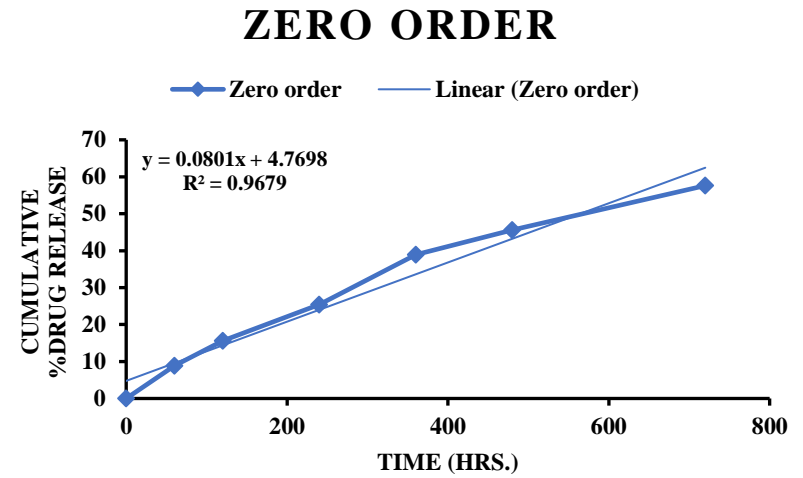
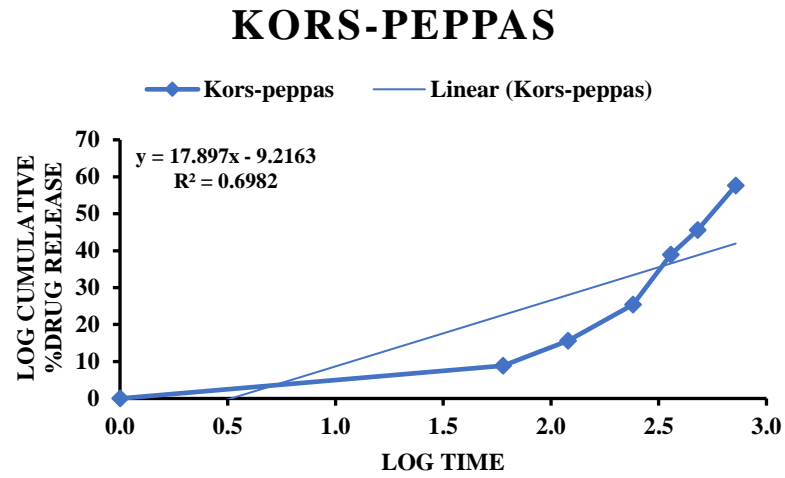
HIGUCHI



HIXSON



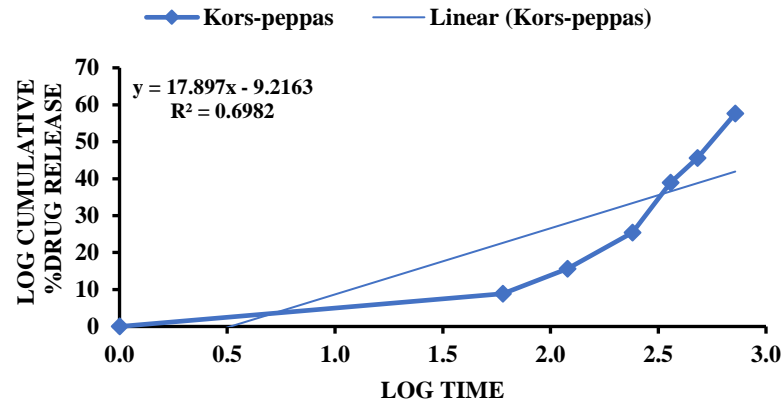
(B) Maclofenamic acid in simulated intestinal medium with pancrelipase



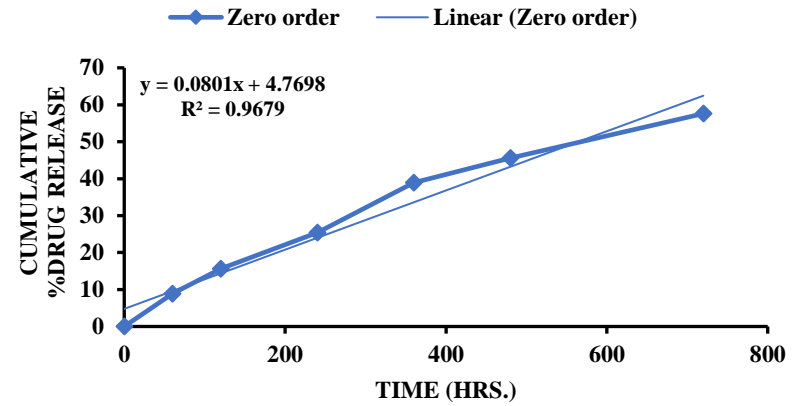
(C) Maclofenamic acid in simulated gastric medium

Figure 24: Kinetics of release of Maclofenamic acid in simulated conditions of intestine medium (A), simulated intestinal medium with pancrelipase (B) and simulated gastric medium (C).

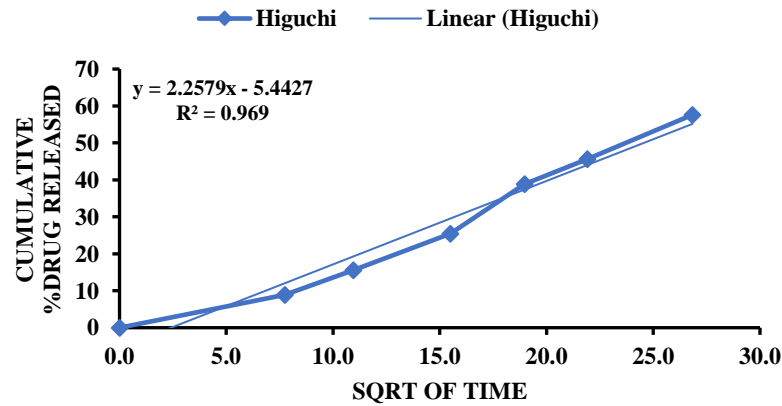
KORS-PEPPAS



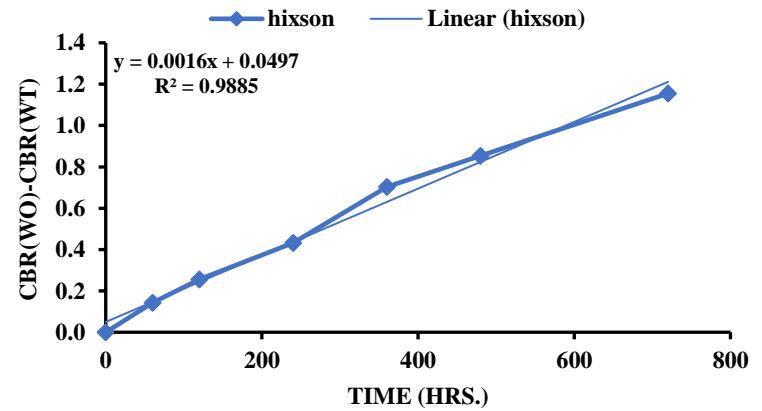
ZERO ORDER



HIGUCHI

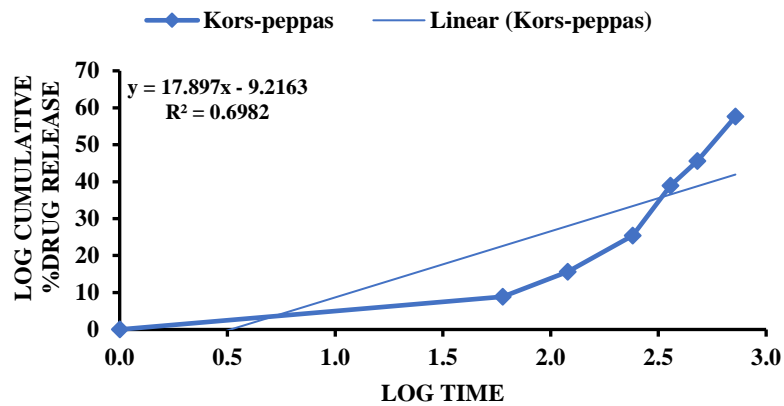


HIXSON

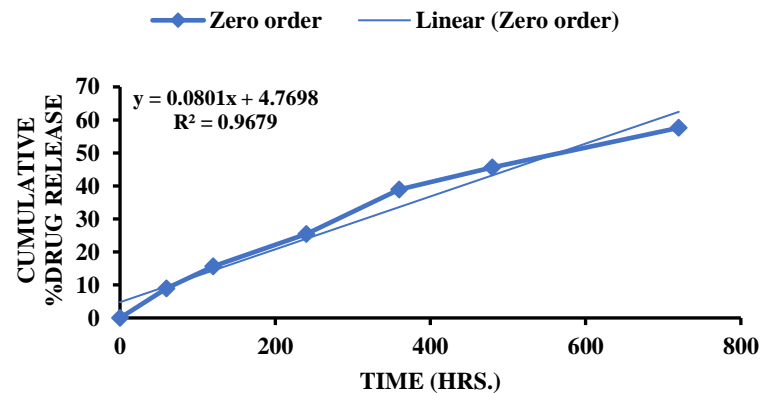


(A) Mefanamic acid in simulated intestinal medium.

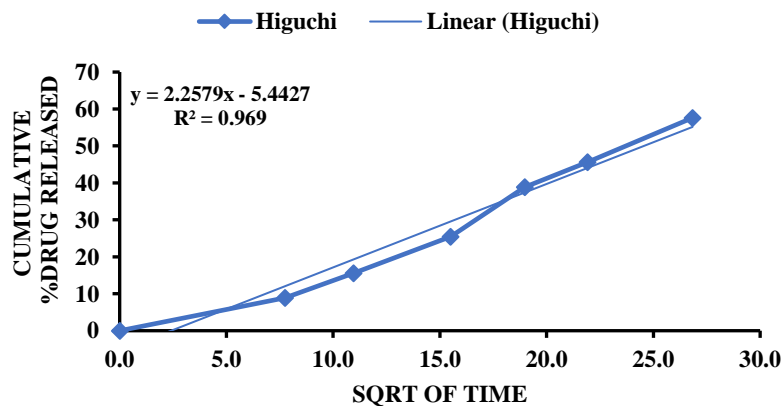
KORS-PEPPAS



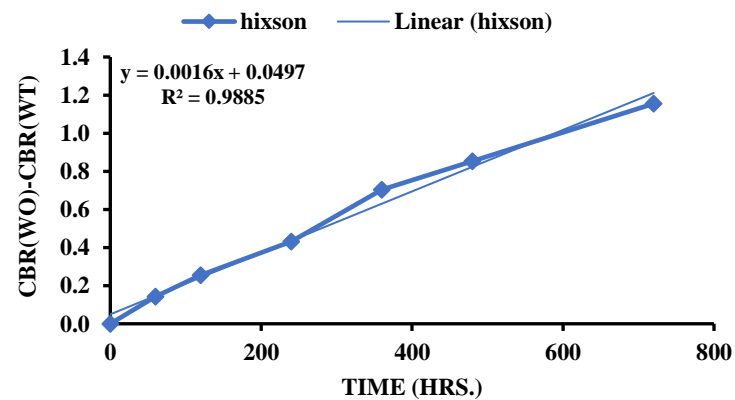
ZERO ORDER



HIGUCHI

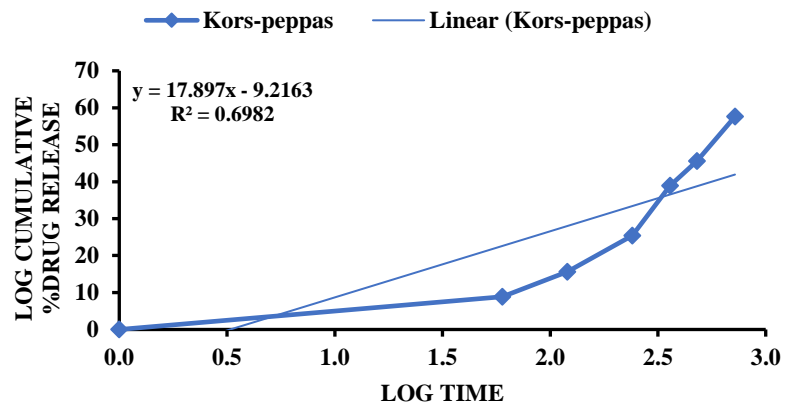


HIXSON

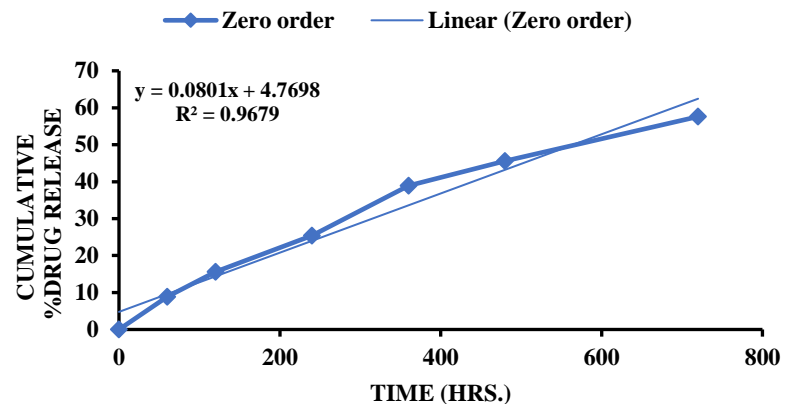


(B) Mefanamic acid in simulated intestinal medium with pancrelipase

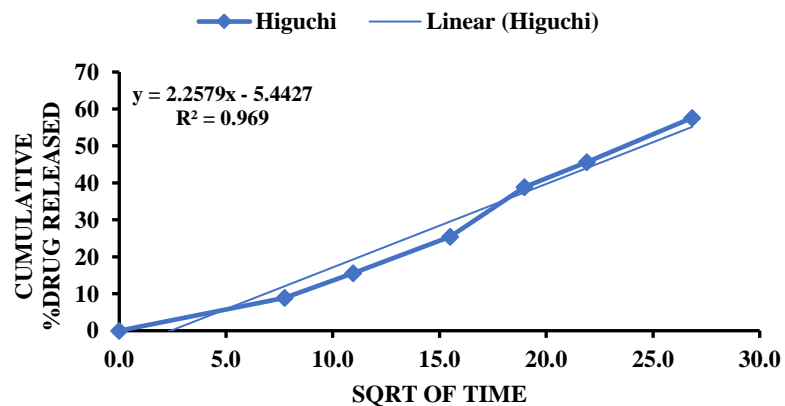
KORS-PEPPAS



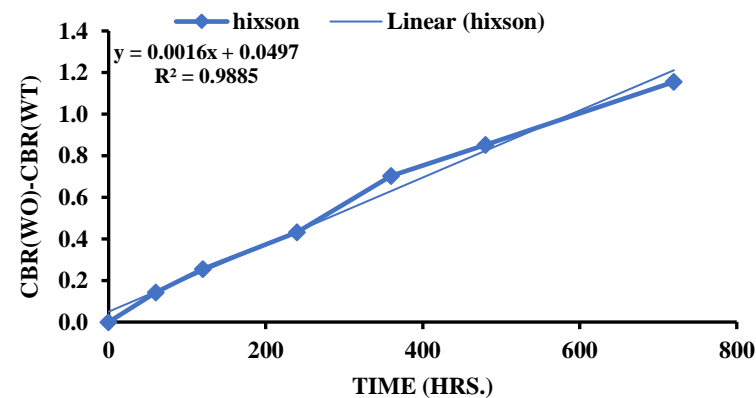
ZERO ORDER



HIGUCHI



HIXSON



(C) Mefanamic acid in simulated gastric medium

Figure 25: Kinetics of release of Mefanamic acid in simulated conditions of intestine medium (A), simulated intestinal medium with pancrelipase (B) and simulated gastric medium (C).

4.4.3. Swelling and matrix erosion

Fig 26 indicates the swelling index and matrix erosion profile for aminated starch-flufenamic acid tablets, where A, E are untreated tablets. The tablets showed a better swelling index in the simulated intestinal media (F, Fig 26) without the loss of matrix as evidenced from the dry weight calculations (B, Fig 26). The swelling index was lower in the simulated intestinal media containing pancrelipase (G, Fig 26) and the matrix erosion begins to appear (C, Fig 26) due to the onset of enzymatic degradation of glycosidic linkages in aminated starch. The swelling index was poor in simulated gastric media (H, Fig 26) and a significant amount of matrix was lost (D, Fig 26) due to the reactivity of imine linkage in aminated starch towards acidic pH.

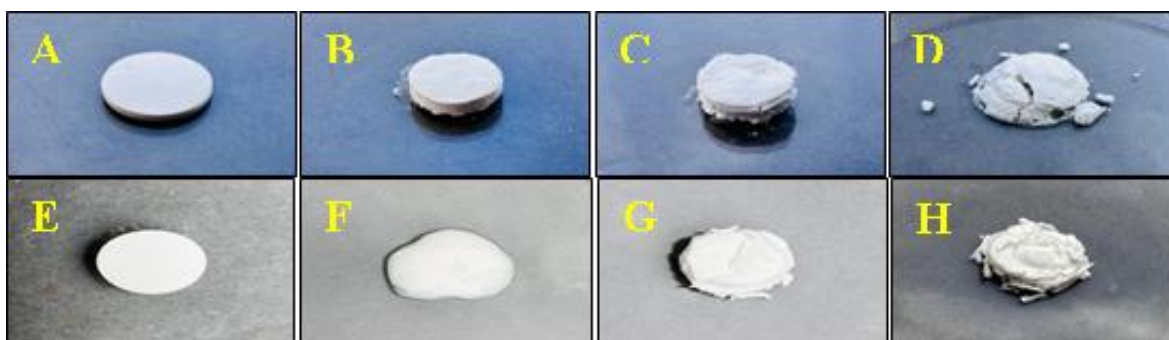


Figure 26: Swelling and matrix erosion studies for aminated-starch-fenamate tablets

The behaviour of tablets in the simulated intestinal media was further assessed by placing them in bulk media in the presence of pancrelipase. Apparently, it was seen that matrix erosion started appearing at 4 hrs, but the swelling was not very prominent. At 12 hrs, the matrix erosion intensified further, and at 24 hrs the complete erosion of matrix occurs resulting in the dissolution of tablets in the media (**Fig 27**). The aminated starch granules at 24 hrs begin to show rapid swelling, which might have prevented the completion of drug release in the bulk media. Furthermore, it is apparent that most of the drug released in the initial 12 hrs can be attributed to the matrix erosion.



Figure 27: Behaviour of tablets in bulk of simulated intestinal media containing pancrelipase.

4.4.4. Mucoadhesive profile

Diaminated starch-fenamic acid tablets showed a 2-fold improvement in the mucoadhesive profile as that of native chitosan. This is indicated by a delayed detachment time of an average 50 hrs for aminated starch, which is 2-fold as compared to chitosan for which the average detachment time is 24 hrs. For native starch tablets, the average detachment time was only 25 minutes (**Fig 28**). The considerable mucoadhesive strength of diaminated starch-fenamic acid tablets may be attributed to their cationic nature due to the presence of amine groups that facilitate their adhesion to the oppositely charged intestinal mucosa [71].

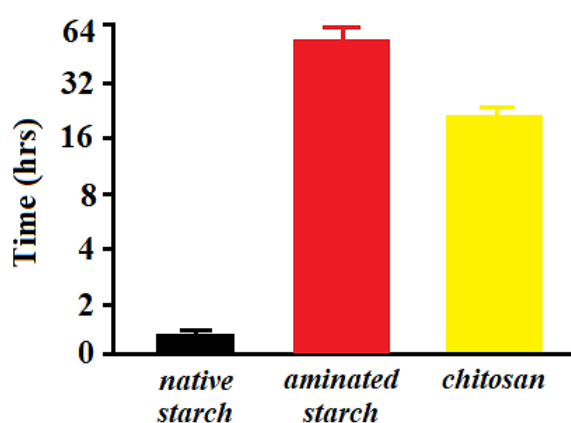


Figure 28: Assessment of the mucoadhesive strength of native starch, aminated starch and chitosan by rotating cylinder method. The values shown in the figure are an average of three experiments.

4.4.5. Zeta potential

As a result of the protonation of amine groups, aminated starch exhibited a conspicuous positive zeta potential under acidic pH conditions, while the zeta potential of unmodified starch approached neutrality. The zeta potential of aminated starch and chitosan diminished as pH levels increased. Conversely, unmodified or native starch displayed a zeta potential that remained unaffected by variations in pH (**Fig 29**). The zeta potential of tested compounds at different physiological pH are listed in **Table 5**.

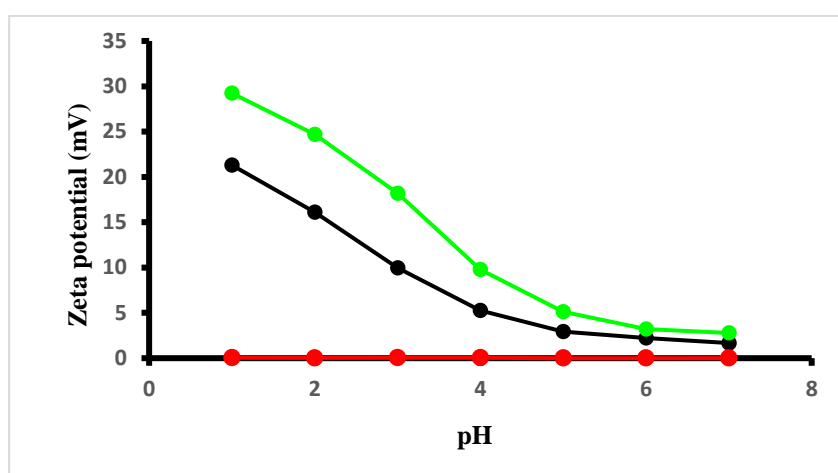


Figure 29: Zeta potential of: Aminated starch (in black), Native starch (in red) and Chitosan (in green) at indicated pH

Table 5: Zeta potential of Aminated starch, native starch and chitosan with respect to pH

pH	Zeta potential (mV)		
	Aminated starch	Native starch	Chitosan
1	21.29	0.04	29.23
2	16.11	0.03	24.67
3	9.97	0.04	18.19
4	5.25	0.04	9.78
5	2.92	0.003	5.1
6	2.21	0.003	3.21
7	1.67	0.001	2.78

4.5. Discussion

Aminated starch was characterized with FTIR spectroscopy, and XRD studies, which also indicated the preferential oxidation of crystalline region. TGA further confirmed these observations. The drug-release profile was studied in simulated gastric media, and simulated intestinal media with and without pancrelipase enzyme and the data were fitted to various mathematical models to evaluate the release kinetics. Rotating cylinder method was used to study mucoadhesive potential of tablets. The tablets achieved an initial fast release of fenamates, which eventually slows down after 12 h. Drug release was not completed in the simulated intestinal media (both with and without pancrelipase) which may be due to the stability of imine bond in aminated starch at weakly acidic pH. Drug release was completed in simulated acidic media even though initial release kinetics resembled that of the simulated intestinal media due to the hydrolysis of imine functionality at strongly acidic pH. The protonation of primary amine groups leading to considerable swelling prevents premature release of drug from tablets in both simulated gastric and intestinal media. Therefore, the aminated starch containing primary amine group and an imine functionality may serve as an ideal intestine targeted drug delivery system due to its stability at weakly acidic pH, controlled drug release profile and a remarkable mucoadhesive potential.

4.6. Conclusion

Aminated starch-fenamate tablets achieve a controlled release profile in the simulated intestinal media with and without the presence of pancrelipase enzyme. After an initial fast release of the drug, a controlled release profile is reached at 10 hrs due to the stability of imine linkage in aminated starch towards weakly acidic media. Furthermore, primary amines achieve sufficient protonation at this pH to maintain an ideal swelling index which facilitates a controlled release profile from the system. Whereas in the simulated gastric

media, the drug release was fast initially due to the degradation of imine linkage at strongly acidic media. However, the release profile followed that of the simulated intestinal media till 10 hrs due to the contribution of primary amine groups that become heavily protonated at acidic pH and gain sufficient swelling index to prevent a premature drug release and a burst release. The drug release is rather completed in the simulated gastric media pertaining to the degradation of carrier system which becomes devoid of the amine appendages owing to the hydrolysis of imine functionality at strongly acidic pH. The aminated starch-fenamate tablets show a remarkable mucoadhesive potential which is critical for the targeted drug delivery to the intestine. Furthermore, the controlled release profile achieved by aminated starch for fenamate NSAIDs may be useful for the prevention of ulcerogenicity.

4.7. Summary Points

- Mucoadhesive, controlled release tablets of fenamic acid based NSAIDs, based on aminated starch were prepared
- Thermogravimetric analysis and x-ray diffraction suggest preferred amination of the amylose component of starch
- The drug-release profile was studied in vitro in the simulated gut media in the presence of amylose digesting pancrelipase enzyme
- The tablets showed a slow and sustained (controlled) release of fenamic acid based NSAIDs
- Drug release was not completed till 24 h in different media indicating a slow-release profile
- The protonation of primary amine groups leading to considerable swelling prevents premature release of drug from tablets in simulated gut media
- Stability of imine linker in simulated intestine media was responsible for a slower drug release
- Susceptibility of imine linker toward acidic pH resulted in a completed drug release in the simulated gastric media
- Appreciable mucoadhesive strength of aminated starch tablets further suggests their efficacy in the gut environment.

Chapter 5: Design of magnetically guided drug delivery systems for V amylose drug complexes

5.1 Introduction and background

The area of material science has recently been exploiting natural polymers for the design of magnetic nanoparticle-based drug delivery systems (MDDs). Magnetic nanoparticles (MNP) comprise ferromagnetic, paramagnetic and superparamagnetic materials. Their unique physico chemical property renders them valuable and customizable drug nanocarriers in targeted drug delivery, tumor detection and as contrast agents in magnetic resonance imaging. The particles are made up of a magnetite core and natural polymers that serve as a shell [136]. Because of their low toxicity, ease of surface modification, biocompatibility and magnetic feature, MNPs are considered as next-generation drug/gene carriers with immense utility in diagnostics, theranostic and clinical science.

Magnetic nanoparticles have emerged as versatile entities with multifaceted roles in advancing both targeted drug delivery and theranostics, combining therapeutic and diagnostic functionalities within a unified platform [113]. In the domain of targeted drug delivery, magnetic nanoparticles function as carriers for therapeutic agents, affording a means to transport drugs, peptides, nucleic acids, and other cargoes to specific anatomical sites. Their modifiable surface properties permit functionalization with targeting ligands, enabling precise recognition and binding to particular cells or tissues. Following targeting, the nanoparticles can be maneuvered and concentrated at the intended location through the application of external magnetic fields, thereby augmenting drug accumulation while mitigating systemic exposure. This targeted strategy elevates the therapeutic efficacy of drugs and diminishes off-target effects, ultimately enhancing patient outcomes.

Magnetic nanoparticles also assume a substantial role in the realm of theranostics, a fusion of therapeutic and diagnostic elements. Integration of imaging agents, such as contrast agents for magnetic resonance imaging (MRI) or fluorescence probes, allows for real-time visualization of nanoparticle dispersion and therapeutic effects. This diagnostic facet provides clinicians with invaluable insights into treatment progress, thereby aiding the optimization of therapeutic strategies [136].

Moreover, magnetic nanoparticles facilitate triggered drug release. Capitalizing on their responsiveness to external magnetic fields, researchers can provoke controlled release of therapeutic payloads at specific locales, thereby refining the precision and timing of drug administration. This feature proves particularly advantageous for on-demand drug release in response to disease-associated cues.

The biocompatibility and surface engineering of magnetic nanoparticles enable their safe interaction with biological systems, ameliorating potential concerns regarding toxicity and immune reactions. Their diminutive size allows for passive accumulation in tumor tissues via the enhanced permeability and retention (EPR) effect, rendering them promising candidates for cancer theranostics [137].

In synthesis, magnetic nanoparticles function as adaptable platforms in the domain of targeted drug delivery and theranostics. Their capabilities encompass the transport of therapeutics, the targeting of designated sites, the provision of imaging contrast, and the facilitation of controlled release under the influence of external magnetic fields. This renders them indispensable tools for the design of tailored and effective therapeutic interventions. As research advances, magnetic nanoparticle-based approaches are poised to persistently shape the landscape of precision medicine by offering innovative resolutions for heightened therapeutic outcomes and enhanced patient care.

Among several MNPs, iron oxide is the most preferred owing to its superparamagnetic nature at room temperature. But due to its hydrophobic nature, it tends to agglomerate and form large clusters with reduced colloidal stability [114]. Another problem is the oxidation of the MNPs due to their large surface to volume ratio, which necessitates coating of the iron oxide core with functional shell containing long chain molecules to not only enhance colloidal stability but also minimize residual magnetization [115].

Non-steroidal anti-inflammatory drugs (NSAIDs) are often prescribed for the treatment of pain and inflammation associated with cancer treatment and have been reported to inhibit the expression of androgen receptor responsible for prostate tumor progression [138]. Flufenamic acid *N*-(α,α,α -trifluoro-*m*-tolyl) or FFA is a member of the anthranilic acid derivatives class of NSAIDs works by blocking crucial mediators of inflammation and pain; cyclooxygenase 1 and 2 enzymes. Their mechanism of action principally involves the inhibition of prostaglandin F synthase and activation of TRPC6 enzyme [139]. To enhance the therapeutic efficacy of antitumor drugs, Flufenamic acid has been reported to combat tumor associated inflammation in synergism with sorafenib mesoporous silica nanomatrix in recurrent breast and hepatocellular carcinoma [140]. It has also demonstrated to act as an antagonist to metabolizing enzymes such as AKR1C1 (aldo keto reductase family 1, member C1) responsible for bladder tumor progression in cisplatin based chemopreventive therapy in vitro [141].

In drug delivery, host-guest complexation with natural polysaccharides is of paramount value and can be used to encapsulate drugs within host cavity to improve their efficacy, stability, and tumor cell targeting. Starch having α Amylose, beside chitosan, is a biodegradable and biocompatible polysaccharide that can be easily modified and processed into various forms, such as microparticles, nanoparticles, and hydrogels, making it a suitable material for drug encapsulation. The encapsulation of NSAIDs in α

Amylose can improve their stability, solubility, and controlled release behaviour, as well as reduce their toxicity and side effects during chemotherapy. For instance, starch-based nanoparticles can protect NSAIDs from degradation in the acidic environment of the stomach and allow targeted release in the colon, which can reduce the risk of gastrointestinal side effects such as ulcers and achieve intended therapeutic response [142]. Similarly starch-based hydrogels can also be used for topical delivery of NSAIDs promoting the local treatment of pain and inflammation with reduced systemic absorption [126]. The two major components of starch are: the linear amylose connected by alpha 1-4 glycosidic linkages (which accounts for only 20-30% of starch) and highly branched amylopectin linked with alpha 1-6 glycosidic linkages [96]. Amylose has been known to form inclusion complexes with alcohols, esters, fatty acids and aromatic compounds owing to its tightly packed helical structure, and remarkable resistance towards enzymatic degradation in intestines [94]. In an attempt to design bioligand friendly and biocompatible magnetic nanoparticle, starch complexed with Flufenamic acid was exploited in the present study, as coating to deliver the drug to morbid tissues. In our previous work it has already been demonstrated that V Amylose forms stable complexes with Flufenamic acid that favor intestinal targeting in simulated conditions and subsequent releasing the payload in colon due to presence of amylase. The work also supported the idea that the Flufenamic complexes of amylose have the potential to be used as enteric coating and food matrix applications[143]. Thus, the present study was done to synthesize magnetic nanoparticles coated with V Amylose Flufenamic acid complex as shell to obtain magnetically guided drug delivery vehicle for theranostic applications.

5.2. Methodology

5.2.1. Materials

Flufenamic acid (98% pure), analytical grade native starch (NS), iron (III) chloride hexahydrate and sodium hydroxide was purchased from Sigma Aldrich company. All other reagents were of analytical grade.

Methodology

5.2.2. Preparation of V Amylose Flufenamic acid (NS FFA) complexes

Various NS FFA were prepared by acidification method. Principally 1.2 gm of native starch was dispersed in 200ml of 0.1 mol/L KOH solution at 85°C for 60 min with uninterrupted agitation until it turned to a homogenous paste which was further cooled. To this paste different amounts of FFA were added. A set of five V Amylose flufenamic acid complexes were synthesized with increasing ratios of FFA to CS:1/80,1/20,1/10 and 1/5 w/v. A white precipitate was obtained by adding 0.1 mol/L of phosphoric acid to these complexes with gentle stirring for 24 hours at 30°C. The precipitate was further isolated by centrifugation at 10,000 g for 25 min at 4°C and washed with 50% v/v ethanol [49].

5.2.3. Preparation of magnetic nanoparticles coated with V Amylose flufenamic acid complex (MNPs)

2 gm V amylose drug complex was dissolved in water at stirred mechanically at 40°C. 11nmol of iron (III) chloride hexahydrate was added. The suspension was precipitated by adding 15 ml of NaOH (30% solution) dropwise. The resulting black mixture was recovered by applying a magnet. The mixture was further washed with deionized water and dried in vacuum oven at 30°C for 24 h.

5.2.4. Physical Investigations

FTIR analysis of NS FFA complexes and MNPs was done on Perkin Elmer Frontier Fourier transformed spectrometer with a DTGS detector. The dried sample was grounded

with anhydrous KBr and pressed to form a pellet to be observed in the range of 4400-400 cm^{-1} . X Ray diffractogram was carried out in a Bruker diffractometer to assess the conformation and structure of different FFA NS. The generator worked on a 40KVx25 mA. A reversed-phase HPLC for the assessment of Flufenamic acid complexed with NS was done. RP C18 column was employed for chromatographic separation with a mobile phase constituted by a mixture of acetonitrile and water aqueous solution (50:50, v/v) with a flow rate of 1.0 mL/min. The HPLC system was performed at room temperature (25 ± 1 °C). The injection volume was 20 μL and the detector was set to 214 nm and. Prior to use, acetonitrile and HPLC water were filtered with a 0.45 μm filter and degassed for 30 min. All samples were filtered through a 0.45 μm PVDF membrane filter from Millipore, USA.

Extreme caution was exercised while preparing samples for analyzing FTIR, XRD, UV VIS, HPLC, SEM and TGA so as to ensure the following errors do not affect the quality of sample prepared and final measurement:

- i) Static error which includes reading, characteristic and environmental error.
- ii) Instrument loading error
- iii) Systemic or random errors

All the instruments were handled with precision and care following the standard operating procedure.

5.3. Results and discussion

The peaks of pure flufenamic acid and V Amylose with KOH and their complexes are given below. The pure Flufenamic acid FTIR spectra in **Fig 30** showed characteristic NH

stretching at 3401.07 cm^{-1} , whereas the peaks at 1669.76 and 1127.05 can be assigned to COOH and CF_3 functional groups of FFA.

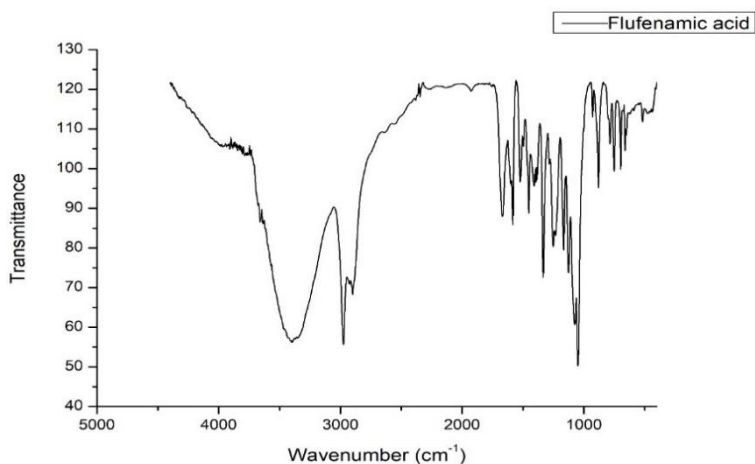


Figure 30: FTIR of flufenamic acid

The V Amylose and V Amylose in KOH spectra in **Fig 31** indicate a wide band of OH bond at around 3437.83 cm^{-1} and CH stretching at 2073.57 cm^{-1} . The peak at around 1633.85 cm^{-1} can be assigned to C=O stretching. On comparing the IR spectrum of pure V Amylose and V Amylose in KOH we didn't find any significant difference in IR peaks. This suggests that KOH has not altered the properties of V Amylose. After

complexing with FFA however the absorption peaks at 1417cm^{-1} suggest the successful formation of V Amylose FFA conjugates.

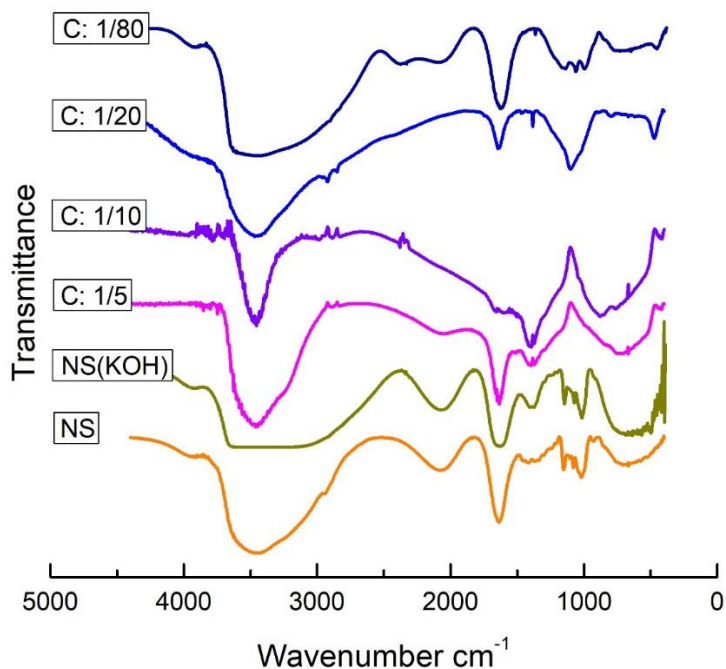


Figure 31: FTIR of pure V Amylose, V Amylose in KOH, complex 1/5, 1/10, 1/20 and 1/80.

The XRD patterns of FFA, V Amylose and 1/5 conjugate are given below. The XRD of pure FFA (**Fig 32**) displayed characteristic bands indicative of the highly crystalline structure of FFA at 13° , 17° and 25° . The XRD of V Amylose gives distinct diffraction peaks at 15.00° , 22.86° and a doublet at 17.04° and 17.86° corresponds to A type crystalline structure of amylose. Moreover, the appearance of an ambiguous peak at 47° can be attributed to the absence of moisture or the addition of phosphoric acid. On complexation of V Amylose with FFA the characteristic band of the drug, however appears weak but a distinct peak at 35.00° confirms the formation of 1/5 complex (**Fig 33**).

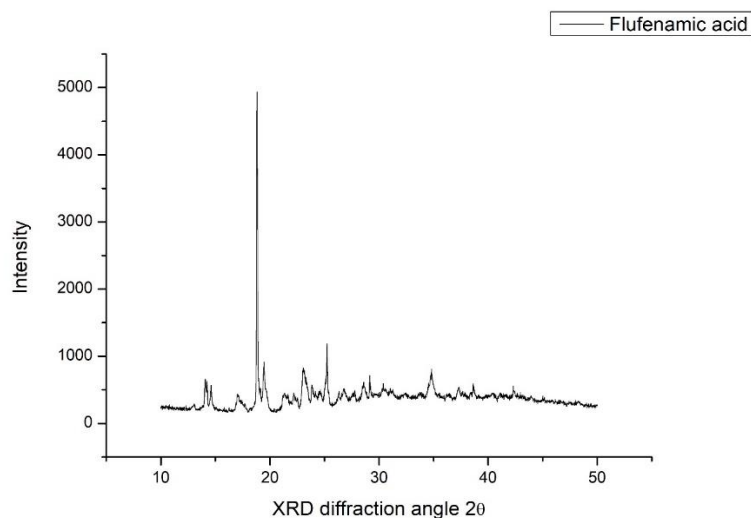


Figure 32: XRD of pure Flufenamic acid

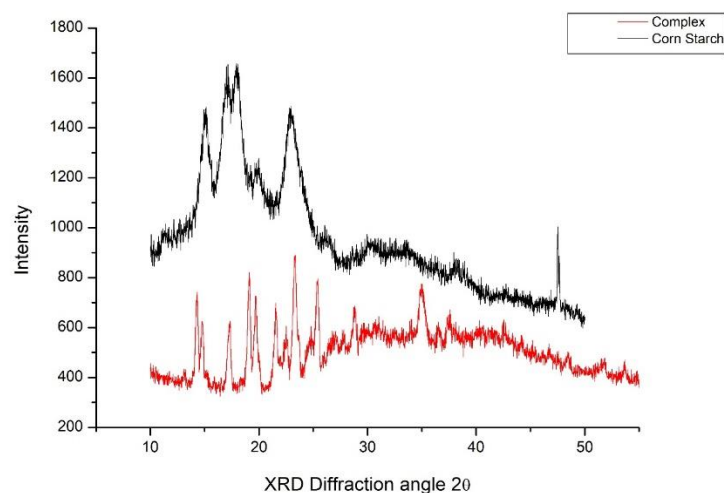
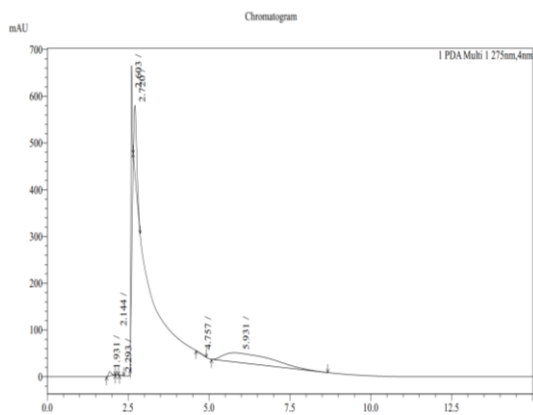


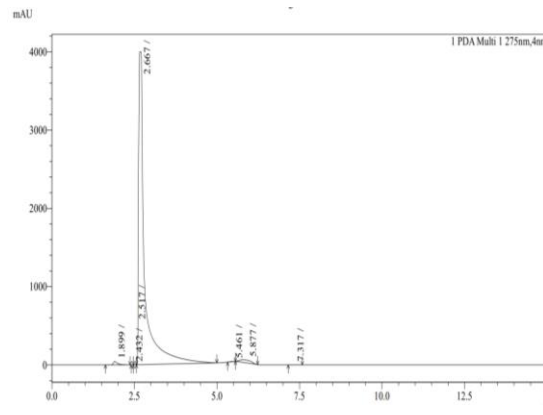
Figure 33: XRD of V Amylose (black) and complex of 1/5 ratio (red)

The chromatogram for NS in KOH and various FFA NS complexes has been given below.

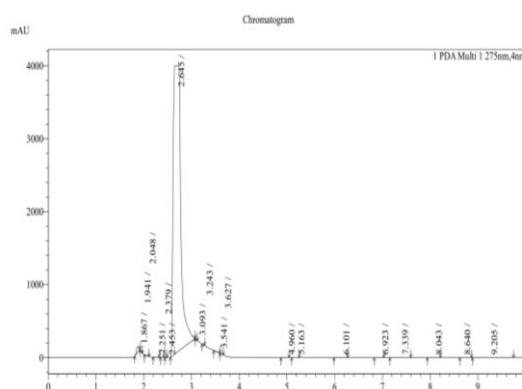
The chromatogram for NS in KOH shows two separate peaks with a retention time of 2.603 and 2.720 suggesting the presence of amylopectin and amylose components in **Fig 34(a)**. The HPLC peaks for various FFA NS complexes 1/5, 1/10, 1/20 and 1/80 are given in **Fig 34(b), 34(c), 34(d), 35(e)** with a retention time of 2.667, 2.645, 2.656 and 2.635 respectively which are appearing between the RT of amylopectin and amylose indicating the formation of conjugates with amylose which gets precipitated due to leaching as amylopectin goes away to water.



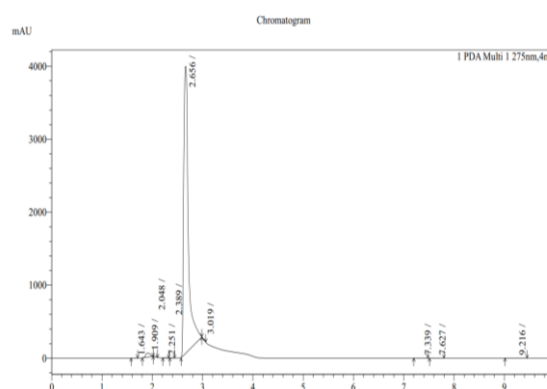
(a)



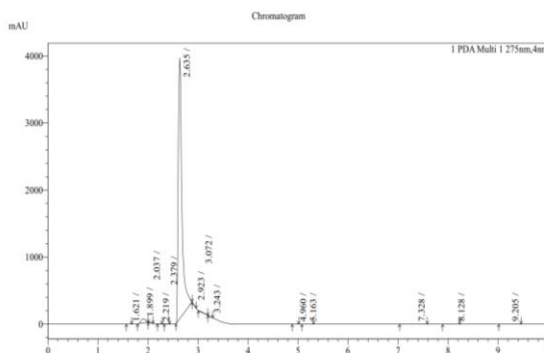
(b)



(c)



(d)



(e)

Figure 34: (a) Chromatogram for NS in KOH, (b) Chromatogram for complex 1/5, (c) Chromatogram for complex 1/10, (d) Chromatogram for complex 1/20 and (e) Chromatogram for complex 1/80

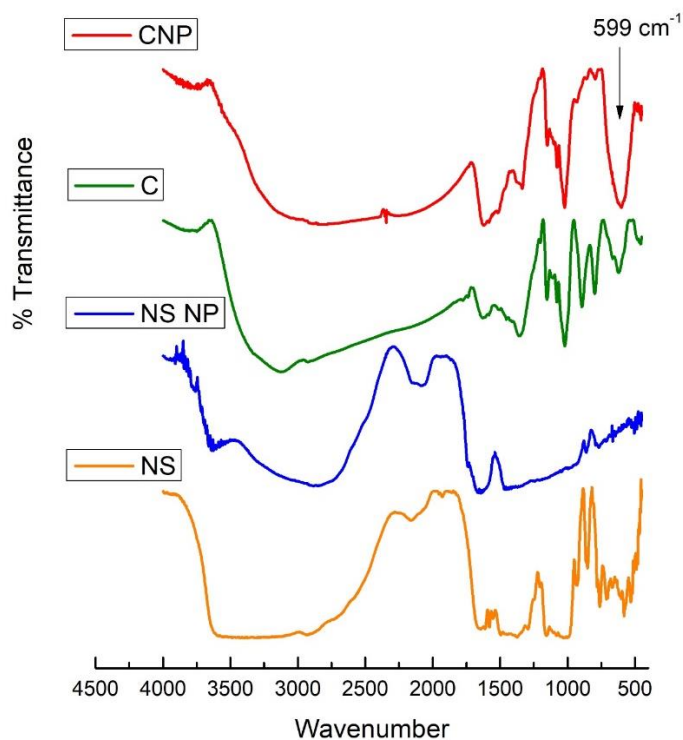


Figure 35: FTIR spectra of Native *V* Amylose (NS), Native *V* amylose nanoparticle (NS NP) and *V* Amylose flufenamic acid complex (C), and magnetic nanoparticles coated with *V* Amylose flufenamic acid complex (CNP)

FTIR spectra of Native *V* Amylose (NS), nanoparticle of NS (NS NP), complex of *V* Amylose and drug (C) and prepared magnetic nanoparticle (CNP) presented characteristic bands in **Fig 35**. The absorption at 3420 cm^{-1} can be assigned to OH group of starch. The peak at around 1633.85 cm^{-1} is attributed to an intermolecular H-bond involving the carboxyl group. The absorption peak at 1154.29 cm^{-1} can be assigned to C-O stretching. The absorbance at 599 cm^{-1} can be assigned to Fe-O group of magnetite in CNP and indicates the successful formation of magnetite core.

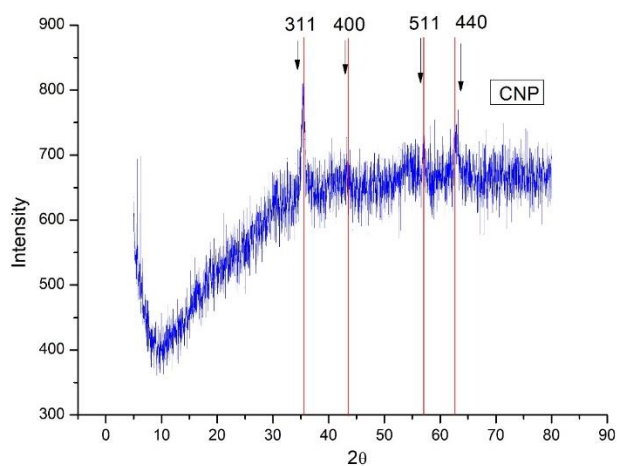


Figure 36: XRD diffractogram of prepared magnetic nanoparticles coated with V Amylose Flufenamic acid complex (CNP)

XRD analysis was carried out to see the crystal structure and phase purity of prepared magnetic nanoparticles. Four characteristic peaks (according to X'pert high score database) with their indices marked at (311), (400), (511), (440) were observed for CNP indicating the successful formation of pure iron oxide core with a spinel structure necessary for MDDs and other theranostic applications (**Fig 36**) [144].

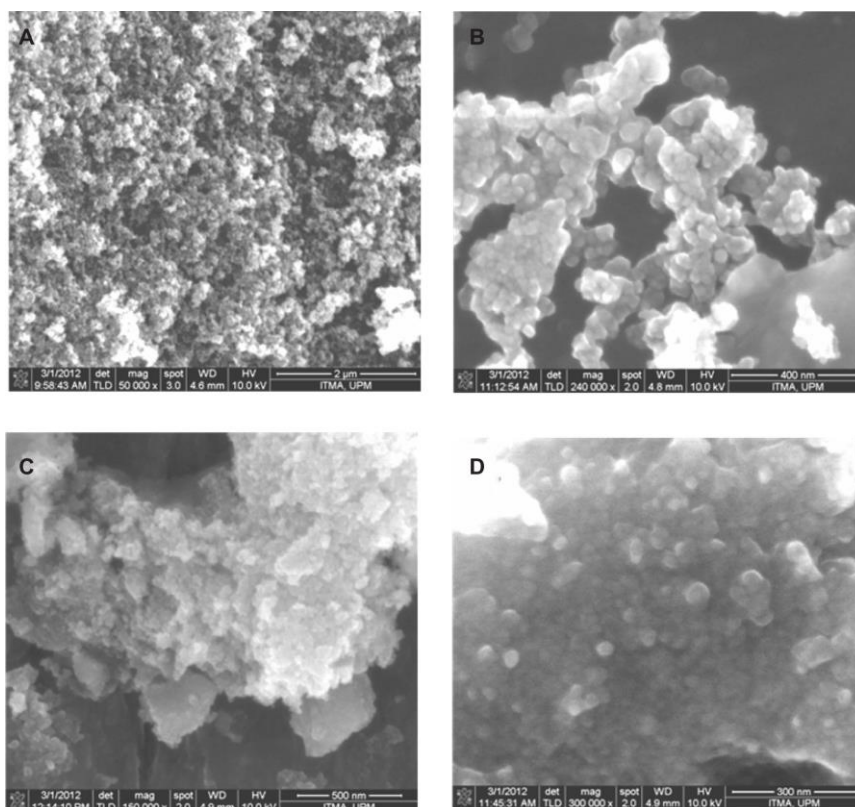


Figure 37: SEM images of (A) magnetic nanoparticles at 50,000' magnifications, (B) magnetic nanoparticles at 240,000' magnification, (C) magnetic nanoparticles coated with V Amylose-flufenamic complex at 150,000' magnification (D) magnetic nanoparticles coated with V Amylose-flufenamic acid complex at 300,000' magnification

At different magnifications, SEM analysis also demonstrated that the produced magnetic nanoparticles had a spherical form. A small size range of around 11-13 nm in diameter was confirmed by TEM examination, as shown in **Fig 37 (A-D)**. The mean size of the iron oxide nanoparticles coated with V Amylose Flufenamic acid was in the range of 14 ± 3 nm, while the average size of the magnetic nanoparticles was 11.4 ± 2.2 nm. (**Fig 38**).

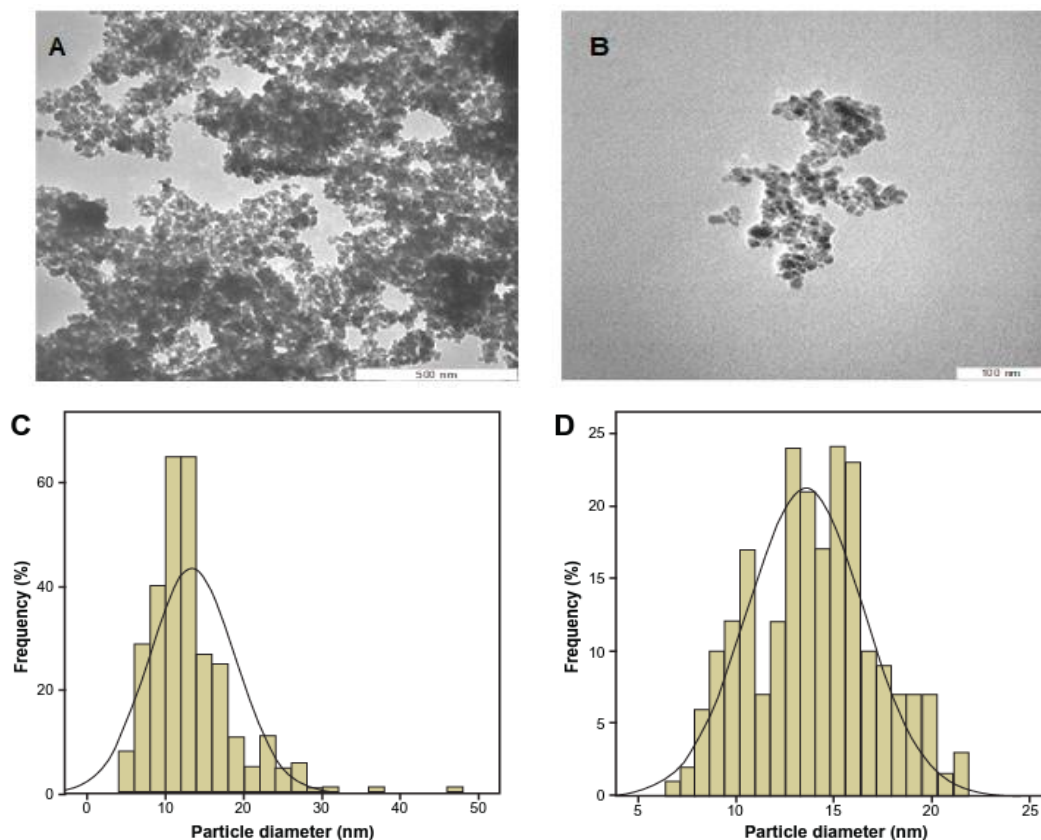


Figure 38: TEM images of (A) magnetic nanoparticle with 500 nm bar, (B) magnetic nanoparticle coated with V Amylose flufenamic acid complex with 100 nm magnetic bar, (C) particle diameter of magnetic nanoparticle, and (D) particle diameter of magnetic nanoparticle coated with V Amylose flufenamic acid complex

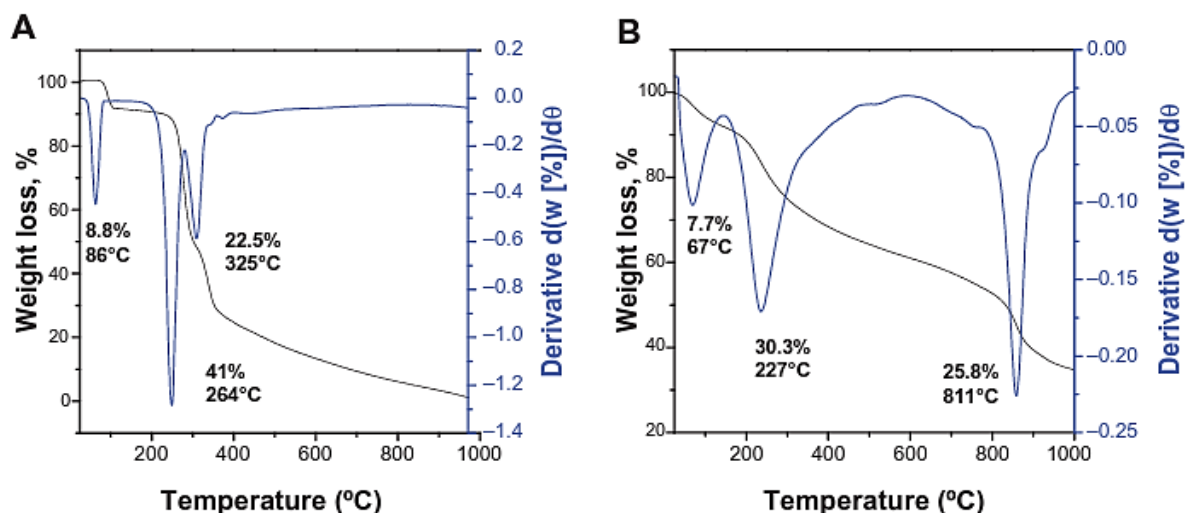


Figure 39: TGA analysis of (A) V Amylose flufenamic acid complex (B) magnetic nanoparticles coated with V Amylose flufenamic acid complex

The amylose drug complex's TGA curve indicates that the first weight loss occurred at 86 °C (8.8%), possibly as a result of the elimination of crystalline water. According to the differential

thermogravimetric curves, weight loss begins at 41.0 °C (264 °C) and 22.5 °C (22.5%) (**Fig 39 A**). The coating caused a change in the curved shape of the thermogravimetric-derivative thermogravimetric thermograms. The initial weight loss at 67 °C was attributed to the water that had been chemically and freely adsorbed. At 227 °C, the V Amylose flufenamic acid complex began to degrade, which is higher than the temperature at which the pure complex breaks down. The modest mass drop (25.8%) at 811 °C is caused by the coating breaking down (**Fig 39 B**). The temperature range is greater than that of the pure free V Amylose flufenamic acid complex, suggesting that the complex's thermal stability was improved by the magnetic nanocarrier.

5.4. Conclusion

Magnetic nanoparticles hold a pivotal role in the realm of targeted drug delivery and theranostics, effectively merging therapeutic and diagnostic functions within one framework. Within targeted drug delivery, magnetic nanoparticles serve as excellent carriers for therapeutic agents, offering a platform to convey drugs, peptides, nucleic acids, and other therapeutic cargoes to specific sites. Their modifiable surface properties enable functionalization with targeting ligands, enabling precise recognition and binding to particular cells or tissues. Upon successful targeting, these nanoparticles can be guided and concentrated at the intended site using externally applied magnetic fields, thereby enhancing drug accumulation while minimizing systemic exposure. This targeted approach significantly enhances therapeutic efficacy while concurrently mitigating off-target effects, ultimately leading to improved patient outcomes.

The magnetic nanoparticles also contribute significantly to the realm of theranostics and diagnostics. By incorporating imaging agents such as contrast agents for magnetic resonance imaging (MRI) or fluorescence probes, these nanoparticles enable real-time visualization of nanoparticle distribution and therapeutic effects. This endows clinicians with invaluable

insights into the progression of treatments, thereby facilitating the optimization of therapeutic strategies. Leveraging their responsiveness to external magnetic fields, researchers can fine tune the controlled release of therapeutic payloads at specific locations, thus elevating the precision and timing of drug administration. This attribute proves exceptionally advantageous for on demand drug release, responding to disease associated cues.

The innate biocompatibility and tailored surface engineering of magnetic nanoparticles endorse their safe interaction with biological systems, thereby ameliorating concerns pertaining to potential toxicity and immune reactions. Their submicron dimensions facilitate their passive accumulation in tumor tissues through the enhanced permeability and retention (EPR) effect, which renders them promising candidates for cancer theranostics. Starch drug coated magnetic nanoparticles have high colloidal stability and biocompatibility with reasonable magnetic properties. They are valuable in targeting the delivery of therapeutics at deliberated sites in vivo in many diseased conditions. The study was conducted to synthesize and characterize magnetic nanoparticles coated with V Amylose flufenamic acid complex. First, complexes of V Amylose and flufenamic acid were synthesized and then MNPs using iron (III) chloride and sodium hydroxide were prepared for surface coating. FTIR and XRD results indicated successful V Amylose drug complex and magnetite core formation. The synthesized magnetic nanosystem can be used as magnetic tracer for probing the drug pharmacokinetics. The prepared particles hold a promising approach to deliver NSAIDs prescribed along with anti-cancer drugs to specifically deliver the deliberated therapeutic at desired site. As research progresses, magnetic nanoparticle-based approaches are poised to perpetually reshape the landscape of precision medicine, offering innovative solutions.

Conclusion and Future Prospects

Given the widespread use of NSAIDs, it is imperative to refine their administration for safety and efficacy. One promising approach is the controlled release of NSAIDs using natural polysaccharides, specifically V-amylose. V-amylose's structural uniqueness and resistance to enzymatic breakdown makes it an ideal enteric coating, preventing premature drug release in the stomach and enabling targeted delivery to the colon. The utilization of V-amylose and aminated starch, in present work as innovative drug delivery systems, demonstrated promising potential for enhancing therapeutic outcomes associated with the delivery of ulcerogenic NSAIDs. The exploration of V-amylose as a carrier for fenamates, a class of NSAIDs, highlighted its unique physicochemical properties, including biocompatibility, hydrophobic interior, and hydrophilic exterior. The formation of inclusion complexes with Flufenamic acid further, presented a controlled and sustained drug release profile, particularly in simulated intestinal conditions. This approach minimized gastrointestinal side effects and showcases stability over a range of pH and temperature conditions, supporting its potential for intestinal drug delivery applications.

Notably, aminated starch-fenamate tablets demonstrated controlled release profiles in simulated intestinal media, with stability attributed to imine linkages under weakly acidic conditions. The mucoadhesive potential of these tablets is crucial for targeted drug delivery to the intestine, presenting a controlled release profile and mitigating ulcerogenicity. Furthermore, the incorporation of magnetic nanoparticles in drug delivery and theranostics offers a multifaceted approach. The synthesis of magnetic nanoparticles coated with V-Amylose-flufenamic acid complexes demonstrated successful core formation and holds promise for delivering NSAIDs along with anti-cancer drugs to specific sites under the influence of external magnetic field. As research in magnetic nanoparticle-based approaches progresses, the landscape of precision medicine is expected to undergo continuous transformation, offering

innovative solutions for targeted and personalized therapeutic interventions. Investigations into the pharmacokinetics and toxicity profiling of drug-loaded V-amylose and aminated starch formulations in the intestine are essential for clinical translation. These studies will provide crucial insights into the safety and efficacy of these delivery systems, paving the way for potential therapeutic applications. Pharmacokinetics and appraisal of toxicity of drug loaded V Amylose can be done in vivo and using CaCO₂ cell line. Since degradation of matrix tablets in gastric medium resulted in complete drug loss, a different approach without opening ring of starch can be performed while attaching primary amine groups to the periphery of starch molecule. The formulation of mucolytic or mucopermeable drug delivery carriers by conjugating the diaminated amylose with NSAIDs (in the form of ester) in presence of strong mucolytic agent such as N acetyl cysteine may also result in improved mucosal drug delivery and better patient compliance. Additionally, the synthesis and characterization of magnetic nanoparticles coated with V-Amylose-flufenamic acid complexes open avenues for magnetically guided drug delivery approaches, especially in the realm of precision medicine. As research progresses, understanding the interplay between these natural polysaccharides and therapeutic agents will likely lead to the development of more tailored and efficient drug delivery systems. The integration of magnetic nanoparticles in theranostics offers a promising avenue for real-time monitoring and precise targeting, revolutionizing the landscape of personalized medicine. Continued exploration and refinement of these strategies hold immense potential for addressing current challenges and advancing the field of drug delivery and theranostics into new frontiers.

References

- [1] J. Zhang, P. Zhan, and H. Tian, “Recent updates in the polysaccharides-based Nano-biocarriers for drugs delivery and its application in diseases treatment: A review,” *Int. J. Biol. Macromol.*, vol. 182, pp. 115–128, 2021, doi: 10.1016/j.ijbiomac.2021.04.009.
- [2] Y. Sun, X. Jing, X. Ma, Y. Feng, and H. Hu, “Versatile types of polysaccharide-based drug delivery systems: From strategic design to cancer therapy,” *Int. J. Mol. Sci.*, vol. 21, no. 23, pp. 1–21, 2020, doi: 10.3390/ijms21239159.
- [3] P. Prasher *et al.*, “Chemico-Biological Interactions Targeting mucus barrier in respiratory diseases by chemically modified advanced delivery systems,” *Chem. Biol. Interact.*, vol. 365, no. July, p. 110048, 2022, doi: 10.1016/j.cbi.2022.110048.
- [4] M. Jelkmann *et al.*, “Chitosan: The One and Only? Aminated Cellulose as an Innovative Option for Primary Amino Groups Containing Polymers,” *Biomacromolecules*, vol. 19, no. 10, pp. 4059–4067, 2018, doi: 10.1021/acs.biomac.8b01069.
- [5] Y. Xu, Y.-J. Wu, P.-L. Sun, F. Zhang, R. J. Linhardt, and A.-Q. Zhang, “Chemically modified polysaccharides: Synthesis, characterization, structure activity relationships of action,” *Int. J. Biol. Macromol.*, vol. 132, pp. 970–977, Jul. 2019, doi: 10.1016/j.ijbiomac.2019.03.213.
- [6] and K. W. L. Ying Zhang, Hon Fai Chan, “Advanced Materials and Processing for Drug Delivery: The Past and the Future,” *Adv Drug Deliv Rev*, vol. 65, no. 1, pp. 104–120, 2014, doi: 10.1016/j.addr.2012.10.003.Advanced.
- [7] B. Layek and S. Mandal, “Natural polysaccharides for controlled delivery of oral therapeutics: a recent update,” *Carbohydr. Polym.*, vol. 230, p. 115617, 2020, doi: 10.1016/j.carbpol.2019.115617.
- [8] S. H. Lee, R. Bajracharya, J. Y. Min, J. W. Han, B. J. Park, and H. K. Han, “Strategic approaches for colon targeted drug delivery: An overview of recent advancements,” *Pharmaceutics*, vol. 12, no. 1, 2020, doi: 10.3390/pharmaceutics12010068.
- [9] M. Cui, M. Zhang, and K. Liu, “Colon-targeted drug delivery of polysaccharide-based nanocarriers for synergistic treatment of inflammatory bowel disease: A review,” *Carbohydr. Polym.*, vol. 272, no. August, p. 118530, 2021, doi: 10.1016/j.carbpol.2021.118530.
- [10] V. C. Ibekwe, M. K. Khela, D. F. Evans, and A. W. Basit, “A new concept in colonic drug targeting: A combined pH-responsive and bacterially-triggered drug delivery technology,” *Aliment. Pharmacol. Ther.*, vol. 28, no. 7, pp. 911–916, 2008, doi: 10.1111/j.1365-2036.2008.03810.x.
- [11] M. Z. I. Khan, H. P. Štedul, and N. Kurjaković, “A pH-dependent colon-targeted oral drug delivery system using methacrylic acid copolymers. II. Manipulation of drug release using Eudragit® L100 and Eudragit S100 combinations,” *Drug Dev. Ind. Pharm.*, vol. 26, no. 5, pp. 549–554, 2000, doi: 10.1081/DDC-100101266.

- [12] A. Rubinstein, "Microbially controlled drug delivery to the colon," *Biopharm. Drug Dispos.*, vol. 11, no. 6, pp. 465–475, 1990, doi: 10.1002/bdd.2510110602.
- [13] E. Solheim and R. R. Scheline, "Metabolism of alkenebenzene derivatives in the rat I. P-methoxyallylbenzene (estragole) and p-methoxypropenylbenzene (anethole)," *Xenobiotica*, vol. 3, no. 8, pp. 493–510, 1973, doi: 10.3109/00498257309151538.
- [14] J. Varshosaz, "Dextran conjugates in drug delivery," *Expert Opin. Drug Deliv.*, vol. 9, no. 5, pp. 509–523, 2012, doi: 10.1517/17425247.2012.673580.
- [15] M. A. Hussain, K. Abbas, I. Jantan, and S. N. A. Bukhari, "Polysaccharide-based materials in macromolecular prodrug design and development," *Int. Mater. Rev.*, vol. 62, no. 2, pp. 78–98, 2017, doi: 10.1080/09506608.2016.1209617.
- [16] A. K. Philip and B. Philip, "Colon targeted drug delivery systems: A review on primary and novel approaches," *Oman Med. J.*, vol. 25, no. 2, pp. 70–78, 2010, doi: 10.5001/omj.2010.24.
- [17] P. J. Pentikäinen, P. J. Neuvonen, and C. Backman, "Human pharmacokinetics of tolfenamic acid, a new anti-inflammatory agent," *Eur. J. Clin. Pharmacol.*, vol. 19, no. 5, pp. 359–365, 1981, doi: 10.1007/BF00544587.
- [18] F. Directions, "Controlled Drug Delivery Systems : Current Status and," *Molecules*, vol. 26, p. 5905, 2021.
- [19] R. Fatima *et al.*, "Diversity of Rationally Modified Polysaccharides for Pharmaceutical Applications," *ChemistrySelect*, vol. 8, no. 20, May 2023, doi: 10.1002/slct.202300941.
- [20] L. Li *et al.*, "Dual-Responsive Alginate Hydrogel Constructed by Sulfhydryl Dendrimer as an Intelligent System for Drug Delivery," *Molecules*, vol. 27, no. 1, pp. 1–13, 2022, doi: 10.3390/molecules27010281.
- [21] A. S. Eltaweil, M. S. Ahmed, G. M. El-Subruiti, R. E. Khalifa, and A. M. Omer, "Efficient loading and delivery of ciprofloxacin by smart alginate/carboxylated graphene oxide/aminated chitosan composite microbeads: In vitro release and kinetic studies," *Arab. J. Chem.*, vol. 16, no. 4, p. 104533, 2023, doi: <https://doi.org/10.1016/j.arabjc.2022.104533>.
- [22] B. Singh, V. Sharma, M. Mohan, Rohit, P. Sharma, and K. Ram, "Design of ciprofloxacin impregnated dietary fiber psyllium-moringa gum-alginate network hydrogels via green approach for use in gastro-retentive drug delivery system," *Bioact. Carbohydrates Diet. Fibre*, vol. 29, p. 100345, 2023, doi: <https://doi.org/10.1016/j.bcdf.2022.100345>.
- [23] T. Long *et al.*, "Gelatin/alginate-based microspheres with sphere-in-capsule structure for spatiotemporal manipulative drug release in gastrointestinal tract," *Int. J. Biol. Macromol.*, vol. 226, pp. 485–495, 2023, doi: <https://doi.org/10.1016/j.ijbiomac.2022.12.040>.
- [24] A. Rashidy Ahmady, A. Solouk, S. Saber-Samandari, S. Akbari, H. Ghanbari, and B. E. Brycki, "Capsaicin-loaded alginate nanoparticles embedded polycaprolactone-

- chitosan nanofibers as a controlled drug delivery nanoplatform for anticancer activity,” *J. Colloid Interface Sci.*, 2023, doi: <https://doi.org/10.1016/j.jcis.2023.01.139>.
- [25] L. S. Devi, A. J. Das, and A. B. Das, “Characterization of high amylose starch-microcrystalline cellulose based floatable gel for enhanced gastrointestinal retention and drug delivery,” *Carbohydr. Polym. Technol. Appl.*, vol. 3, p. 100185, 2022, doi: <https://doi.org/10.1016/j.carpta.2022.100185>.
- [26] N. Sivapragasam, P. Thavarajah, J. B. Ohm, K. Margaret, and D. Thavarajah, “Novel starch based nano scale enteric coatings from soybean meal for colon-specific delivery,” *Carbohydr. Polym.*, vol. 111, pp. 273–279, 2014, doi: [10.1016/j.carbpol.2014.04.091](https://doi.org/10.1016/j.carbpol.2014.04.091).
- [27] V. Taghipour-Sabzevar *et al.*, “Targeted delivery of a short antimicrobial peptide against CD44-overexpressing tumor cells using hyaluronic acid-coated chitosan nanoparticles: An in vitro study,” *J. Nanoparticle Res.*, vol. 22, no. 5, 2020, doi: [10.1007/s11051-020-04838-2](https://doi.org/10.1007/s11051-020-04838-2).
- [28] Y. Liang *et al.*, “Self-crosslinkable chitosan-hyaluronic acid dialdehyde nanoparticles for CD44-targeted siRNA delivery to treat bladder cancer,” *Bioact. Mater.*, vol. 6, no. 2, pp. 433–446, 2021, doi: [10.1016/j.bioactmat.2020.08.019](https://doi.org/10.1016/j.bioactmat.2020.08.019).
- [29] A. P. Bagre, K. Jain, and N. K. Jain, “Alginate coated chitosan core shell nanoparticles for oral delivery of enoxaparin: In vitro and in vivo assessment,” *Int. J. Pharm.*, vol. 456, no. 1, pp. 31–40, 2013, doi: <https://doi.org/10.1016/j.ijpharm.2013.08.037>.
- [30] M. A. Collier *et al.*, “Host-mediated Leishmania donovani treatment using AR-12 encapsulated in acetalated dextran microparticles,” *Int. J. Pharm.*, vol. 499, no. 1–2, pp. 186–194, 2016, doi: [10.1016/j.ijpharm.2016.01.004](https://doi.org/10.1016/j.ijpharm.2016.01.004).
- [31] M. A. Collier *et al.*, “Saquinavir Loaded Acetalated Dextran Microconfetti – a Long Acting Protease Inhibitor Injectable,” *Pharm. Res.*, 2016, doi: [10.1007/s11095-016-1936-y](https://doi.org/10.1007/s11095-016-1936-y).
- [32] C. J. Batty, E. A. Amouzougan, M. A. Carlock, T. M. Ross, E. M. Bachelder, and K. M. Ainslie, “Sustained delivery of CpG oligodeoxynucleotide by acetalated dextran microparticles augments effector response to Computationally Optimized Broadly Reactive Antigen (COBRA) influenza hemagglutinin,” *Int. J. Pharm.*, vol. 630, p. 122429, 2023, doi: <https://doi.org/10.1016/j.ijpharm.2022.122429>.
- [33] Z. Xie *et al.*, “Acetalated dextran microparticles for the smart delivery of pyraclostrobin to control Sclerotinia diseases,” *Carbohydr. Polym.*, vol. 291, p. 119576, 2022, doi: <https://doi.org/10.1016/j.carbpol.2022.119576>.
- [34] Z. Wang and S. A. Meenach, “Dry powders based on mucus-penetrating nanoparticles entrapped microparticles for pulmonary delivery of Tobramycin,” in *2014 40th Annual Northeast Bioengineering Conference (NEBEC)*, Apr. 2014, pp. 1–2, doi: [10.1109/NEBEC.2014.6972969](https://doi.org/10.1109/NEBEC.2014.6972969).
- [35] D. A. Hendy *et al.*, “Delivery of Small Molecule Mast Cell Activators for West Nile Virus Vaccination Using Acetalated Dextran Microparticles,” *Int. J. Pharm.*, p. 122658, 2023, doi: <https://doi.org/10.1016/j.ijpharm.2023.122658>.

- [36] M. Akrami-Hasan-Kohal, M. Eskandari, and A. Solouk, "Silk fibroin hydrogel/dexamethasone sodium phosphate loaded chitosan nanoparticles as a potential drug delivery system," *Colloids Surfaces B Biointerfaces*, vol. 205, p. 111892, 2021, doi: <https://doi.org/10.1016/j.colsurfb.2021.111892>.
- [37] O. Iqbal *et al.*, "Moxifloxacin loaded nanoparticles of disulfide bridged thiolated chitosan-eudragit RS100 for controlled drug delivery," *Int. J. Biol. Macromol.*, vol. 182, pp. 2087–2096, 2021, doi: <https://doi.org/10.1016/j.ijbiomac.2021.05.199>.
- [38] M. ur Rehman Kashif *et al.*, "Chitosan/guar gum-based thermoreversible hydrogels loaded with pullulan nanoparticles for enhanced nose-to-brain drug delivery," *Int. J. Biol. Macromol.*, vol. 215, pp. 579–595, 2022, doi: <https://doi.org/10.1016/j.ijbiomac.2022.06.161>.
- [39] A. L. Onugwu, A. A. Attama, P. O. Nnamani, S. O. Onugwu, E. B. Onuigbo, and V. V. Khutoryanskiy, "Development and optimization of solid lipid nanoparticles coated with chitosan and poly(2-ethyl-2-oxazoline) for ocular drug delivery of ciprofloxacin," *J. Drug Deliv. Sci. Technol.*, vol. 74, p. 103527, 2022, doi: <https://doi.org/10.1016/j.jddst.2022.103527>.
- [40] A. Sood, A. Gupta, R. Bharadwaj, P. Ranganath, N. Silverman, and G. Agrawal, "Biodegradable disulfide crosslinked chitosan/stearic acid nanoparticles for dual drug delivery for colorectal cancer," *Carbohydr. Polym.*, vol. 294, p. 119833, 2022, doi: <https://doi.org/10.1016/j.carbpol.2022.119833>.
- [41] F. Mirjalili and M. Mahmoodi, "Controlled release of protein from gelatin/chitosan hydrogel containing platelet-rich fibrin encapsulated in chitosan nanoparticles for accelerated wound healing in an animal model," *Int. J. Biol. Macromol.*, vol. 225, pp. 588–604, 2023, doi: <https://doi.org/10.1016/j.ijbiomac.2022.11.117>.
- [42] Y. Wang *et al.*, "Chitosan/hyaluronan nanogels co-delivering methotrexate and 5-aminolevulinic acid: A combined chemo-photodynamic therapy for psoriasis," *Carbohydr. Polym.*, vol. 277, p. 118819, 2022, doi: <https://doi.org/10.1016/j.carbpol.2021.118819>.
- [43] S. P. Akhlaghi, S. Saremi, S. N. Ostad, R. Dinarvand, and F. Atyabi, "Discriminated effects of thiolated chitosan-coated pMMA paclitaxel-loaded nanoparticles on different normal and cancer cell lines," *Nanomedicine Nanotechnology, Biol. Med.*, vol. 6, no. 5, pp. 689–697, 2010, doi: <https://doi.org/10.1016/j.nano.2010.01.011>.
- [44] Y. Zhang *et al.*, "Encapsulation of honokiol into self-assembled pectin nanoparticles for drug delivery to HepG2 cells," *Carbohydr. Polym.*, vol. 133, pp. 31–38, 2015, doi: [10.1016/j.carbpol.2015.06.102](https://doi.org/10.1016/j.carbpol.2015.06.102).
- [45] R. Sabra, N. Billa, and C. J. Roberts, "Cetuximab-conjugated chitosan-pectinate (modified) composite nanoparticles for targeting colon cancer," *Int. J. Pharm.*, vol. 572, p. 118775, 2019, doi: <https://doi.org/10.1016/j.ijpharm.2019.118775>.
- [46] W. C. Obiro, S. Sinha Ray, and M. N. Emmambux, "V-amylose Structural Characteristics, Methods of Preparation, Significance, and Potential Applications," *Food Rev. Int.*, vol. 28, no. 4, pp. 412–438, 2012, doi: <https://doi.org/10.1016/j.ijpharm.2019.118775>.

- 10.1080/87559129.2012.660718.
- [47] N. Ab'lah, C. Y. L. Yusuf, P. Rojsitthisak, and T. W. Wong, "Reinvention of starch for oral drug delivery system design," *Int. J. Biol. Macromol.*, vol. 241, p. 124506, Jun. 2023, doi: 10.1016/j.ijbiomac.2023.124506.
- [48] P. Prasher, R. Fatima, and M. Sharma, "Therapeutic delivery with V-amylose," *Drug Dev. Res.*, vol. 82, no. 6, pp. 727–729, Sep. 2021, doi: 10.1002/ddr.21804.
- [49] R. Fatima, M. Sharma, and P. Prasher, "Targeted delivery of flufenamic acid by V-amylose," *Ther. Deliv.*, vol. 12, no. 8, pp. 575–582, Aug. 2021, doi: 10.4155/tde-2021-0020.
- [50] A. Elmas, G. Akyüz, A. Bergal, M. Andaç, and Ö. Andaç, "Mathematical modelling of drug release," *Res. Eng. Struct. Mater.*, vol. 6, no. 4, pp. 327–350, 2020, doi: 10.17515/resm2020.178na0122.
- [51] D. Y. Arifin, L. Y. Lee, and C. H. Wang, "Mathematical modeling and simulation of drug release from microspheres: Implications to drug delivery systems," *Adv. Drug Deliv. Rev.*, vol. 58, no. 12–13, pp. 1274–1325, 2006, doi: 10.1016/j.addr.2006.09.007.
- [52] J. Siepman, "Mathematical modeling of bioerodible, polymeric drug delivery systems," *Adv. Drug Deliv. Rev.*, vol. 48, no. 2–3, pp. 229–247, Jun. 2001, doi: 10.1016/S0169-409X(01)00116-8.
- [53] L. S. Koester, G. G. Ortega, P. Mayorga, and V. L. Bassani, "Mathematical evaluation of in vitro release profiles of hydroxypropylmethylcellulose matrix tablets containing carbamazepine associated to β -cyclodextrin," *Eur. J. Pharm. Biopharm.*, vol. 58, no. 1, pp. 177–179, Jul. 2004, doi: 10.1016/j.ejpb.2004.03.017.
- [54] J. Siepman and F. Siepman, "Mathematical modeling of drug delivery," *Int. J. Pharm.*, vol. 364, no. 2, pp. 328–343, Dec. 2008, doi: 10.1016/j.ijpharm.2008.09.004.
- [55] C. G. Biliaderis and G. Galloway, "Crystallization behavior of amylose-V complexes: Structure-property relationships," *Carbohydr. Res.*, vol. 189, no. C, pp. 31–48, Jun. 1989, doi: 10.1016/0008-6215(89)84084-4.
- [56] R. F. Tester, J. Karkalas, and X. Qi, "Starch - Composition, fine structure and architecture," *Journal of Cereal Science*, vol. 39, no. 2. Academic Press, pp. 151–165, Mar. 01, 2004, doi: 10.1016/j.jcs.2003.12.001.
- [57] L. Tan and L. Kong, "Starch-guest inclusion complexes: Formation, structure, and enzymatic digestion," *Crit. Rev. Food Sci. Nutr.*, vol. 60, no. 5, pp. 780–790, 2020, doi: 10.1080/10408398.2018.1550739.
- [58] L. Phuong Ta, E. Bujna, S. Kun, D. Charalampopoulos, and V. V. Khutoryanskiy, "Electrosprayed mucoadhesive alginate-chitosan microcapsules for gastrointestinal delivery of probiotics," *Int. J. Pharm.*, vol. 597, no. February, 2021, doi: 10.1016/j.ijpharm.2021.120342.
- [59] A. Dadkhah Tehrani and M. Parsamanesh, "Preparation, characterization and drug delivery study of a novel nanobiopolymeric multidrug delivery system," *Mater. Sci.*

- Eng. C*, vol. 73, pp. 516–524, Apr. 2017, doi: 10.1016/j.msec.2016.12.103.
- [60] A. Nouri and S. Khoee, “Preparation of amylose-poly(methyl methacrylate) inclusion complex as a smart nanocarrier with switchable surface hydrophilicity,” *Carbohydr. Polym.*, vol. 246, no. May, p. 116662, Oct. 2020, doi: 10.1016/j.carbpol.2020.116662.
- [61] P. Prasher, M. Sharma, and S. P. Singh, “Drug encapsulating polysaccharide-loaded metal nanoparticles: A perspective drug delivery system,” *Drug Dev. Res.*, vol. 82, no. 2, pp. 145–148, Apr. 2021, doi: 10.1002/ddr.21754.
- [62] N. Masina *et al.*, “A review of the chemical modification techniques of starch,” *Carbohydr. Polym.*, vol. 157, pp. 1226–1236, Feb. 2017, doi: 10.1016/j.carbpol.2016.09.094.
- [63] S. H. Mahmoudi Najafi, M. Baghaie, and A. Ashori, “Preparation and characterization of acetylated starch nanoparticles as drug carrier: Ciprofloxacin as a model,” *Int. J. Biol. Macromol.*, vol. 87, pp. 48–54, Jun. 2016, doi: 10.1016/j.ijbiomac.2016.02.030.
- [64] D. Zhou, S. Liu, H. Song, X. Liu, and X. Tang, “Preparation and characterization of chemically modified high amylose maize starch-ascorbyl palmitate inclusion complexes in mild reaction condition,” *LWT*, vol. 142, p. 110983, May 2021, doi: 10.1016/J.LWT.2021.110983.
- [65] D. Yu, S. Xiao, C. Tong, L. Chen, and X. Liu, “Dialdehyde starch nanoparticles: Preparation and application in drug carrier,” *Chinese Sci. Bull.*, vol. 52, no. 21, pp. 2913–2918, Nov. 2007, doi: 10.1007/s11434-007-0388-5.
- [66] T. L. Carlson, J. Y. Lock, and R. L. Carrier, “Engineering the Mucus Barrier,” *Annu. Rev. Biomed. Eng.*, vol. 20, pp. 197–220, 2018, doi: 10.1146/annurev-bioeng-062117-121156.
- [67] R. A. Cone, “Barrier properties of mucus,” *Adv. Drug Deliv. Rev.*, vol. 61, no. 2, pp. 75–85, 2009, doi: 10.1016/j.addr.2008.09.008.
- [68] P. Prasher, R. Fatima, and M. Sharma, “Cationic polysaccharides: emerging drug delivery vehicle across the physiological mucus barrier,” *Future Med. Chem.*, vol. 14, no. 8, pp. 531–533, Apr. 2022, doi: 10.4155/fmc-2021-0296.
- [69] R. Fatima *et al.*, “Aminated Polysaccharides: Unveiling a new frontier for enhanced therapeutic efficacy,” *J. Drug Deliv. Sci. Technol.*, vol. 89, p. 105090, Nov. 2023, doi: 10.1016/j.jddst.2023.105090.
- [70] A. Nouri, M. Jelkmann, S. Khoee, and A. Bernkop-Schnürch, “Diaminated Starch: A Competitor of Chitosan with Highly Mucoadhesive Properties due to Increased Local Cationic Charge Density,” *Biomacromolecules*, vol. 21, no. 2, pp. 999–1008, 2020, doi: 10.1021/acs.biomac.9b01665.
- [71] M. Jelkmann, C. Lechner, C. Menzel, V. Krebs, and A. Bernkop-Schnürch, “Cationic starch derivatives as mucoadhesive and soluble excipients in drug delivery,” *Int. J. Pharm.*, vol. 570, no. September, p. 118664, 2019, doi: 10.1016/j.ijpharm.2019.118664.

- [72] P. Luo, L. Liu, W. Xu, L. Fan, and M. Nie, "Preparation and characterization of aminated hyaluronic acid/oxidized hydroxyethyl cellulose hydrogel," *Carbohydr. Polym.*, vol. 199, no. February, pp. 170–177, 2018, doi: 10.1016/j.carbpol.2018.06.065.
- [73] E. Amar-Lewis *et al.*, "Quaternized starch-based carrier for siRNA delivery: From cellular uptake to gene silencing," *J. Control. Release*, vol. 185, no. 1, pp. 109–120, 2014, doi: 10.1016/j.jconrel.2014.04.031.
- [74] S. Nadanaciva, M. D. Aleo, C. J. Strock, D. B. Stedman, H. Wang, and Y. Will, "Toxicity assessments of nonsteroidal anti-inflammatory drugs in isolated mitochondria, rat hepatocytes, and zebrafish show good concordance across chemical classes," *Toxicol. Appl. Pharmacol.*, vol. 272, no. 2, pp. 272–280, 2013, doi: 10.1016/j.taap.2013.06.019.
- [75] P. L. Beck *et al.*, "Mechanisms of NSAID-induced gastrointestinal injury defined using mutant mice," *Gastroenterology*, vol. 119, no. 3, pp. 699–705, 2000, doi: 10.1053/gast.2000.16497.
- [76] M. Whitehouse, "Drugs to Treat Inflammation: A Historical Overview," *Front. Med. Chem. - (Volume 4)*, pp. 707–729, 2012, doi: 10.2174/978160805207310904010707.
- [77] I. K. Oktavianti, I. Thalib, and E. Suhartono, "The protective efficacy of quercetin on mefenamic acid-induced gastric mucosal damage," *Int. J. Pharm. Clin. Res.*, vol. 8, no. 10, pp. 1390–1395, 2016.
- [78] K. Rainsford and P. Stetsko, "Gastrointestinal mucosal injury following repeated daily oral administration of conventional formulations of indometacin and other non-steroidal anti-inflammatory," *J. Pharm. Pharmacol.*, vol. 55, no. 5, pp. 661–668, 2003, doi: 10.1211/0022357021134.
- [79] W. Lee *et al.*, "Mefenamic Acid-Upregulated Nrf2/SQSTM1 Protects Hepatocytes against Oxidative Stress-Induced Cell Damage," *Toxics*, vol. 11, no. 9, p. 735, Aug. 2023, doi: 10.3390/toxics11090735.
- [80] M. J. D. Daniels *et al.*, "Fenamate NSAIDs inhibit the NLRP3 inflammasome and protect against Alzheimer's disease in rodent models," *Nat. Commun.*, vol. 7, pp. 24–30, 2016, doi: 10.1038/ncomms12504.
- [81] P. S. Khansari and R. F. Halliwell, "Mechanisms underlying neuroprotection by the NSAID mefenamic acid in an experimental model of stroke," *Front. Neurosci.*, vol. 13, no. FEB, pp. 1–10, 2019, doi: 10.3389/fnins.2019.00064.
- [82] S. K. Chiou and S. Mandayam, "NSAIDs enhance proteasomic degradation of survivin, a mechanism of gastric epithelial cell injury and apoptosis," *Biochem. Pharmacol.*, vol. 74, no. 10, pp. 1485–1495, 2007, doi: 10.1016/j.bcp.2007.07.024.
- [83] K. M. Kim, J. J. Song, J. Y. An, Y. T. Kwon, and Y. J. Lee, "Pretreatment of acetylsalicylic acid promotes tumor necrosis factor-related apoptosis-inducing ligand-induced apoptosis by down-regulating BCL-2 gene expression," *J. Biol. Chem.*, vol. 280, no. 49, pp. 41047–41056, 2005, doi: 10.1074/jbc.M503713200.

- [84] M. J. Redlak, J. J. Power, and T. A. Miller, "Role of mitochondria in aspirin-induced apoptosis in human gastric epithelial cells," *Am. J. Physiol. - Gastrointest. Liver Physiol.*, vol. 289, no. 4 52-4, pp. 731–738, 2005, doi: 10.1152/ajpgi.00150.2005.
- [85] P. Pyrko *et al.*, "Downregulation of survivin expression and concomitant induction of apoptosis by celecoxib and its non-cyclooxygenase-2-inhibitory analog, dimethyl-celecoxib (DMC), in tumor cells in vitro and in vivo," *Mol. Cancer*, vol. 5, pp. 1–16, 2006, doi: 10.1186/1476-4598-5-19.
- [86] A. A. R. Mehihi, A. A. R. Kubba, W. A. Shihab, and L. H. Tahtamouni, "New tolfenamic acid derivatives with hydrazine-1-carbothioamide and 1,3,4-oxadiazole moieties targeting VEGFR: synthesis, in silico studies, and in vitro anticancer assessment," *Med. Chem. Res.*, vol. 32, no. 11, pp. 2334–2348, Nov. 2023, doi: 10.1007/s00044-023-03137-4.
- [87] G. G. Graham, *Compendium of Inflammatory Diseases*. Basel: Springer Basel, 2016.
- [88] T. D. Warner, F. Giuliano, I. Vojnovic, A. Bukasa, J. A. Mitchell, and J. R. Vane, "Nonsteroid drug selectivities for cyclo-oxygenase-1 rather than cyclo-oxygenase-2 are associated with human gastrointestinal toxicity: A full in vitro analysis," *Proc. Natl. Acad. Sci. U. S. A.*, vol. 96, no. 13, pp. 7563–7568, 1999, doi: 10.1073/pnas.96.13.7563.
- [89] I. Bjarnason, J. Hayllar, A. N. dre. J. Macpherson, and A. N. thon. S. Russell, "Side effects of nonsteroidal anti-inflammatory drugs on the small and large intestine in humans," *Gastroenterology*, vol. 104, no. 6, pp. 1832–1847, 1993, doi: 10.1016/0016-5085(93)90667-2.
- [90] H. Kankaanranta and E. Moilanen, "Flufenamic and tolfenamic acids inhibit calcium influx in human polymorphonuclear leukocytes.," *Mol. Pharmacol.*, vol. 47, no. 5, pp. 1006–13, May 1995, [Online]. Available: <http://www.ncbi.nlm.nih.gov/pubmed/7746266>.
- [91] J. H. Paik, J. H. Ju, J. Y. Lee, M. D. Boudreau, and D. H. Hwang, "Two opposing effects of non-steroidal anti-inflammatory drugs on the expression of the inducible cyclooxygenase: Mediation through different signaling pathways," *J. Biol. Chem.*, vol. 275, no. 36, pp. 28173–28179, 2000, doi: 10.1074/jbc.M002329200.
- [92] S. Bindu, S. Mazumder, and U. Bandyopadhyay, "Non-steroidal anti-inflammatory drugs (NSAIDs) and organ damage: A current perspective," *Biochem. Pharmacol.*, vol. 180, p. 114147, 2020, doi: 10.1016/j.bcp.2020.114147.
- [93] I. Bjarnason, C. Scarpignato, E. Holmgren, M. Olszewski, K. D. Rainsford, and A. Lanas, "Mechanisms of Damage to the Gastrointestinal Tract From Nonsteroidal Anti-Inflammatory Drugs," *Gastroenterology*, vol. 154, no. 3, pp. 500–514, 2018, doi: 10.1053/j.gastro.2017.10.049.
- [94] P. Prasher, R. Fatima, and M. Sharma, "Therapeutic delivery with V-amylose," *Drug Dev. Res.*, vol. 82, no. 6, pp. 727–729, 2021, doi: 10.1002/ddr.21804.
- [95] N. Ab'lah, C. Y. L. Yusuf, P. Rojsitthisak, and T. W. Wong, "Reinvention of starch for oral drug delivery system design," *Int. J. Biol. Macromol.*, vol. 241, p. 124506, Jun.

- 2023, doi: 10.1016/j.ijbiomac.2023.124506.
- [96] L. Zhang *et al.*, “Structural and release properties of amylose inclusion complexes with ibuprofen,” *J. Drug Deliv. Sci. Technol.*, vol. 31, pp. 101–107, 2016, doi: 10.1016/j.jddst.2015.12.006.
- [97] L. Yang, B. Zhang, J. Yi, J. Liang, Y. Liu, and L. M. Zhang, “Preparation, characterization, and properties of amylose-ibuprofen inclusion complexes,” *Starch/Staerke*, vol. 65, no. 7–8, pp. 593–602, 2013, doi: 10.1002/star.201200161.
- [98] X. Cai, L. Yang, L. M. Zhang, and Q. Wu, “Evaluation of amylose used as a drug delivery carrier,” *Carbohydr. Res.*, vol. 345, no. 7, pp. 922–928, 2010, doi: 10.1016/j.carres.2010.02.008.
- [99] R. Cohen, Y. Orlova, M. Kovalev, Y. Ungar, and E. Shimoni, “Structural and functional properties of amylose complexes with genistein,” *J. Agric. Food Chem.*, vol. 56, no. 11, pp. 4212–4218, 2008, doi: 10.1021/jf800255c.
- [100] M. Rezvani, J. Mohammadnejad, A. Narmani, and K. Bidaki, “Synthesis and in vitro study of modified chitosan-polycaprolactam nanocomplex as delivery system,” *Int. J. Biol. Macromol.*, vol. 113, pp. 1287–1293, 2018, doi: 10.1016/j.ijbiomac.2018.02.141.
- [101] A. Marinopoulou, D. Christofilos, J. Arvanitidis, and S. N. Raphaelides, “Interaction of Tretinoin and Nimesulide with Amylose Matrices,” *Starch/Staerke*, vol. 73, no. 1–2, pp. 1–15, 2021, doi: 10.1002/star.202000054.
- [102] F. M. Carbinatto, T. S. Ribeiro, L. A. Colnago, R. C. Evangelista, and B. S. F. Cury, “Preparation and Characterization of Amylose Inclusion Complexes for Drug Delivery Applications,” *J. Pharm. Sci.*, vol. 105, no. 1, pp. 231–241, 2016, doi: 10.1002/jps.24702.
- [103] G. Galati, S. Tafazoli, O. Sabzevari, T. S. Chan, and P. J. O’Brien, “Idiosyncratic NSAID drug induced oxidative stress,” *Chem. Biol. Interact.*, vol. 142, no. 1–2, pp. 25–41, 2002, doi: 10.1016/S0009-2797(02)00052-2.
- [104] L. F. Siew, S. M. Man, J. M. Newton, and A. W. Basit, “Amylose formulations for drug delivery to the colon: A comparison of two fermentation models to assess colonic targeting performance in vitro,” *Int. J. Pharm.*, vol. 273, no. 1–2, pp. 129–134, Apr. 2004, doi: 10.1016/j.ijpharm.2003.12.015.
- [105] S. Milojevic *et al.*, “Amylose as a coating for drug delivery to the colon: Preparation and in vitro evaluation using 5-aminosalicylic acid pellets,” *J. Control. Release*, vol. 38, no. 1, pp. 75–84, 1996, doi: 10.1016/0168-3659(95)00112-3.
- [106] M. Ganje, S. M. Jafari, A. M. Tamadon, M. Niakosari, and Y. Maghsoudlou, “Mathematical and fuzzy modeling of limonene release from amylose nanostructures and evaluation of its release kinetics,” *Food Hydrocoll.*, vol. 95, no. April, pp. 186–194, 2019, doi: 10.1016/j.foodhyd.2019.04.045.
- [107] P. Prasher, R. Fatima, and M. Sharma, “Resistant starch: ideal candidate for the enteric coating of NSAIDs?,” *Future Med. Chem.*, vol. 13, no. 17, pp. 1411–1414, Sep. 2021, doi: 10.4155/fmc-2021-0160.

- [108] F. Varum, A. C. Freire, H. M. Fadda, R. Bravo, and A. W. Basit, “A dual pH and microbiota-triggered coating (PhloralTM) for fail-safe colonic drug release,” *Int. J. Pharm.*, vol. 583, p. 119379, 2020, doi: 10.1016/j.ijpharm.2020.119379.
- [109] F. Varum, A. C. Freire, R. Bravo, and A. W. Basit, “OPTICORETM, an innovative and accurate colonic targeting technology,” *Int. J. Pharm.*, vol. 583, p. 119372, Jun. 2020, doi: 10.1016/j.ijpharm.2020.119372.
- [110] W. L. Guerra-Ponce *et al.*, “In vitro evaluation of sustained released matrix tablets containing ibuprofen: A model poorly water-soluble drug,” *Brazilian J. Pharm. Sci.*, vol. 52, no. 4, pp. 751–760, 2016, doi: 10.1590/S1984-82502016000400020.
- [111] C. De Brabander, C. Vervaeet, L. Fiermans, and J. P. Remon, “Matrix mini-tablets based on starch/microcrystalline wax mixtures,” *Int. J. Pharm.*, vol. 199, no. 2, pp. 195–203, Apr. 2000, doi: 10.1016/S0378-5173(00)00383-5.
- [112] K. G. Desai, “Properties of tableted high-amylose corn starch-pectin blend microparticles intended for controlled delivery of diclofenac sodium,” *J. Biomater. Appl.*, vol. 21, no. 3, pp. 217–233, 2007, doi: 10.1177/0885328206056771.
- [113] T. Vangijzegem, D. Stanicki, and S. Laurent, “Magnetic iron oxide nanoparticles for drug delivery: applications and characteristics,” *Expert Opin. Drug Deliv.*, vol. 16, no. 1, pp. 69–78, 2019, doi: 10.1080/17425247.2019.1554647.
- [114] T. T. Dung, T. M. Danh, L. T. M. Hoa, D. M. Chien, and N. H. Duc, “Structural and magnetic properties of starch-coated magnetite nanoparticles,” *J. Exp. Nanosci.*, vol. 4, no. 3, pp. 259–267, 2009, doi: 10.1080/17458080802570609.
- [115] H. Aslam *et al.*, “Current and future perspectives of multifunctional magnetic nanoparticles based controlled drug delivery systems,” *J. Drug Deliv. Sci. Technol.*, vol. 67, p. 102946, Jan. 2022, doi: 10.1016/j.jddst.2021.102946.
- [116] X. Cai, L. Yang, L.-M. Zhang, and Q. Wu, “Evaluation of amylose used as a drug delivery carrier,” *Carbohydr. Res.*, vol. 345, no. 7, pp. 922–8, May 2010, doi: 10.1016/j.carres.2010.02.008.
- [117] L. Bisharat, S. A. Barker, A. Narbad, and D. Q. M. Craig, “In vitro drug release from acetylated high amylose starch-zein films for oral colon-specific drug delivery,” *Int. J. Pharm.*, vol. 556, pp. 311–319, 2019, doi: 10.1016/j.ijpharm.2018.12.021.
- [118] A. Marinopoulou, D. Christofilos, J. Arvanitidis, and S. N. Raphaelides, “Study of Molecular Inclusion Complex Formation of Amylose With Indomethacin,” *Starch/Staerke*, vol. 71, no. 7–8, pp. 1–42, 2019, doi: 10.1002/star.201800295.
- [119] I. Lalush, H. Bar, I. Zakaria, S. Eichler, and E. Shimoni, “Utilization of amylose-lipid complexes as molecular nanocapsules for conjugated linoleic acid,” *Biomacromolecules*, vol. 6, no. 1, pp. 121–130, 2005, doi: 10.1021/bm049644f.
- [120] H. Thérien-Aubin, F. Janvier, W. E. Baille, X. X. Zhu, and R. H. Marchessault, “Study of hydration of cross-linked high amylose starch by solid state ¹³C NMR spectroscopy,” *Carbohydr. Res.*, vol. 342, no. 11, pp. 1525–1529, 2007, doi: 10.1016/j.carres.2007.04.014.

- [121] H. S. Azevedo, F. M. Gama, and R. L. Reis, "In vitro assessment of the enzymatic degradation of several starch based biomaterials," *Biomacromolecules*, vol. 4, no. 6, pp. 1703–1712, 2003, doi: 10.1021/bm0300397.
- [122] Y. Liu, H. Xie, and M. Shi, "Effect of ethanol–water solution on the crystallization of short chain amylose from potato starch," *Starch/Staerke*, vol. 68, no. 7–8, pp. 683–690, 2016, doi: 10.1002/star.201500300.
- [123] F. W. D. Tai and M. E. McAlindon, "Non-steroidal anti-inflammatory drugs and the gastrointestinal tract," *Clin. Med. J. R. Coll. Physicians London*, vol. 21, no. 2, pp. 131–134, 2021, doi: 10.7861/CLINMED.2021-0039.
- [124] B. M. Peskar, "Role of cyclooxygenase isoforms in gastric mucosal defence.," *J. Physiol. Paris*, vol. 95, no. 1–6, pp. 3–9, Jan. 2001, doi: 10.1016/s0928-4257(01)00003-1.
- [125] S. Fiorucci, L. Santucci, and E. Distrutti, "NSAIDs, coxibs, CINOD and H2S-releasing NSAIDs: What lies beyond the horizon," *Dig. Liver Dis.*, vol. 39, no. 12, pp. 1043–1051, 2007, doi: 10.1016/j.dld.2007.09.001.
- [126] R. M. Haley and H. A. von Recum, "Localized and targeted delivery of NSAIDs for treatment of inflammation: A review," *Exp. Biol. Med.*, vol. 244, no. 6, pp. 433–444, 2019, doi: 10.1177/1535370218787770.
- [127] M. Aparecida, V. Teixeira, C. F. Garcia, A. Augusto, and G. Faraco, "Maria Aparecida Vieira Teixeira GARCIA 1 *, Cleverson Fernando GARCIA 2 , André Augusto Gomes FARACO 3 1 -," *Wiley Online Libr.*, vol. 72, no. 7–8, p. 44, 2020, doi: 10.1002/star.201900270.This.
- [128] M. Ziegler-Borowska, "Magnetic nanoparticles coated with aminated starch for HSA immobilization- simple and fast polymer surface functionalization," *Int. J. Biol. Macromol.*, vol. 136, pp. 106–114, Sep. 2019, doi: 10.1016/j.ijbiomac.2019.06.044.
- [129] W. Ding, P. Zhao, and R. Li, "Removal of Zn (II) ions by dialdehyde 8-aminoquinoline starch from aqueous solution," *Carbohydr. Polym.*, vol. 83, no. 2, pp. 802–807, 2011, doi: 10.1016/j.carbpol.2010.08.057.
- [130] Y. H. Bae, "Smart polymers in drug delivery," *Pharm. News*, vol. 9, no. 6, pp. 417–424, 2002, doi: 10.1081/e-ebpp-120050557.
- [131] B. Çelik, "Risperidone mucoadhesive buccal tablets: Formulation design, optimization and evaluation," *Drug Des. Devel. Ther.*, vol. 11, pp. 3355–3365, 2017, doi: 10.2147/DDDT.S150774.
- [132] A. Bernkop-Schnürch and S. Steininger, "Synthesis and characterisation of mucoadhesive thiolated polymers," *Int. J. Pharm.*, vol. 194, no. 2, pp. 239–247, 2000, doi: 10.1016/S0378-5173(99)00387-7.
- [133] N. L. Vanier, S. L. M. El Halal, A. R. G. Dias, and E. da Rosa Zavareze, "Molecular structure, functionality and applications of oxidized starches: A review," *Food Chem.*, vol. 221, pp. 1546–1559, 2017, doi: 10.1016/j.foodchem.2016.10.138.

- [134] Y. Liu, V. S. Bryantsev, M. S. Diallo, and W. A. Goddard III, "PAMAM Dendrimers Undergo pH Responsive Conformational Changes without Swelling," *J. Am. Chem. Soc.*, vol. 131, no. 8, pp. 2798–2799, Mar. 2009, doi: 10.1021/ja8100227.
- [135] S. Zhuo, F. Zhang, J. Yu, X. Zhang, G. Yang, and X. Liu, "pH-sensitive biomaterials for drug delivery," *Molecules*, vol. 25, no. 23, pp. 1–20, 2020, doi: 10.3390/molecules25235649.
- [136] X. Mou, Z. Ali, S. Li, and N. He, "Applications of magnetic nanoparticles in targeted drug delivery system," *J. Nanosci. Nanotechnol.*, vol. 15, no. 1, pp. 54–62, 2015, doi: 10.1166/jnn.2015.9585.
- [137] S. Jalali, P. N. Moghadam, and V. Shafiei-Irannejad, "Synthesis of Magnetic Nanocarrier Conjugated by Folate Based on Tragacanth and In Vitro Investigation of their Efficiency on Breast Cancer Cells," *Starch - Stärke*, vol. 75, no. 5–6, May 2023, doi: 10.1002/star.202200092.
- [138] W. Zhu, A. Smith, and C. Y. F. Young, "A Nonsteroidal Anti-Inflammatory Drug, Flufenamic Acid, Inhibits the Expression of the Androgen Receptor in LNCaP Cells," *Endocrinology*, vol. 140, no. 11, pp. 5451–5454, Nov. 1999, doi: 10.1210/endo.140.11.7246.
- [139] V. Prikhodko, D. Chernyuk, Y. Sysoev, N. Zernov, S. Okovityi, and E. Popugaeva, "Potential Drug Candidates to Treat TRPC6 Channel Deficiencies in the Pathophysiology of Alzheimer's Disease and Brain Ischemia," *Cells*, vol. 9, no. 11, 2020, doi: 10.3390/cells9112351.
- [140] Z. Y. Li *et al.*, "Enhancing anti-tumor activity of sorafenib mesoporous silica nanomatrix in metastatic breast tumor and hepatocellular carcinoma via the co-administration with flufenamic acid," *Int. J. Nanomedicine*, vol. 15, pp. 1809–1821, 2020, doi: 10.2147/IJN.S240436.
- [141] R. Matsumoto *et al.*, "Aldo-keto reductase 1C1 induced by interleukin-1 β mediates the invasive potential and drug resistance of metastatic bladder cancer cells," *Sci. Rep.*, vol. 6, no. February, pp. 1–13, 2016, doi: 10.1038/srep34625.
- [142] O. P. Troncoso and F. G. Torres, *Non-conventional starch nanoparticles for drug delivery applications*, vol. 3, no. 6. 2020.
- [143] A. Dimantov, M. Greenberg, E. Kesselman, and E. Shimoni, "Study of high amylose corn starch as food grade enteric coating in a microcapsule model system," *Innov. Food Sci. Emerg. Technol.*, vol. 5, no. 1, pp. 93–100, 2004, doi: 10.1016/j.ifset.2003.11.003.
- [144] L. P. Amador-Gómez, G. Luna Solano, G. R. Urrea-García, R. S. Gines-Palestino, and D. Cantú-Lozano, "Synthesis, Modification, and Characterization of Fe₃O₄@SiO₂-PEI-Dextranase Nanoparticles for Enzymatic Degradation of Dextran in Fermented Mash," *Processes*, vol. 11, no. 1, p. 70, Dec. 2022, doi: 10.3390/pr11010070.

List of Publications

1. **Fatima, R.**, Prasher, P., & Sharma, M., Chellapan, DK., Gupta, G., Singh, SK., Patrawale VB., Dua K. (2023). Aminated Polysaccharides: Unveiling a new frontier for enhanced therapeutic efficacy. *Journal of Drug Delivery Science & Technology*. <https://doi.org/10.1016/j.jddst.2023.105090> [SCI IF 5.0]
2. **Fatima, R.**, Sharma, M., Prasher, P., Singh, S. K., Chellappan, D. K., Kaur, I. P., & Dua, K. (2023). Diversity of Rationally Modified Polysaccharides for Pharmaceutical Applications. *Chemistry Select*, 8(20). <https://doi.org/10.1002/slct.202300941> [SCI IF 2.3]
3. **Fatima, R.**, Sharma, M., Dhiman, A., Arora, A., Mudila, H., Prasher, P. (2023). Targeted delivery of fenamates with aminated starch. *Therapeutic Delivery*, 14(3), 1-10. <https://doi.org/10.4155/tde-2023-0013> [SCI IF 4.2]
4. **Fatima, R.**, Sharma, M., & Prasher, P. (2021). Targeted delivery of flufenamic acid by V-amylose. *Therapeutic Delivery*, 12(8), 575–582. <https://doi.org/10.4155/tde-2021-0020> [SCI IF 4.2]
5. Prasher, P., **Fatima, R.**, & Sharma, M. (2021). Therapeutic delivery with V-amylose. *Drug Development Research*, 82(6), 727–729. <https://doi.org/10.1002/ddr.21804> [SCI IF 3.8]
6. Prasher, P., **Fatima, R.**, & Sharma, M. (2021). Resistant starch: Ideal candidate for the enteric coating of NSAIDs? *Future Medicinal Chemistry*, 13(17), 1411–1414. <https://doi.org/10.4155/fmc-2021-0160> [SCI IF 4.2]
7. Prasher, P., **Fatima, R.**, & Sharma, M. (2022). Cationic polysaccharides: Emerging drug delivery vehicle across the physiological mucus barrier. *Future Medicinal Chemistry*, 14(8), 531–533. <https://doi.org/10.4155/fmc-2021-0296> [SCI IF 4.2]
8. Prasher, P., **Fatima, R.**, Sharma, M., Tynybekov, B., Alshahrani, A. M., Ateşşahin, D. A., ... & Calina, D. (2023). Honokiol and its analogues as anticancer compounds: Current mechanistic insights and structure-activity relationship. *Chemico-Biological Interactions*, 110747. <https://doi.org/10.1016/j.cbi.2023.110747> [SCI IF 5.1]
9. **Fatima, R.**, Sharma, M., Prasher, P., Gupta, G., Singh, S. K., Gulati, M., & Dua, K. (2023). Elucidating the antiviral potential of polysaccharides. *EXCLI Journal*, 22, 108–111. <https://doi.org/10.17179/excli2022-5621> [SCI IF 4.6]

10. **Fatima, R.**, Sharma, M., Prasher, P., Gupta, G., Singh, S. K., Gulati, M., & Dua, K. (2023). Adenocarcinoma - Success so far and the way ahead. *EXCLI Journal*, 22, 329–333. <https://doi.org/10.17179/excli2023-5939> [SCI IF 4.6]
11. **Fatima, R.**, Sharma, M., Prasher, P., Synthesis of magnetic nanoparticles coated with high amylose starch-flufenamic acid complexes: A novel approach for enhanced biomedical applications (**Communicated**)
12. **Fatima, R.**, Prasher, P., & Sharma, M., Singh, S. K., Dua, K. The contemplation of V amylose for the delivery of ulcerogenic NSAIDs (**Communicated**)

Analysis of V Amylose in Controlled Drug delivery

ORIGINALITY REPORT

8% SIMILARITY INDEX	5% INTERNET SOURCES	6% PUBLICATIONS	% STUDENT PAPERS
-------------------------------	-------------------------------	---------------------------	----------------------------

PRIMARY SOURCES

1	discovery.researcher.life Internet Source	1%
2	Akram Nouri, Max Jelkmann, Sepideh Khoei, Andreas Bernkop-Schnürch. "Diaminated Starch: A Competitor of Chitosan with Highly Mucoadhesive Properties due to Increased Local Cationic Charge Density", Biomacromolecules, 2020 Publication	1%
3	www.mdpi.com Internet Source	<1%
4	Cohen, Revital, Yevgenia Orlova, Marina Kovalev, Yael Ungar, and Eyal Shimoni. "Structural and Functional Properties of Amylose Complexes with Genistein", Journal of Agricultural and Food Chemistry, 2008. Publication	<1%
5	Sinha, V.R.. "Polysaccharides in colon-specific drug delivery", International Journal of Pharmaceutics, 20010814 Publication	<1%